Aerodynamic Cooling of Automotive Disc Brakes

A thesis submitted in accordance with the regulations
for the degree of Master of Engineering

by

Arthur Stephens B.Sc. (Eng)

School of Aerospace, Mechanical & Manufacturing Engineering
RMIT University

March 2006

ABSTRACT

Sufficient heat dissipation is crucial to the effective operation of friction based braking systems. Such cooling is generally provided by ensuring a sufficient supply of cooling air to the heated components, hence the aerodynamics in the region of the brake components is extremely important. The objective of the research was to develop an understanding of how aerodynamics could be used to improve the cooling of automotive disc brakes.

Two separate sets of wind tunnel experiments were developed. Tests were performed on a vented disc (rotor) to measure the internal flow through the vents on a rotating vented disc under various conditions, including an isolated disc in still air, the disc in still air with the wheel on, the disc in moving air with the wheel on, and an on-road simulation using a ¼ car. On vehicle tests were also performed in a wind tunnel using a purpose built brake test rig. These tests measured the thermal performance of different brake discs under various operating parameters; including constant load braking, and cooling from high temperature under various speeds, wheels and disc types.

It was found that airflow through vented rotors was significantly reduced during simulated on-road driving, compared to when measured in isolation, but not particularly affected by the vehicles speed. In the situations tested, vented discs offered a 40+% improvement in cooling over an equivalent sized solid rotors. However the research indicates that the greatest benefit of vented rotors over solid will be in vehicles where air entering the wheel cavity is limited, such as low drag vehicles. It was also found that the most significant improvements in brake thermal performance could be achieved by maximising the airflow into the region of the brake components; including increasing the open area of the wheel, and increasing the vehicle velocity. Other improvements can be achieved by using a wheel material with good conductive capability, and increasing the mass of the disc.

Evidence of vortex shedding was also discovered in the airflow at the exit of an internal vented rotor, any reduction in this flow disturbance should lead to increased airflow with associated improvements in thermal performance.

ACKNOWLEDGEMENTS

There are a number of people whose support throughout my candidature made the completion of this thesis possible.

Firstly I would like to thank my supervisors Simon Watkins and Chris Dixon, for their constant support, encouragement and patience.

The School of Aerospace, Mechanical & Manufacturing Engineering at RMIT University, whose support and financial backing made this research possible.

The Ford Motor Company of Australia, by supplying a vehicle and equipment for testing made the experimental work possible.

My fellow postgraduate students, in particular members of the Vehicle Aerodynamics Group, for their time and practical assistance with the experimental work.

The technical staff at RMIT University, for assistance in developing, and maintaining the equipment used in the course of the experiments.

Finally to Trish, without her never ending belief and encouragement, this thesis would never have been completed.

DECLARATION

I certify that except where due acknowledgement has been made, the work presented in this thesis is that of the author alone; the work has not been submitted previously, in whole or in part, to qualify for any other academic award; the content of the thesis is the result of work which has been carried out since the official commencement date of the approved research program; and, any editorial work, paid or unpaid, carried out by a third party is acknowledged.

Arthur Stephens

March 2006

TABLE OF CONTENTS

TABLE OF FIGURES

TABLE OF TABLES

NOMENCLATURE

A_s	Surface Area
A_f	Projected Frontal Area
C_D	Non-dimensional drag co-efficient
CFD	Computational Fluid Dynamics
D	Aerodynamic Drag Force (N)
D_o	Outer Diameter of Rotor
D_i	Inner Diameter of Rotor
DNS	Direct Numerical Simulation
E_b	Braking Energy
f_r	Frequency of Shedding Vortices
FD	Finite Difference
FE	Finite Element
FFT	Fast Fourier Transform
FV	Finite Volume
h	Convection Heat Transfer Co-efficient
Hz	Hertz
Km/h	Kilometres Per Hour
l	Characteristic Length
LES	Large Eddy Simulation
m/s	Metres Per Second
$\dot{m}$	Mass Flowrate
N	Revolution Per Minute
ρ_a	Density of Air
r_o	Outer Radius of Rotor
RANS	Reynolds Averaged Navier Stokes

St	Strouhal Number
T_s	Surface Temperature
T_∞	Temperature of Atmosphere
V	Velocity
V_{ave}	Average Velocity
ω	Angular Velocity

CHAPTER ONE

1 BACKGROUND, OBJECTIVES AND SCOPE

1.1 Background to Research

One of the most important components in a road vehicle is its braking system. The braking system must be able to remove the kinetic and potential energy of the vehicle, to enable safe retardation. In some vehicles this kinetic and potential energy can be converted into electric energy and stored in batteries to be used by the vehicle when required. This is known as regenerative braking. However this type of braking system has limited application and is mainly confined to electric or hybrid electric vehicles. Regenerative braking systems still require a backup system for times when electric braking is insufficient, or when failure occurs, (Westbrook 2001). Friction-braking systems have always been, and are still the universally adopted method of retardation of automobiles. Friction brakes operate by converting the vehicles kinetic and potential energy into thermal energy (heat). The rate of heat generation in a friction braking system is a function of the vehicles mass, velocity, and rate of deceleration. During braking, a large amount of heat can be created and has to be absorbed by brake components in a very short space of time. However the allowable temperatures of the brake and surrounding components limit the amount of thermal energy a brake can store, (Limpert 1975; Sheridan et al. 1988). The absorbed heat must be effectively dissipated to achieve satisfactory performance of the braking system, (Day and Newcomb 1984). If this heat is not dissipated effectively the temperatures in the brake and surrounding components become too high, according to Day (1988) high temperatures are responsible for most problems in vehicle braking systems. Such problems include excessive component wear, squeal, judder and in extreme cases complete failure of the brakes. Any improvements to the cooling characteristics of a braking system will reduce the risk of the above problems and provide safer vehicle transport.

The heat created in braking is generated by friction between the brake rotor and the pad (lining) material. Initially the rotor and adjoining components absorb the heat created, however as braking continues, heat is dissipated through convection to the atmosphere and

conduction and radiation to nearby components. While conduction is an effective mode of heat transfer it can have adverse effects on certain components. According to Limpert (1975) radiation heat transfer from the rotor will have its greatest effect at higher temperatures but must be controlled to prevent tyre damage. Convection to the atmosphere is therefore the primary means of heat dissipation from the brake rotor. Convection heat transfer from the brake components is assisted by cooling air directed at the brake from the forward movement of the vehicle. This airflow must be controlled and directed to the appropriate areas in order to achieve maximum cooling of the brakes.

Aerodynamics has long been used to optimise the airflow around and through vehicles, from reducing aerodynamic drag, to engine cooling and noise reduction, (Hucho 1998). However, little documented research has been conducted on aerodynamic cooling of automotive brakes. It is considered that a more comprehensive understanding of the relationship between brake heat dissipation and aerodynamics could provide significant cooling improvements.

1.2 Scope of the Work

This study is primarily focused on how heat dissipation from brake rotors can be improved by modifying or improving aerodynamic conditions in and around the brake assembly.

The research will address the following questions:

- What are the main factors contributing to effective automobile brake cooling?
- Can heat dissipation from automotive disc brakes be increased by improved local aerodynamics?
- Can the thermal performance of a brake rotor be improved by wheel ventilation?
- Are vented rotors universally better at heat dissipation, or are there times when a solid rotor is better?

1.2.1 Rationale

This research is intended to provide the automobile industry with a better understanding of the requirements of effective aerodynamic brake cooling, as well as recommending methods of improving aerodynamic heat dissipation. The results of the project will

provide information on how and where aerodynamic improvements can be made to automotive brake cooling. Weight reduction is one of the primary design goals in the automotive industry, and by improving brake cooling, the weight of the brake and associated components may be reduced. Other benefits from improved brake cooling include a reduced risk of thermal brake failure (brake fade and fluid vaporisation), longer component life, as well as lower noise and cost. The project will also provide information on how to optimise aerodynamic elements in the early stages of the brake design process to gain substantial improvements in cooling.

1.3 Research Approach

To achieve the stated objectives of the research a detailed review of the relevant literature was completed. An experimental approach was then developed, which involved developing a procedure to study the airflow in and around vented rotors, as well as incorporating a brake test facility into an existing Industrial Wind Tunnel, in order to simulate the airflow around the brakes on a moving vehicle. The experimental work was divided into stages; Stage 1 involved the detailed examination of flow through a vented rotor, and Stage 2 used on-vehicle tests to examine the major parameters that effect brake cooling.

1.3.1 Thesis Structure

The structure of the thesis is as follows:

Chapter 1 (current chapter) introduces the research and outlines the aims, objectives and scope of the work.

Chapter 2 provides a preliminary investigation into the current theory and practices of disc brake cooling and related aerodynamics, and includes a detailed review of the relevant background literature.

Chapter 3 describes the experimental approach adopted in this research. This Chapter also describes test facilities, equipment and instrumentation used in the course of the work.

Chapters 4 and 5 present the experimental work, which is divided into two stages; detailed examination of the airflow through vented brake rotors (Chapter 4), and on-vehicle brake

testing (Chapter 5). A description of the experimental set-up and procedure is given, followed by the results and analysis.

Chapter 6 discusses the major conclusions of the research and outlines recommendations on how the research could be further developed.

The appendices contain additional information supporting the document including; calibration of instruments, preliminary studies and experimental work, calculations and a paper presented to the Society of Automotive Engineers on part of this research.

CHAPTER TWO

2 BACKGROUND RESEARCH IN DISC BRAKES AND RELATED AERODYNAMICS

2.1 Vehicle Braking

2.1.1 Types of Vehicle Brakes

In order to slow or stop a vehicle the kinetic and any potential energy of the vehicle's motion must be contained. In recent years, fuel efficiency (and the reduction of associated exhaust emissions) has become one of the main targets of the automotive industry, and to this end some manufacturers have started producing commercially available electric and hybrid electric vehicles. These vehicles use an electric motor either as the main source of propulsion, or as a secondary source to assist the traditional internal combustion engine. In these vehicles, significant fuel consumption savings can be obtained by re-cycling some of the energy lost in braking into electrical energy. This energy can then stored in batteries and used when required for propulsion of the vehicle, or to power accessories such as air conditioning, lights etc. However it is not possible to recover more than 10-15% of the total energy used in propulsion, (Westbrook 2001), and therefore these vehicles also contain traditional friction brakes as safety backup. Friction brakes operate by converting the energy in the vehicle's motion into heat and dissipating it to the atmosphere, and as such the energy is non-recoverable. In spite of this, the relatively small number of electric and hybrid-electric vehicles in use means that friction brakes are the dominant form of automotive braking systems, and will continue to be for the foreseeable future. Therefore, research continues into ways and means of improving this technology in area such as weight reduction, thermal dissipation and improved safety.

2.1.2 Overview of Friction Braking Systems

Friction brakes operate by converting the vehicles kinetic, and sometimes potential energy into thermal energy (heat). Heat is created due to friction at the interface between a rotor (disc or drum) and stator (pads or shoes). During braking, a large amount of heat can be

created and has to be absorbed by the rotor. The rotor and surrounding components effectively act as temporary thermal storage devices, and sufficient cooling of these components is essential to achieve satisfactory performance of the braking system, (Day and Newcomb 1984). It is therefore vital that heat is effectively dissipated for the successful operation of a braking system.

2.1.3 Types of Friction Braking Systems

Two main types of automotive brakes exist, drum and disc. Drum brakes operate by pressing shoes (stator) radially outwards against a rotating drum (rotor), while disc brakes operate by axially compressing pads (stator) against a rotating disc (rotor) as shown in Figure 2.1.1. A more advanced form of the disc brake is the ventilated or vented disc, where internal cooling is achieved by air flowing through radial passages or vanes in the disc.

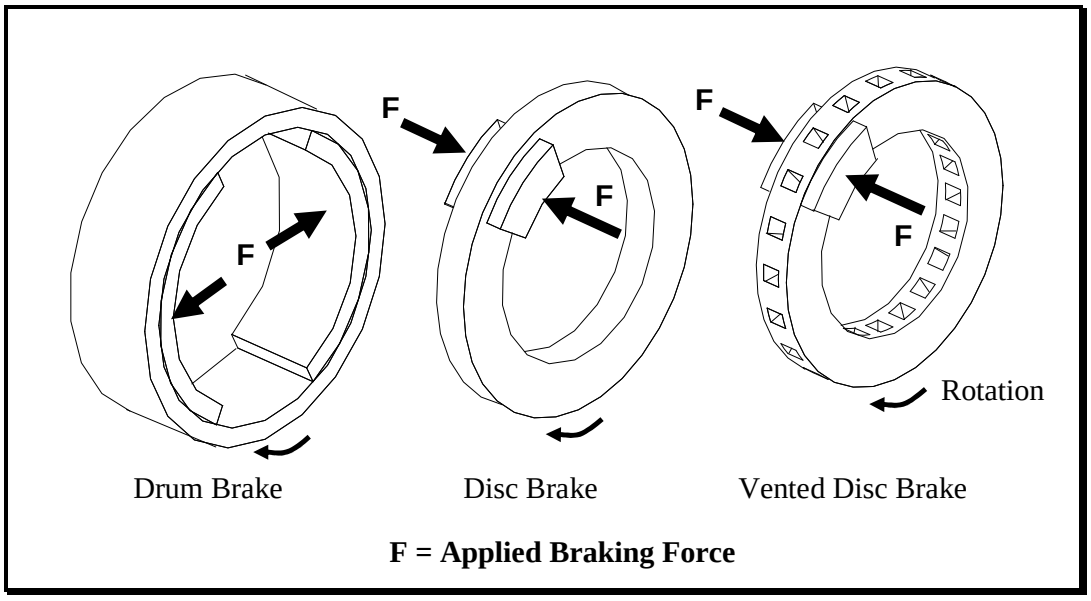

Figure 2.1.1 Schematic View of Drum and Disc Brakes, adapted from Baker (1986)

The various advantages of disc brake over drum has seen them almost universally adopted in passenger cars as well as in the front of light duty trucks, (Limpert 1999), and will therefore be the focus of this research. However, drum brakes are still used in many applications including heavy-duty trucking. The main advantages of disc over drum are:

- The rubbing surfaces of the disc brake are exposed to the atmosphere providing better cooling and reducing the possibility of thermal failure (brake fade and brake fluid vaporisation).

- In drum brakes, expansion of the drum at elevated temperatures will result in longer pedal travel and improper contact between the drum and shoes, whereas in disc brakes elevated temperatures cause an increase in disc thickness, with no adverse effect in braking.
- Disc brake adjustment is achieved automatically whereas drum brakes need to be adjusted as the friction material wears.
- Disc brakes are less sensitive to high temperatures and can operate safely at temperatures of up to 1000°C. Drum brakes due to their geometry and effects on their friction co-efficient, should not exceed 500-600°C, (Limpert 1999).

Brake discs (solid and vented) are generally cast from an iron alloy and machined to the required finish, they are generally shaped like a top hat which provides structural strength to minimise distortion.

2.1.4 Problems Associated With Overheating Brakes

If the temperatures reached in braking become too high, deterioration in braking may result, and in extreme conditions complete failure of the braking system can occur. It can be difficult to attribute thermal brake failure to motor vehicle accidents as normal braking operation may return to the vehicle when the temperatures return to below their critical level, (Hunter et al. 1998). One of the most common problems caused by high temperatures is brake fade; other problems that may occur are excessive component wear, rotor deterioration, and thermally excited vibration (brake judder). Heat conduction to surrounding components can also lead to damaged seals, brake fluid vaporisation, as well as wheel bearing damage, while heat radiated to the tyre can cause damage at tyre temperatures as low as 200°F (93°C), (Limpert 1975). The major problems associated with elevated brake temperatures are outlined below.

Brake Fade

Brake fade is a temporary loss of braking that occurs as a result of very high temperatures in the friction material. The high temperature reduces the coefficient of friction between the friction material and the rotor, and results in reduced braking effectiveness and ultimately failure. Generally fade is designed to occur at temperatures lower than the flame temperature of the friction material to reduce the possibility of fire at extreme temperatures. Normal braking will usually return when temperatures drop below their critical level.

Brake Fluid Vaporisation

Most braking systems are hydraulically actuated, with the exception of heavy-duty trucking. If temperatures reached during braking exceed the boiling point of the hydraulic fluid then brake fluid vaporisation will occur. A vapour lock will then form in the hydraulic circuit, and as gas is more compressible than liquid the pedal stroke is used to compress this gas without actuating the brakes. Brake fluid is hydroscopic causing it to absorb water from the atmosphere over time; this may result in a reduced boiling temperature of the fluid, (Hunter et al. 1998). Therefore it is usually recommended by vehicle manufacturers to replace brake fluid periodically.

Excessive Component Wear

High temperatures in the braking system can form thermal deformation of the rotors leading to uneven braking, accelerated wear and premature replacement. The life of the friction material is also temperature dependent, at higher temperatures chemical reactions in the friction material may cause a breakdown in its mechanical strength, which reduces braking effectiveness and causes rapid wear. The wear of frictional material is directly proportional to contact pressure, but exponentially related to temperature, (Day and Newcomb 1984); therefore more rapid wear will occur at elevated temperatures.

Thermal Judder

On application of the vehicles brakes, low frequency vibrations may occur, these vibrations can be felt by the driver as body shake, steering shake and in some cases an audible drone, (Kao et al. 2000). This phenomenon is known as 'judder'. Two types of judder exists; hot (or thermal judder) and cold judder. Cold judder is caused by uneven thickness of the rotor, known as disc thickness variation, this leads to deviations in contact pressure as the pads connect with the rotor. This results in uneven braking or brake torque variation. The second type, thermal judder, occurs at elevated temperatures, and is caused by thermal deformation of the rotor. When a rotor containing a cold disc thickness variation is subjected to braking, the contact pressure in the thicker parts will be much greater than the thinner parts. As a result, the thicker parts become hotter causing uneven thermal expansion of the rotor, which compounds the original disc thickness variation and creates a "self accelerating instability", (Little et al. 1998). Thermal judder can also be a result of 'hotspots' on the rotor surface. Hotspots can be caused by localised contact between the pads and rotor resulting in small areas of very high temperatures, >700 °C, which causes a thermal disc thickness variation. This thermal disc thickness variation

may develop into a permanent disc thickness variation due to a phase change from pearlite to martensite, (Kao, et al. 2000), when cast iron is cooled rapidly. Martensite occupies a larger volume than pearlite, and therefore a cold disc thickness variation is formed and the problem is again compounded.

2.1.5 Dissipation of Heat from Disc Brakes

The rise in temperature of the brake disc in any braking operation will depend on a number of factors including the mass of the vehicle, the rate of retardation, and the duration of the braking event. In the case of short duration brake applications with low retardation, the rotor and friction material may absorb all of the thermal energy generated. As a result very little heat dissipation occurs as the temperature rise in the rotor is minimal. In extreme braking operations such as steep descents or repeated high speed brake applications, sufficient heat dissipation becomes critical to ensure reliable continued braking. As the rotor temperature rises it begins to dissipate heat, at steady-state conditions heat generated through braking equals heat dissipation and no further heating occurs. If the heat generation is greater than the dissipation then the temperature will rise, the rate of this rise will depend of the relative quantities of each. If sufficient heat dissipation does not occur the temperature of the rotor and friction material can reach critical levels and brake failure may occur.

Heat dissipation from the brake disc will occur via conduction through the brake assembly and hub, radiation to nearby components and convection to the atmosphere. At high temperatures heat may create chemical reactions in the friction material, which may dissipate some of the braking energy. However research conducted by Day and Newcomb (1984) indicated this to be less than two per cent of the total energy dissipated. While conduction is an effective mode of heat transfer it can have adverse effects on nearby components. Such effects include damaged seals, brake fluid vaporisation, as well as wheel bearing damage. Radiation heat transfer from the rotor will have its greatest effect at higher temperatures but must be controlled to prevent beading of the tyre, (Limpert 1975). It is estimated that the amount of heat dissipation through radiation under normal braking conditions is less than 5% of the total heat dissipated, (Noyes and Vickers 1969; Limpert 1975).

Convection to the atmosphere must then be the primary means of heat dissipation from the brake rotor. Convection is governed by the expression:

$$Q=hA_s(T_s-T_\infty) \qquad \textbf{Equation 2.1.1}$$

also know as Newton's law of cooling.

Where:

Q = the rate of heat transfer (Watts),

h = the convection heat transfer coefficient (W/m^2 k),

A_s = the surface area of the rotor (m^2), and

T_s *and* T_∞ are the surface temperatures of the brake rotor and ambient air temperature respectively.

It can be seen from this expression that in order to maximise heat transfer from the rotor (increase Q) and keep the rotor temperature (T_s) to a minimum, the value of heat transfer coefficient (h), or the surface area (A_s) needs to be increased. As it is required to keep T_s to a minimum, improvements must be made through increasing the heat transfer coefficient (h) and or the surface area (A_s) of the rotor. The amount by which the surface area can increase is confined by the diameter of the wheel and the requirements of minimising unsprung mass[1], so improvements in cooling can best be made through increased values of the heat transfer coefficient, (Limpert 1975). This heat transfer coefficient is dependent on the boundary layer, which is influenced by surface geometry, the nature of the fluid motion around the rotor, as well as thermodynamic and fluid transfer properties, (Incropera and DeWitt 1996).

The use of an internally ventilated rotor will increase both surface area (extra internal area exposed to the atmosphere) and the heat transfer coefficient, due to forced convection created by the internal airflow, with negligible influence on unsprung mass. The material selection and the physical dimensions of the rotor will also have a direct bearing on cooling ability. Analytical work by Rusnak et al. (1970) found that the steady state surface temperatures decrease with increasing thermal conductivity of the rotor. This was mainly attributed to the ability of high conductive materials to transmit heat into the hub

[1] Un-sprung mass = The mass of a vehicle which is not supported by the suspension, comprising of mass of wheels, tires, brakes hubs, etc., and approximately 50% of the mass of the suspension links, drive shafts and shock absorbers.

and wheel assembly, which act as a heat sink. However, as discussed previously this is not a particularly advantageous situation, and therefore the more energy dissipated to the surrounding air the better. The greater the volume of air which interacts with the heated elements the greater the heat dissipation. The study of aerodynamics has long been used to optimise the airflow around passenger vehicles, from aerodynamic drag reduction to passenger comfort. In order to identify how aerodynamics could be further employed to enhance brake cooling a thorough review of the subject matter must first be undertaken.

2.2 Vehicle Aerodynamics

As an automobile travels through the atmosphere, air is forced through and around the vehicle. The aerodynamic interaction between this air and the moving vehicle has a large influence on vehicle performance, safety, comfort, stability, visibility and cooling. This airflow must be understood and controlled in order to provide the optimum conditions for the vehicles movement. Therefore road vehicle aerodynamics has become an important part of vehicle development in recent years.

Initially work in aerodynamics has concentrated on the reduction of aerodynamic drag; the resistive force acting on a moving vehicle due to the displacement of the surrounding air. At high speeds (100 km/hr) aerodynamic drag accounts for approximately 75% of the total resistance to motion of the vehicle, (Hucho 1998), the rest is mostly rolling resistance. Therefore significant savings in fuel consumption and emissions can be obtained from minimising aerodynamic drag. As a result, drag reduction is one of the primary focuses of ground vehicle aerodynamics. In recent years aerodynamic drag has become an important marketing feature for new vehicles, and the non-dimensional aerodynamic drag coefficient "C_D" has been compared in importance to the compression ratio of the internal combustion engine, (Hucho 1998). The C_D values for typical passenger cars has dropped from about 0.5 in the 1960's to around 0.3 in the early 1990's, however it appears to be rising again as the demand for large and four wheel drive vehicles increases. Drag reduction may also adversely effect the vehicle braking system in the following ways:

- The reduction in aerodynamic drag also reduces aerodynamic braking, increasing the load on the vehicle braking system particularly at higher speeds[2].
- The result of reducing the aerodynamic drag of a vehicle is a smoother path for the air to flow around the vehicle, which reduces the cooling airflow available to the vehicle, (Garrett and Munson 1983).
- Reducing aerodynamic drag will allow higher vehicle speeds for a given engine power, potentially increasing braking duty.

However important the goal of low aerodynamic drag may be, vehicle aerodynamics is concerned with many other aspects of the vehicle performance. The directional stability will be greatly affected by the overall flow field around the vehicle. For optimal performance of the engine, sufficient combustion air must be supplied, air for cooling (engine, brakes, electronics etc) and cabin ventilation must also be considered. The flow field around the vehicle should be controlled to minimise cabin noise as well as dirt deposition from spray water that may impair the driver's visibility or the effectiveness of the lights. The following table adapted from Hucho (1998) outlines the areas of the vehicle which are directly influenced by aerodynamics:

Vehicle Aerodynamics				
Cooling	**Performance**	**Comfort**	**Stability**	**Visibility**
Engine	Fuel Economy	Ventilation	Directional	Dirt
Transmission	Emissions	Heating	Crosswind Sensitivity	Splash & Spray
Brakes	Maximum Speed	Air conditioning		Wiper Lift off
Condenser	Acceleration	Wind Noise		

Table 2.2.1 Spectrum of Tasks for Vehicle Aerodynamics, Hucho (1998)

Clearly from the above table the wide range of areas that aerodynamics has to cover is apparent. This spectrum of tasks often creates conflicting requirements, the best engine cooling is provided with large openings at the front of the vehicle, however these openings

[2] $D=\frac{1}{2}\rho V^2 C_d A$

Where D = Aerodynamic Drag
ρ = Density of Air
V = Vehicle Velocity
C_d = Non-dimensional Drag Co-efficient
A_F = Project Frontal Area of the Vehicle

tend to increase aerodynamic drag. Furthermore vehicles are not specifically designed around aerodynamic considerations; function, safety, economy, aesthetics, etc, are generally the objectives of the design. These requirements will be strongly influenced by aerodynamics, but the final result may be a compromise to suit all needs and desires.

2.2.1 Development of Road Vehicle Aerodynamics

The early stages of road vehicle aerodynamics involved developing ideas and shapes from the aeronautical industry and applying them to ground vehicles. Ground vehicles are essentially bluff bodies and many of the aerodynamic requirements for aircraft are significantly different, as they tend to have aerodynamic characteristics more similar to buildings rather than aircraft, (Cooper 1992). Although some benefits were transferred, the area of aerodynamics dealing with ground vehicles had to be developed independently, mainly through experimentation. This experimentation can be performed using 1:1 scale, reduced scale or by utilising the fundamental thermal and fluid mechanics equations and locally solving them using a Finite Element (FE) or Finite Difference (FD) approach. In recent years the development of Computational Fluid Dynamics (CFD) has complemented and in some cases taken over from some of the experimental aerodynamic testing. However it is useful to note that in spite of the advances in CFD, large scale wind tunnel facilities are still being constructed, including the $120 million Sverdrup Wind Tunnel in Michigan, the Hyundai Wind Tunnel in Korea, and the $37.5 million DaimlerChrysler Wind Tunnel in Michigan. CFD is however playing an increasing role. The wind tunnel is still the most reliable tool available for aerodynamic testing, (Cooper 1992), and for the foreseeable future aerodynamics will still utilise experimentation. Some of the major tools of aerodynamics are outlined in the following passages.

2.2.1.1. Wind Tunnels

The wind tunnel is the primary tool of aerodynamics; it provides a controlled environment that enables simulation of airflow experienced by a moving vehicle. There are two main types of wind tunnel used in road vehicle aerodynamics, the Gottingen type and the Eiffel type. In the former the air circulates in a closed circuit and in the latter the air re-circulates within the confines of a building. These two types of tunnel can have closed, open or partially open jets. With open jets the flow can expand around the test vehicle, while closed sections do not permit this; partially open jets allow limited expansion. Wind tunnels are usually designed with a specific function, some are built to study effects of

engine load, ambient temperature, solar radiation etc, and are know as climatic chambers. Generally climatic chambers have poor aerodynamic simulation characteristics, as this is not their primary function. Aeroacoustic tunnels are used to measure wind noise and are generally open jet as the plenum can be lined with noise suppression covering. Increasingly tunnels are built for a combination of functions, and may contain moving ground floors and/or boundary layer suppression, with chassis and/or brake dynamometers to simulate on road conditions.

Issues Associated with Wind-Tunnel Testing

A wind tunnel is not capable of exactly reproducing all on-road conditions, it can only simulate some of them. As a result there are many potential errors and issues which need to be considered before undertaking wind-tunnel simulations. One such concern with closed jet wind tunnels is the close proximity of the test section walls to the test vehicle; generally it is desirable to have negligible influence on the test object from test section boundaries, requiring working sections to be relatively large. When driving on road, only the ground provides a solid boundary, therefore an open jet tunnel is generally favoured for road vehicle aerodynamics. Another important factor that must be considered in wind-tunnel testing of vehicles (particularly in closed test sections), is blockage ratio. Blockage ratio is the ratio of the projected frontal area of the test object, to the cross-sectional area of the wind-tunnel test section, it is often expressed as a percentage:

$$B = \frac{A_C}{A_T} \times 100\% \qquad \textbf{- Equation 2.2.1}$$

Where: B = the blockage ratio

A_C = the projected frontal area of the test object

A_T = the cross sectional area of the tunnel.

The effect of blockage is an increase in the velocity of the local flow stream around the test object, due to a reduction in area for the flow. Typical blockage ratios for full-scale automotive wind tunnels are between 5 and 10%, although blockage ratios of up to 20% have been used, (Hucho 1998).

Most vehicle wind tunnels represent the road as a stationary floor, and not a moving ground as on-road driving. The result of this is an altered flow field around the vehicle from both the development of a boundary layer on the wind-tunnel floor, and the absence of rotating wheels. The most obvious way of solving this issue is to include a moving ground floor in the wind tunnel, however the relative effort in developing this, coupled

with the financial implication, have meant simpler techniques have been developed, (Hucho 1998). These methods include:

- boundary layer suction, (boundary layer thickness is reduces by removing air from the tunnel floor);
- second floor method, (the vehicle is placed on a second floor above the level of the boundary layer);
- blowing air (blowing air into the boundary layer to accelerate the flow, compensating for the reduction in flow caused by the boundary layer).

2.2.1.2. Flow Measuring Devices

Various flow-measuring devices are used in aerodynamics, for steady state measurements pitot static tubes and vane anemometers are commonly used. For unsteady or fluctuating air flows the device must be capable of measuring the instantaneous flow at a point or in a plane, both in magnitude and direction. Instruments which are capable of measuring these turbulent velocity fluctuations include hot-wire anemometers, and dynamic Cobra probes, (both of which may disturb the flow). Laser Doppler anemometers and particle image velocimetry, are also capable of turbulent flow measurements, and have the added advantage of not disturbing the flow, however both are expensive and difficult to use in the real world environment.

2.2.1.3. Flow Visualisation

Flow visualisation can provide qualitative (and in some cases quantitative) data about the flow field around a test body; it is often a useful first stage in aerodynamic testing. Visualisation of the flow can be useful in determining areas of flow separation, re-attachment, and circulation, it can be used to determine the optimum locations for mounting flow or pressure measuring devices. Visualisation can be achieved with:

- Wool tufts - short lengths of yarn taped at one end to the surface of the test object.
- Smoke generation – smoke is injected into the area of interest and the path of the flow stream can be traced.
- Pressure Sensitive Paint (PSP) - PSP fluoresces under short wave light, as the pressure increases with the wind-on, collisions between the oxygen and the paint reduce the fluorescence of the paint. The detectable change in fluorescence from wind-on to wind-off condition can be used to calculate surface pressure; both qualitative and

quantitative data may be obtained. However this technique is limited to relatively high dynamic pressures.

- China clay – a mixture of fine clay and kerosene is applied to the test surface, and the surface shear stress from the airflow drags the mixture into the path of the flow stream.
- Flow visualisation in water - the test object is placed in a stream of moving water, neutrally buoyant dyes are injected which colour the flow path. The flow conditions within the water stream should be similar to those in the actual flow field. To achieve this all relevant dimensionless parameters must have the same corresponding values, they are then said to possess geometric, kinematic, dynamic, and thermal similarity. Still photographs or video can then be used to study the flow stream.

2.2.1.4. Computational Fluid Dynamics

The high financial implications and the long development time associated with wind-tunnel development of vehicles shapes has led the automotive industry to look for cheaper viable alternatives. Computational fluid dynamics relies on the use of computers to locally solve the equations that describe the motion of fluids, and can be used to simulate the airflow around vehicles. The mathematical equations that govern the motion of a fluid are based on the principles of conservation of mass, momentum and energy. The majority of CFD software is based on the Navier-Stokes equations; these are a set of second-order non-linear partial differential equations, which (apart from certain specific situations) cannot be solved analytically. Therefore CFD techniques use approximations of the Navier-Stokes equations, which can be solved numerically, (Blazek 2001). These approximations use such techniques as Euler-method, Reynolds Averaged Navier-Stokes (RANS), Large Eddy Simulation (LES), and Direct Numerical Simulation (DNS). Numerical methods such as finite element, finite volume and finite difference are then used to solve these equations. As numerical solutions can only provide results at specific points, the model must first be divided into a number of discrete points or a grid, the approximation equations are then solved at each grid point. The final result is a series of numbers, which are usually displayed as a graphic for ease of understanding. The density of the grid size will have a direct bearing on the accuracy of the results as well as the computational time required to complete the simulation. CFD simulations are useful for predicating flow field trends in the early stages of vehicle development, as shape modification is possible without the need to build the physical model. CFD solutions seldom replace wind-tunnel testing as accurate quantitative data is usually not possible, it

can however ensure time in the wind-tunnel is used more efficiently, (Hucho 1998). It should be noted that CFD is still a developing technology, and is undergoing rapid development.

2.2.1.5. Reduced Scale Testing

Due the scales involved it is not always practical or cost effective to perform aerodynamic testing on full-size objects. Model-scale testing offers advantages in cost and time, and is usually part of the early stage of new vehicle development. However in order for results from model tests to be valid for the full-size equivalent, certain conditions must be met. In general there must be kinematic similarity between model test and the full-size on-road equivalent. This means that the Reynolds number for the model should equal the full size Reynolds number. The dimensionless Reynolds number represents the relative effects of viscosity and inertia on the flow, and if these effects are the same for the model as the full-size object there is kinematic similarity. In order to achieve this, the wind-tunnel velocity may need to be increased by the same scale as the test vehicle dimensions are to the model. This can introduce compressibility effects, (Cooper 1992) or may be beyond the capabilities of the wind tunnel. Road vehicles are however bluff bodies and are not particularly sensitive to Reynolds number, so aerodynamic testing for models can provide reasonably valid results at lower than full-scale Reynolds numbers, as long as the Reynolds number effects are understood, (Watkins 2001).

2.3 Aerodynamics and Brake Cooling

As previously stated, the primary means of heat dissipation from a brake rotor is by convection. Increasing either the surface area of the rotor *(A_s)* or the heat transfer coefficient *(h)* will improve convection. In order to maximise cooling by convection, a sufficient supply of cooling air must interact with the heated elements. Clearly cooling can be improved by guiding air towards the appropriate parts, many examples of this can be seen in motor racing, however this may have a negative effect on the vehicles drag, (Jerhamre and Bergstrom 2001). Consequently a compromise must be achieved between effective cooling and minimum drag. The situation is further complicated by the nature of the airflow in the vicinity of the brake rotor. Generally this airflow is extremely unsteady and turbulent, (Fabijanic 1996), and is influenced by the local geometry and vehicle

velocity. However it is very difficult to relate cooling to the geometry of components or vehicle speed, (Jerhamre and Bergstrom 2001). The airflow is further affected by the pumping action of internally vented rotors, and pitching of the moving vehicle creating its own pumping effect. The nature of the flow in and around the brake rotor also means that a single Reynolds number cannot fully describe the flow in this region, (Sheridan et al. 1988; Jerhamre and Bergstrom 2001). The flow may be laminar on the face of the rotor and turbulent within and exiting the vanes.

The selection of wheel will also have an influence on the aerodynamics in the vicinity of the brake components, a more open wheel (large open area) will allow more cooling flow to reach the rotor. Significant improvements in cooling were found by (Sheridan et al. 1988) when comparing the effect of two different wheels on brake cooling. The comparison was made between a steel wheel with an open area of 80 cm^2, and an aluminium wheel with double the open area, the improved cooling was attributed in part to the larger vent area. Garrett and Munson (1983) estimated that for a medium size family car a minimum open area should be 70 cm^2, but found improvements could be achieved with openings of up to 150 cm^2.

To date little work has been done on this particular area of aerodynamics, and research has generally been limited to the effects of lift and drag caused by wheels both fixed and rotating including Fabijanic (1996) and Axon, et al. (1999). The relationship between the flow within the wheel-well with lift and drag has also been studied experimentally and computationally using CFD, (Fabijanic 1996; Axon, et al. 1999). Fabijanic (1996) showed the flow within the wheel arch to be very unsteady, and alternated from entering the wheel arch to exiting at the same position with no obvious periodicity. This flow is further complicated by the movement of the suspension creating an air pumping effect within the wheel arch. Most aerodynamic research in the area of brake cooling has focused on the airflow through internally ventilated rotors in isolation, and has not considered the effect on the flow under normal driving conditions.

2.3.1 Aerodynamics of Vented Brake Discs

The need for increased cooling of disc brakes led to the development of vented rotor discs, however the advantages of vented discs over solid discs is the subject of some conjecture. The primary advantage of vented rotors is increased heat dissipation from internal

pumping of air, however under slow speeds the pumping action of the vanes is minimal and only becomes pronounced as rotor speed increases, (Day and Newcomb 1984). At higher speeds the airflow flowing around the disc as a result of the forward movement of the vehicle, tends to prevent effective pumping of air through the vanes, (Limpert 1975). Early work by Limpert (1975) indicated that the heat dissipation from internal ventilation amounted to about one third of the total heat dissipation from the rotor, but suggested it was the larger surface area and not the pumping action that made the major contribution to cooling. While vented rotors do provide a larger surface area for heat dissipation, and extra airflow from the pumping effects of the vanes, it must be remembered that they will usually have a reduced mass than their equivalent solid rotor and therefore have less capacity to store thermal energy. Much of this work has involved attempts to increase the flow through internally ventilated rotors. One approach has been the use of curved vanes instead of straight vanes ones. Curved vanes can create additional cooling in two ways; firstly an increase in surface area of up to 30% can be achieved, (Limpert 1975), and secondly optimisation of the vanes can improve the pumping efficiency. Daudi (1999) used commercially available CFD software to compare the flow generated by straight and curve vane rotors, and found significant reductions in rotor temperatures using curved vane rotors when operating in still air. However curved vane rotors add to manufacturing complexity and introduce the need for different rotors for each side of the car, (Hudson and Ruhl 1997; Zhang 1997), potentially resulting in four different rotors for a given vehicle.

Many attempts have been made to improve the cooling ability of straight vane ventilated rotors. Zhang (1997) proposed a redesign of vented rotors to include an optimised number of flow passages, improved rounding on inlet vanes, and a long-short alternative vane configuration. This design contains twice the number of outlet vanes as inlet vanes, in order to reduced inlet blockages and guide to flow though the exit more easily. The configuration was modelled on CFD software and a 42% increase in flow through the vanes is claimed, however no experimental verification is given. A similar technique was used by Daudi (1999) to develop a rotor with three times the number of outlet vanes as inlet vanes, providing 35% more flow through the vanes when tested on a model in still air. A long-short vane rotor configuration was also devised by Kubota et al. (2000), this was tested using a one-tenth scale disc brake assembly model submersed in a water tank to find a relationship between rotor shape and cooling performance. Hudson and Ruhl

(1997) looked at ways of increasing the centrifugal pumping of existing vented rotors by using traditional turbo-machinery techniques to improve flow condition at the inlet to the vanes. Airflow from the modified rotor were measured at the outlet of the vanes (without wheel and tyre blockage or an external airflow) using an adapted three hole pitot static tube at the outlet of the vanes. The results of these modifications are presented in Table 2.3.1. The modifications were designed to reduce flow separations and decrease losses while keeping the symmetry of existing vented rotors. Experimental on-vehicle testing of the modified rotor resulted in temperatures of between 3-6% lower than the production rotor at the end of a ten stop fade test. Daudi (1998) also concluded from CFD modelling that increased airflow through a vented rotor could be achieved by allowing air to enter the vents from both the inboard and outboard side of the rotor. Another development has been the cross-drilled or axial cooled rotor; this increases the surface area presented to the atmosphere and can potentially improve cooling, however the rotor mass and friction area are reduced. Analytical work by Limpert (1975) showed that the addition of axial cooling passages reduced cooling effectiveness; this is mainly attributed to the increased heat flux.

Visualisation of the flow through ventilated rotors by Kubota, et al. (2000) using scale models submerged in water, indicated significant regions of separated flow within the vanes of the rotor, which would indicate that increased flow could be achieved with optimised designs. Measurement of the airflow through the vanes of a vented rotor is extremely difficult while on the vehicle, so it is usually done in isolation, [see Hudson and Ruhl (1997) and Jerhamre and Bergstrom (2001)]. Sisson (1978) developed the following empirical equation from measurements of the flow through a series of vented rotors in isolation at varying speeds in still air:

$$V_{ave} = \omega D_O \sqrt{-0.0201 + (0.2769 \times D_I) - (0.0188 \times D_I^2)} \qquad \textbf{\textit{Equation 2.3.1}}$$

Where

V_{ave} *= average velocity of airflow through vanes (m/sec)*

ω *= angular velocity (rads* s^{-1}*)*

D_O *= outer diameter of rotor (m)*

D_I *= inner diameter of rotor (m)*

This relationship was valid for the range of rotors tested from outside diameters of 9 inches to 16 inches and inside diameters of 4 inches to 7 inches (101 – 178 mm).

Similar work by Limpert (1975) also produced an expression for the average velocity through a rotor:

$$V_{ave} = \frac{V_{in}}{2}\left(1 + \frac{A_{in}}{A_{out}}\right), \qquad V_{in} = 0.052N(D_O^2 - D_I^2)^{1/2} \qquad \textbf{Equation 2.3.2}$$

Where

N = revs per minute of rotor

V_{in} *= air velocity at inlet (m/sec)*

A_{in} *= vent area inlet* (m^2)

A_{out} *= vent area outlet* (m^2)

It should be noted that neither equation caters for the number of vanes in the rotor, as both authors found that the number of vanes did not affect the amount of air pumped, provided that the flow areas were the same. However Zhang (1998) concluded that a square cross section provides the lowest wetted perimeter and therefore lowest viscous friction losses, as it has the shortest perimeter than any other rectangular shape. Thus the optimum number of vanes could be calculated using the formula:

$$Z = \frac{\pi D}{w + t} \qquad \textbf{Equation 2.3.3}$$

Where: Z = number of vanes,

D = the mid diameter of the rotor,

w = the flow passage width,

t = the thickness of the vanes.

Hudson and Ruhl (1997) used turbomachinery techniques to improve the airflow through a typical ventilated rotor, and compared experimental findings with values expected from both Limpert and Sisson's equation. Hudson and Ruhl (1997) suggest three improvements to the existing brake rotor including a rounded inlet chamfer, a rounded inlet horn and a pre-impeller, all of which reduces the number of sharp edges the flow interacts with. The results of these experiments are compared to results obtained analytically from both Sisson's and Limpert's equations in Table 2.3.1. Sisson's relationship yields values of average velocity higher than Limpert's, although both appear to give reasonable correlation with the average velocity recorded by Hudson and Ruhl (1997).

Average Vent Flow Velocity (m/s) – Calculated vs. Measured						
	Calculated		**Measured - Improved Rotor**			
RPM	**Limpert**	**Sisson**	**Prod.**	**Cham.**	**Horn**	**PreImp.**
600	0.80	1.20	0.957	1.058	1.264	1.526
800	1.07	1.60	1.159	1.281	1.688	1.967

Table 2.3.1 Average vent velocity as measured at 1 cm beyond vane outlet, Hudson and Ruhl (1997).

It must be remembered that the above results were obtained from experimental work conducted on rotors operating in still air, which is considerably different to that experienced by a rotor under normal operating conditions. Also the effects of vehicle velocity or inlet restrictions such as splash shields, callipers and suspension geometry etc were not considered. To measure the airflow in this region in the correct operational environment on-road or full-scale wind-tunnel tests are required. However, no published material is evident, due to the level of difficult involved in completing these tests. Increasingly Computational Fluid Dynamics is being used in an effort to reduce the need for and to complement wind-tunnel testing. Jerhamre and Bergstrom (2001) found good correlation between the experimental results and the results obtained from a CFD simulation for a rotor operating in still air. Others including, Sheridan et al. (1988), Zhang (1997) and Daudi (1999) have used thermal modelling and CFD techniques to improve the cooling of brakes, but these have not included experimental validation.

2.3.1.1. Centrifugal Fan Theory Applied to Vented Brake Rotors

Internally vented rotors are designed to generate airflow in a similar way to a centrifugal fan or blower; airflow is created through a combination of airflow deflection and centrifugal force, (Bleier 1997). Turbomachinery theory and the theory of centrifugal fan design have been used by Hudson and Ruhl (1997) in an attempt to improve the airflow though these rotors. The vane or blade configuration is essential in centrifugal fans, however for simplicity and ease of manufacture brake rotors usually contain simple straight vanes with radial configuration. The main types of blade configuration used in centrifugal fans, and their potential for use in brake rotors is examined in the following section. Diagrams of these configurations can be seen in Figure 2.3.1. It should be noted

that centrifugal fans are generally fabricated, whereas brake rotors are cast. Therefore the relative advantages of the various types of centrifugal fan may not be easily transferred to brake rotor applications.

Centrifugal Fans with Aerofoil Blades.

This type of fan has the best mechanical efficiency, therefore for a given power input it will displace the largest volume of air, however efficiency is a very minor consideration in brake rotors. The benefit of maximum airflow for cooling far outweighs any possible gains in efficiency, (Hudson and Ruhl 1997). This type of vane configuration is widely used in clean air and ventilation systems.

Centrifugal Fans with Backward-Curved Blades

These vanes are curved in the opposite direction of rotation and are of uniform thickness; they have slightly lower efficiency than aerofoil blades but can handle contaminated air streams. They are commonly used in air extraction systems, and in boilers for both induced and forced draft systems.

Centrifugal Fans with Backward-Inclined Blades

This vane configuration is one of the most economical to construct; its performance is similar to backward curved fans although slightly lower in mechanical efficiency and in structural strength.

Centrifugal Fans with Radial-Tip Blades

These vanes are curved at the leading edge but the blade tips are radial, generally used in large sizes, (diameters 750 mm to 1500 mm). The shape of the radial tip fan blades allows self-cleaning, and is often employed in areas with high temperature and high concentration of solids.

Centrifugal Fans with Forward-Curved Blades

Vanes are curved in direction of rotation, with a large blade angle; these fans will generate flow rates much greater than any other type of centrifugal fan. They are often used when compactness is more important than efficiency, which would appear to make them the most suited to a brake rotor configuration.

Centrifugal Fans with Straight Radial Blades

This configuration is most often employed in brake rotors; straight vanes allow the same rotor to be used on both sides of the vehicle as well as being simple to cast. Radial blade

fans are rugged and self-cleaning, but have low efficiency due to the non-tangential flow conditions at the leading edge.

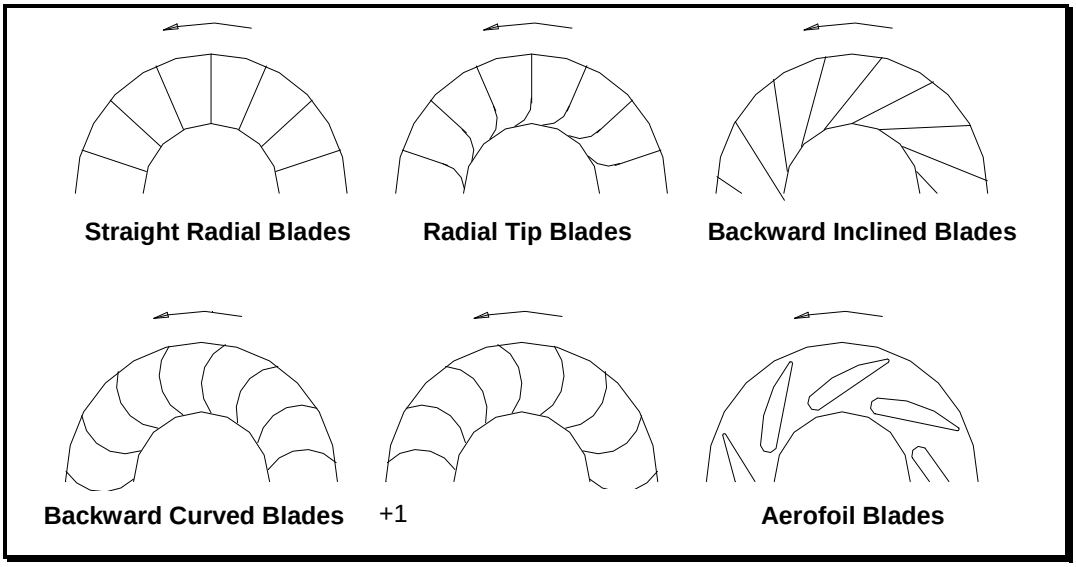

Figure 2.3.1 Various Blade Configurations of Centrifugal Fans Adapted from Bleier (1997)

Apart from vane configuration there are other techniques used in centrifugal fan design that are applicable in ventilated rotors. Centrifugal fans are usually designed from empirical data and experience of the designer rather than by design calculation, (Bleier 1997). The number of vanes and hence the number of flow passages is crucial in centrifugal fans. The flow passage must be narrow enough for good guidance of the flow stream but wide enough to ensure resistance to flow is a minimum. For centrifugal fans there are well documented recommended numbers of vanes for the various configurations ranging from 9-12 for backward inclined and backward curved fans, to 24-64 for forward curved fans, (Bleier 1997). Experimental work by Sisson (1978) showed the number blades (when varying from 20 to 40) to have little effect on the flow through brake rotors. Daudi (1999) used CFD techniques to study the flow in varying number of flow passages in a brake rotor, and found the optimum number to be 72, using a long-short vane configuration. The use of these partial blades at the outer portion can reduce the flow area where it is largest and channel the airflow, but these outer blades are not considered beneficial in centrifugal fans as it doubles the number of flow restrictions which is the main source of turbulence. In brake rotors the losses due to this turbulence may be insignificant compared to the gains in cooling provided by the additional thermal mass and surface area.

2.3.2 Predicting Brake Disc Temperature

The temperature a brake disc will attain during braking is directly proportional to the initial kinetic and potential energy of the vehicle. All the energy of acceleration must be dissipated in braking, either through the engine, aerodynamic or frictions braking systems. For a vehicle braking on a flat surface the energy created in braking will be, (Limpert 1999), (neglecting engine or aerodynamic braking):

$$E_b = \frac{1}{2} m(v_1^2 - v_2^2) + \frac{1}{2} I(\omega_1^2 - \omega_2^2) \qquad \textbf{\textit{Equation 2.3.4}}$$

Where:

$m = mass\ of\ vehicle$

$v_1, v_2 = velocity\ at\ start\ and\ end\ of\ braking$

$I = inertia\ of\ moving\ parts\ of\ engine\ and\ transmission$

$\omega_1, \omega_2 = angular\ velocity\ at\ start\ and\ end\ of\ braking$

if $v_2 = 0$ then

$$E_b = \frac{1}{2} m v_1^2 + \frac{1}{2} I \omega_1^2 \qquad \textbf{\textit{Equation 2.3.5}}$$

and $v = r\omega$, then

$$E_b = \frac{1}{2} m(1 + \frac{I}{r^2 m}) v_1^2 = \frac{k m v_1^2}{2}, \qquad \textbf{\textit{Equation 2.3.6}}$$

$k = 1 + \frac{1}{r^2 m}$ (a correction factor for rotating masses in drive train and engine)

Where

$r = tyre\ radius$

train

The value of k is dependent on the gear, but values for a typical passenger range from about 1.05 in high gear to 1.5 in low gear, (Limpert 1999). For a vehicle travelling on a slope the energy required in braking is given by:

$$E_b = Wh + \frac{km}{2}(v_1^2 - v_2^2) \qquad \textbf{\textit{Equation 2.3.7}}$$

Where

$W = vehicle\,weight\ mg\ (N)$

$h = vertical\,drop\ (m)$

As well as this, braking will also be assisted slightly by the rolling resistance of the wheels and from aerodynamic drag; it is only possible to obtain an estimation of the energy generated in braking from the above equations under certain assumptions. If we assume the brake components absorb all the heat energy, as in the case of a single stop, (Limpert 1975), it is possible to obtain an estimation of the energy absorbed by the rotor. However according to Garrett and Munson (1983) it is not possible to analytically predict the rate of heat dissipation from the rotor with any degree of accuracy, and any estimation of heat dissipation must be through empirical means. Without knowledge of the heat dissipation rate, it is extremely difficult to accurately predict the temperatures reached in braking. The estimation may be further complicated if multiple brake applications, aerodynamic drag and engine braking consideration are incorporated. The chart shown in Figure 2.3.2 shows the relationship between vehicle velocity and the aerodynamic drag force for a typical large modern family sedan, with a projected frontal area of 2.0 m^2 and a C_D value of 0.31.

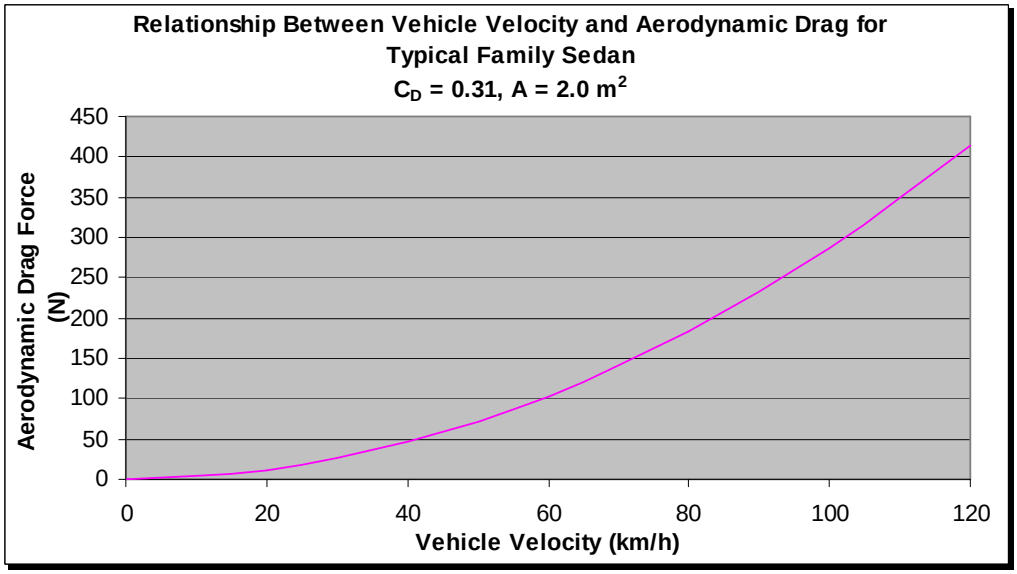

Figure 2.3.2 Aerodynamic Drag Force Vs Velocity for Typical Family Sedan

However for a repeated brake applications such as a down hill descent, a simple expression cannot be used to determine temperature as heat will be dissipated from the brake components, and actual temperature prediction becomes more complex, (Sheridan et al. 1988). A simplified energy balance of the process is shown in Figure 2.3.3.

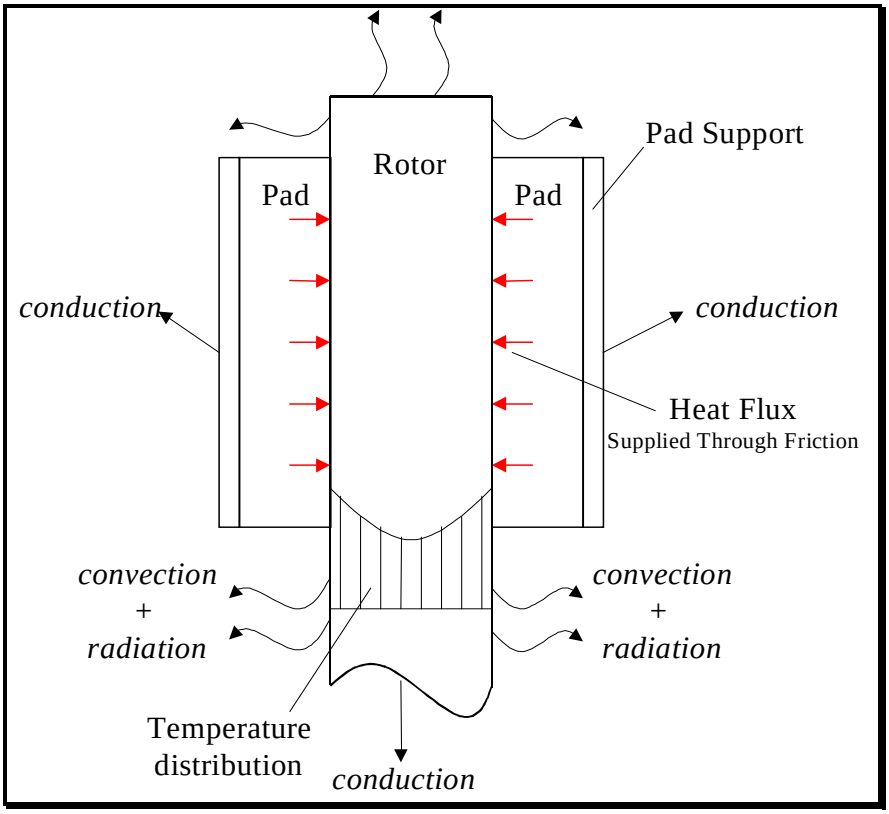

Figure 2.3.3 Heat Dissipation from Disc Rotor, adapted from Limpert, (1999)

As can be seen from the above diagram the temperature distribution is quite complex, the heat flux will vary with time, a linearly decreasing heat flux is often assumed, (Sisson 1978). The heat transfer coefficient *(h)* will rarely be constant, although an average value is usually assumed. Noyes and Vickers (1969) developed a thermal model based on the numerical finite difference method, and made the following conclusions on energy flows at the end of 10 stops from 60 mph:

- 60% of the energy is dissipated by convection,
- 34% remains as stored thermal energy,
- remainder is lost by radiation and conduction to the lining.

This appears to agree with Sheridan et al. (1988) who found that about 90% of heat dissipation is by convection to the atmosphere in almost all braking conditions. Limpert (1975) presented equations for predicting the bulk temperature of disc brakes; the expression however assumes a lumped temperature distribution.

In order to accurately determine brake temperatures at a particular time *(t)* in the braking phase, knowledge of the heat transfer coefficient is required. The heat transfer coefficient *(h)* will depend on the airflow in the region of the brake rotor, and the vehicle speed. It will therefore vary constantly throughout the braking process. It is generally considered extremely difficult to obtain accurate values of the heat transfer coefficient, with errors of between 10 and 30% considered acceptable, (Limpert 1975). Limpert (1975) also presented empirical equations for heat transfer coefficients for both solid and vented rotors. These equations were obtained experimentally and are based on Reynolds number, with different forms for laminar and turbulent flow.

There have also been many attempts to model both the transient and steady state temperatures of brake rotors with varying degrees of success. Many examples are found in the literature including Noyes and Vickers (1969), Sisson (1978), Day and Newcomb (1984) and Sheridan et al. (1988), and the accuracy of these models is usually determined by the heat transfer coefficient. The level of complexity of the models generally reflected the technology available at the time, with the complexity increasing with advancing computer technology. In recent years advances in computer technology has enabled CFD solutions of the fundamental thermo-fluid equations. This approach has allowed models to move away from bulk temperature analysis to determine both the temperature profiles and the air velocity contours on the surface of the brake rotor. Research conducted by Jones et al. (1995) found excellent correlation between experimental and CFD results. Krusemann and Schmidt (1995) also found CFD to be a useful tool for understanding the air in, around and through the brake disc. More recent work by Jerhamre and Bergstrom (2001) found that by comparing CFD studies with experimental findings, “acceptable accuracy” could be obtained from standard CFD software. In many cases the accuracy of CFD is dependent on cell size, which is in turn limited by computer power.

2.4 Experimental Techniques

The most straightforward brake testing conducted on a vehicle is usually on a test track. The instruments are placed on the vehicle and the brake performance is assessed over a series of predefined test. However these tests may only occur at the final stages of design, and it may be difficult to obtain quantitative data, as the variables are not easy to control. Other tests may be carried out on a brake dynamometer; essentially this simulates on-road braking in a controlled environment. Tests are carried out with the vehicle stationary, but

with the wheels rotating, allowing repeatable data to be collected, although some real world parameters are absent such as airflow around the vehicle, atmospheric winds, lateral forces induced by cornering etc. As dynamometer tests are only possible on a vehicle late in its development period, manufacturers are turning more and more to computer simulations for all aspects of vehicle design. However the high standards of performance and safety required in braking make the physical testing of components essential, (Kruger et al. 1995).

2.4.1 Disc Brake Temperature Measurement

Exact temperature determination of a brake rotor presents a number of problems. Firstly there is obvious difficulty in obtaining the accurate temperature from a spinning disc, and secondly it is unlikely that a uniform temperature exists over the entire rotor, (Idogaki et al. 1987). Any temperature measuring system must consider both radial and circumferential temperature gradients. The system must also provide a quick enough response to accommodate rapid temperature changes as well as having enough range to cover all temperatures from ambient to in excess of 700 °C, (Eisengraber et al. 1999). Thermocouples provide a rapid response and can be obtained to suit the particular temperature range. However the difficulties in obtaining an accurate temperature from the rotating disc must be addressed. Methods frequently used are embedding thermocouples in the pad, embedding thermocouples in the rotor, or rubbing thermocouples mounted on the side of the rotor, (Limpert 1975). All of these solutions present their own problems. Thermocouples imbedded in the rotor require a slip-ring arrangement to transmit the output to a logging device, (Limpert 1975), and because the measurement is taken at a fixed point, this temperature may not be representative of the overall disc temperature, (Eisengraber et al. 1999). Pad embedded thermocouples only measure temperatures at a fixed radius and assume no circumferential temperature gradient; also the temperature in the pad may lag or differ from the rotor. Rubbing thermocouples also measure at a fixed radius but can be adjusted easily, however the accuracy of these is further complicated by factors such as self heat generation by friction on the disc and heat transfer from the disc to the thermocouple, (Limpert 1975). It must also be noted that depending on the response time of the thermocouple and the rotational speed of the rotor, the temperature response of pad imbedded and rubbing thermocouples can be averaged over several rotations of the disc, (Eisengraber et al. 1999). Limpert (1975) concluded that rubbing thermocouples generally yielded temperatures of up to 17 °C higher than the actual temperature due to the

heat generated by the sliding thermocouple. However Eisengraber et al. (1999) believed rubbing thermocouples consistently unvalued the temperature by up to 70 °C, and concluded that instantaneous temperature could only be reliably obtained by permanently fixed thermocouples.

Clearly the above methods of temperature measurement can be employed when considering the rotor temperature as uniform. To measure the temperature distributions on a brake rotor, non contact temperature measuring devices are used. Infrared thermometers and cameras (known as pyrometry) have been used successfully in measuring the disc brake temperatures, (Woodward et al. 1993; Dinwiddie and Lee 1998; Little et al. 1998; Eisengraber et al. 1999). However measuring the temperature of a rotating brake disc via infra red radiation also presents some problems. Firstly the braking operation creates dust, which can obscure the sensor, and secondly the emissivity of the material may change with temperature. Systems developed by Idogaki et al. (1987) and Woodward et al. (1993) have successfully overcome these problems. One major advantage of optical pyrometry is the ability to measure temperature gradients and hotspots in the brake rotor, this can be achieved by sequencing the scanning frequency of the pyrometer to match the rotational velocity of the rotor, (Little et al. 1998; Idogaki et al. 1987). In recent years the development of high-speed infrared cameras has enabled easier measurement of rotor temperatures. Dinwiddie and Lee (1998) used such a system to measure the development of hotspots on the surface of a rotor when studying the thermal judder phenomenon.

2.5 Conclusions from Background Research

The considerable numbers of problems caused by excessive brake temperatures makes it an important topic of research, both from an economic and safety point of view. Although there has been limited research into the aerodynamic aspect of brake cooling, it appears that there is further scope for improved cooling in this area. It is first necessary to understand the main parameters that effect the cooling of disc brakes, and establish how best cooling could be achieved. The current research illustrates that there are no clearly accepted methods of how to achieve optimal brake cooling. It was generally agreed that vented discs achieve superior cooling than solid discs, however according to Limpert (1975) this may depend on the type of braking operation. There are also differing views

on the design of vented rotors, however from this review it would appear that the best possible design would contain forward curved vanes, with an alternative long/short configuration, as suggested by Daudi (1999). This type of rotor would displace the maximum amount of air for a given speed, and the curved vanes combined with short vanes at the exit would also give the maximum possible surface area to interact with the airflow. The number of vanes and the vane angles may need to be optimised for each particular application.

Most of the research into the topic appears to be either from an aerodynamic approach where airflows are examined, or from a brake cooling approach where disc temperatures are examined. Rarely has the research attempted to relate airflow measurements to the thermal performance of the braking system. In the design of vehicles, aerodynamic work is usually applied late in the design process and is usually of secondary concern to other aerodynamic considerations such as drag and vehicle stability, and therefore optimal aerodynamics for brake cooling may not always be achieved. Secondary aerodynamic effects such as the wheel or the wheel arch geometry have been given little attention in previous work. Although Garrett and Munson (1983) believed that the open area of the wheel should be 70 cm^2 or greater, attempts to reduce vehicle drag have resulted in smaller open areas in many standard vehicles.

The most recent work in the field used the latest in CFD techniques in an attempt to model and improve the airflow in the vicinity of the brake rotor. Much of this work has been involved in the evaluation of the application of CFD to this type of problem. Comprehensive experimental testing seldom follows up the work. In addition the real flow regime is not axis-symmetric around the rotor, and the accuracy of computational work is constrained by the difficulty in modelling the complex vehicle geometry in the vicinity of the brake rotor, (Zhang 1995).

Measuring the flow through vented rotors is the most common method of accessing their ability to displace air. Most of this work has been conducted by measuring the airflow at the outlet of a rotating brake rotor in still air; this is a vastly different environment to the actual working condition of the rotor. Airflow around the rotor (due to the flow imposed by the forward motion of the vehicle), may have a considerable effect on its ability to displace air. It is known that the airflow within this region is extremely unsteady and turbulent, however it is unclear what happens to the flow through vented rotors under

these conditions. CFD studies have shown that warm air exiting from the vanes may actually re-circulate again through the vane inlets, (Jerhamre and Bergstrom 2001), this may well be true for lower vehicle velocities. For higher vehicle velocities it is believed that the pumping effect of a vented rotor is reduced as air attempts to enter the outlet of the vanes, (Limpert 1975). A clearer understanding this flow may present opportunities to improve the overall flow in this region, and hence improve the cooling performance of the braking system.

CHAPTER THREE

3 RESEARCH METHODOLOGY

3.1 Introduction

From the review of the background material it is evident that improvements in automotive brakes could be achieved with a better understanding of the aerodynamics in the region of the brake rotor and surrounding components. Generally aerodynamics are optimised in a passenger vehicle for such things as minimum aerodynamic drag, reduced cabin noise, maximising engine-cooling etc, and aerodynamic cooling of brakes is of secondary concern. In the vehicle development stage it is usually only when a representative vehicle is available that a true understanding of its aerodynamic characteristics can be obtained, (Garrett and Munson 1983). Therefore, with the exception of racing vehicles, little is known about the aerodynamic cooling capabilities of the braking system until very late in the vehicle development, and the efficient use of air to cool brakes tends to be underdeveloped. The amount of research into the aerodynamic aspect of brake cooling has been limited, even though most of the heat generated in braking is dissipated to the air as it flows around the rotor and thermally linked components. The gap of aerodynamic research in brake cooling has been narrowed in recent years by some CFD modelling of brake rotors in isolation and in some cases within the vehicle body; however without realistic experimental validation of these studies it is difficult to access their accuracy.

In this chapter a research methodology is outlined, in order to develop an understanding of the main parameters which affect disc brake cooling, and to understand the airflow through vented rotors both in still air and on-road conditions. A description of the experimental equipment is also given.

3.2 Research Methodology

Depending on the type of disc employed (solid or vented), there can be two separate but interacting flow fields contributing to the cooling of automotive disc brakes. One is the airflow through a vented rotor as a result of the rotation of the wheel (vent airflow), and the second is the airflow induced around the rotor as a result of the forward movement of the vehicle (external airflow). Both are complicated by the influence of the wheel and body structure as well as the vehicle speed. There are three possible approaches that could be adopted when looking at this particular type of engineering problem: analytical, computational and experimental. An analytical approach is often the first step in any engineering development, and although sometimes many assumptions have to be made it can serve as a good guide, but due to the complexity of solving the governing equations detailed accuracy is not possible. It is widely agreed that an analytical approach is limited to very simple or specific cases due to the complex nature of thermo-fluid problems. Computational approaches are rapidly developing and much work has been done on the evaluation of their accuracy, however with the complication of two separate flow fields, results may be questionable without experimental validation. It is extremely difficult to use CFD for predicting performance where complex geometry shapes are associated with high Reynolds number separated flows. Experimental methods are the most tried and trusted, and as the airflow in the region of interest is extremely complex and turbulent, this approach was considered the most suited for the problem under investigation.

3.2.1 Design of Experiments

The experimental work was divided into two separate phases. The first phase of the experiments was designed to establish quantitative data on the airflow through a standard vented brake rotor, independent of the vehicle, and subsequently in a simulated version of the on-road condition. As discussed, the aerodynamic cooling from automotive disc brakes can be as a result of two separate but interacting flow patterns, internal and external flow. An understanding of the contribution of both these flows to the cooling of the rotors needed to be obtained. Measurement of the flow within the rotor vents was not practical due to the size of the passage, complexity of instrumentation due to rotation, and any flow-measuring devices within the passage would restrict the flow. Therefore the flow was measured at the outlet of the vents. The extremely turbulent and three-dimensional nature of the airflow in this region means that any flow-measuring device must be capable

of measuring multidirectional flows, as well as mean and time varying flows. Traditionally the airflow though vented rotors was measured using pitot static tubes, (Hudson and Ruhl 1997) or hot wire anemometers, (Jerhamre and Bergstrom 2001), however these devices present their own disadvantages when used to measure this flow. Pitot static tubes are not suited to fluctuating or turbulent flows, and hot wires are not particularly robust. Dynamic Cobra probes offer a real, robust method of measuring and analysing flow (see Hooper, (1997); Hooper, (1995); Watkins et al. (2002)), and were used to measure the flow at the outlet of a vented brake rotor.

The second phase of experiments was performed on-vehicle, and was designed to determine the main parameters (including aerodynamic) that affect the thermal behaviour of the rotors in braking. By measuring the rotor temperatures directly during heating and cooling cycles, the major parameters affecting the rates of heating, cooling and heat dissipation could be evaluated. The parameters under examination included the effect of rotor type, wheel type and vehicle velocity. Generally on-vehicle brake testing is done on a brake dynamometer or the vehicle is instrumented and the testing is performed on-road or on a test track. Performing these tests on-road introduces a number of difficulties, including repeatability, safety and complications with instrumentation. Dynamometer testing also has limitations, since it does not usually replicate the aerodynamic cooling provided by the forward movement of the vehicle. Therefore a system of brake testing which combined the advantages of both testing options was developed. A brake test facility was incorporated into the existing RMIT Industrial Wind Tunnel in order to allow stationary brake testing similar to a dynamometer, while allowing equivalent on-road wind velocities to be included in the tests. The simulation does differ slightly from the on-road condition due to the absence of a moving ground floor. However the test wheel is rotating as with a moving ground, and the repeatable nature of the testing allows for comparative testing of such parameters as rotor type, wheel type and vehicle velocity.

3.3 Experimental Equipment and Instrumentation

3.3.1 Equipment

3.3.1.1. RMIT Industrial Wind Tunnel

The tests were conducted in the RMIT Industrial Wind Tunnel in order to simulate the local airflow in the region of the brake rotor. The RMIT Wind Tunnel is a Gottingen type (closed return), with a 2m x 3m x 9m closed working section. A schematic view of the tunnel is given in Figure 3.3.1. Retractable turning vanes allow access of full size vehicles, however due to the relatively small size of the tunnel compared to a road vehicle, blockage must be carefully considered, see Section 5.2. The salient details of the tunnel are given in Table 3.3.1.

RMIT Industrial Wind Tunnel	
Turbulence intensity	1.8%
Test section dimensions	2m × 3m cross-section x 9m long
Contraction ratio	2:1
Maximum velocity	40 m/s

Table 3.3.1 Salient Details of the RMIT Industrial Wind Tunnel

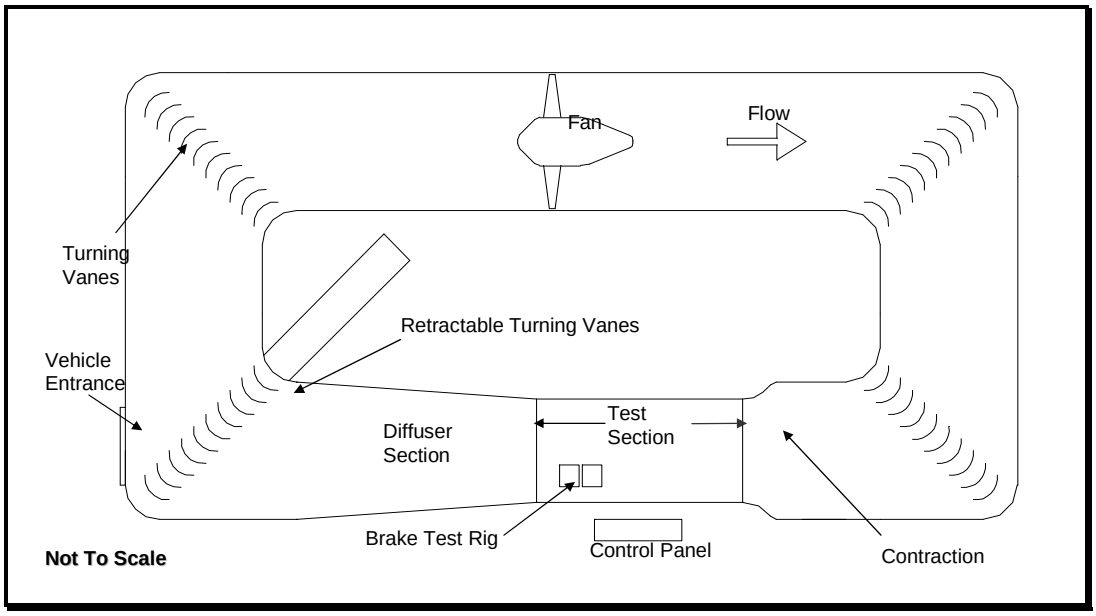

Figure 3.3.1 Schematic View of RMIT Industrial Wind Tunnel

3.3.1.2. Rotor Test Bench

The rotor test bench was developed to enable rotation of a brake rotor independently of the vehicle, both with and without the presence of the wheel. The rig consists of a 3-phase motor mounted on a stand with a direct connection to the brake rotor see Figure 3.3.2. The height of the test bench above the ground was chosen to ensure the rotor was clear of any boundary layer ground effects. The motor is powered through a variable frequency controller, enabling speeds from 0-3000 RPM (0-50 Hz). A digital tachometer directed at the shaft provided confirmation of the rotational velocity.

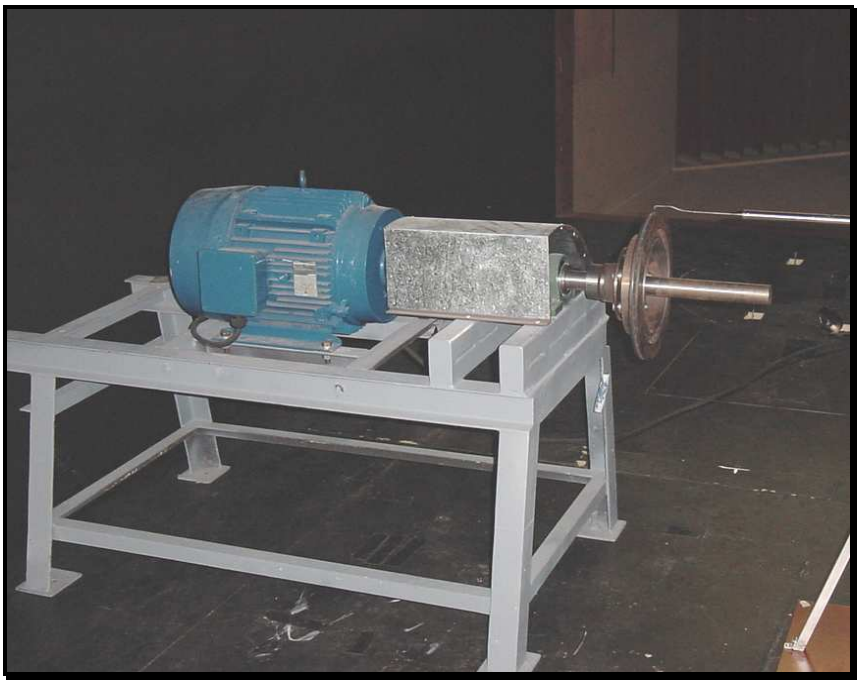

Figure 3.3.2 Brake Rotor Airflow Test Bench

3.3.1.3. Brake Test Rig

The Brake Test Rig, located in the working section of the wind tunnel, was developed by the author in conjunction with technical staff in RMIT University's school of Aerospace, Mechanical and Manufacturing Engineering. The rig was designed specifically to examine aerodynamic cooling of automobile braking systems for both this research, and future commercial applications. The device enabled the wheel of the test vehicle to be rotated independent of the engine, which together with the airflow in the tunnel, allowed simulation of the local flow field around the brake and surrounding components.

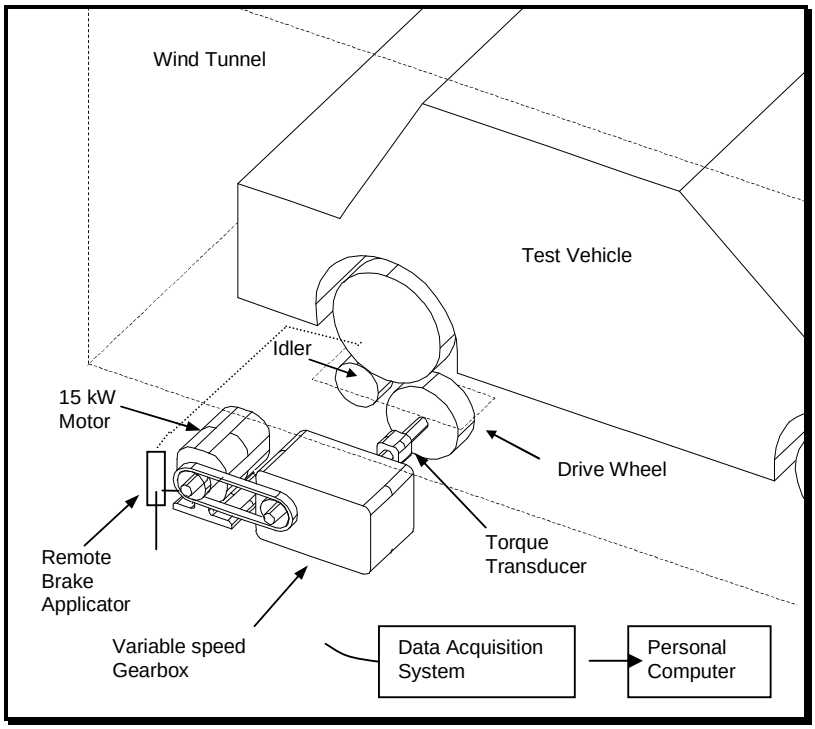

Figure 3.3.3 Schematic of Brake Test Rig

As can be seen in Figure 3.3.3 the wheel of the test vehicle can be positioned on a pair of supporting wheels, a driver and an idler. The drive wheel is driven from a 15 kW three-phase induction motor via a variable speed gearbox and a torque transducer. The motor is controlled by a variable frequency inverter, which as well as enabling a full range of speed control (0 to 3000 RPM), provides a slow start-up and stopping sequence to reduce shock loads. The variable speed gearbox is an enclosed belt drive type, which consists of a vee-belt mounted between two variable diameter pulleys. Speed variation is obtained by simultaneous adjustment of the diameter of both pulleys through an external handle. The test rig also contains a remote brake applicator; this enables external operation of the test vehicle's brake. The applied brake load could be measured indirectly from the torque transducer using the following formula:

$$T_{Brake} = [T_{Measured} - T_{Initial}] \frac{D_{Vehicle}}{D_{Drive\ Wheel}} \qquad \textbf{Equation 3.3.1}$$

Where: T_{Brake} = *applied brake torque*

$T_{Measured}$ = *torque measured by transducer*

$T_{Initial}$ = *measured torque before brake was applied*

$D_{Vehicle}$ = *rolling diameter of wheel on test vehicle*

$D_{Drive\ Wheel}$ = *diameter of drive wheel*

3.3.1.4. Test Vehicle

The vehicle used for the test was a 1999 Ford AU Falcon, which was supplied by Ford Australia. The Falcon is a four-door passenger sedan, and accounted for about 30% of the sales in the Australian large car market in 2000 (Commonwealth Department of Industry 2001). This vehicle shown in Figure 3.3.4 is very similar to many large mass-produced passenger vehicles in Europe, North America and elsewhere.

Figure 3.3.4, Ford Falcon AU Passenger Vehicle

3.3.1.5. Ford Falcon One-Quarter Buck

The one-quarter car buck (partial car) shown in Figure 3.3.5 allows simulation of the local airflow around the front quarter of the vehicle. The buck used was taken from an AU Falcon similar to the test vehicle.

Figure 3.3.5 Ford Falcon One-Quarter Car Buck

3.3.1.6. Brake Rotors

Three different cast iron brake rotors were used in the tests; a 303 mm vented rotor, an equivalent 303 mm solid disc rotor, and a smaller 287 mm solid disc rotor. Full details are given in Table 3.3.2.

Rotor	Mass (kg)	Thickness	No. of Vents
287 mm Solid	5.14	10.5 mm	N/A
303 mm Solid	7.34	15 mm	N/A
303 mm Vented	7.75	18 mm (6+6+6)	37

Table 3.3.2 Brake Rotor Details

3.3.1.7. Wheels

Two standard production wheels were used 15” and 16” steel wheels, as well as a modified 15” and an after market 15” alloy. The details are given in Table 3.3.3.

Wheel	Open Area	Rolling Diameter
15” Steel	40 cm^2	625 mm
15” Steel (modified)	108 cm^2	625 mm
15” Alloy	590 cm^2	625 mm
16” Steel	40 cm^2	650 mm

Table 3.3.3 Wheel Details

3.3.2 Instrumentation

3.3.2.1. Dynamic Cobra Probe

A high frequency four-hole Dynamic Cobra Probe manufactured by Turbulent Flow Industries was used for airflow measurement through the vented rotor. This probe has a multifaceted head that contains four pressure taps, which can measure flow fields within a range of ±45°. Any flow measured outside the acceptance range of the probe is automatically rejected. From the four pressure taps the Cobra probe is capable of providing mean and time-varying values of: velocity (3-components), and local static pressure; thus pitch and yaw angles, as well as turbulence characteristics (all six components of Reynolds stresses) can be calculated. The maximum frequency response is 1,500 Hz, which is obtained utilising dynamic calibration. The probe is connected to a personal computer via an analog to digital (A/D) card, where data can be displayed in real-time or stored for later analysis. Real-time frequency analysis can also be performed. The probe is operated by specially developed commercial software, which controls data acquisition, processing and display of data. A schematic of the probe is given in Figure 3.3.6. Information on the calibration of the probe is given in Appendix A.1, further information on the Cobra Probe can be found in Hooper, (1997); Hooper, (1995); Watkins et al. (2002).

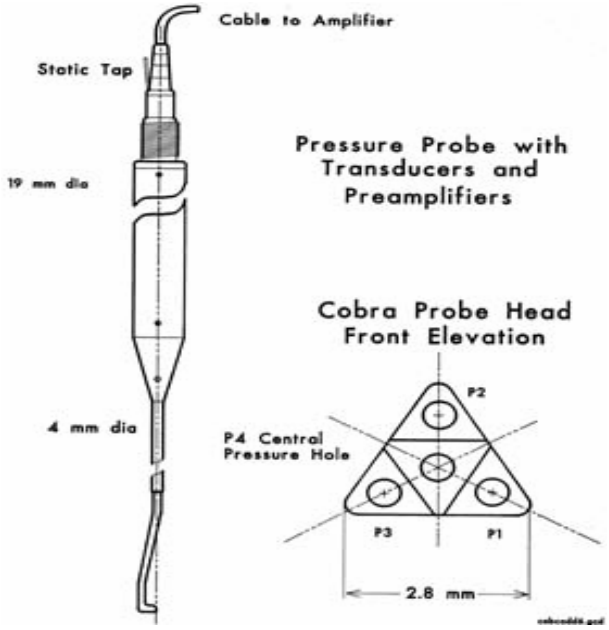

Figure 3.3.6 Dynamic Cobra Probe, (Hooper and Musgrove 1997)

3.3.2.2. Three-Axis Traverse

The Cobra Probe was mounted on a three-axis traverse enabling movement in the vertical and horizontal planes as well as 360° rotation about the probe axis. The traverse was controlled from integrated software on the digital computer and linked to the Cobra Probe software. This enables simultaneous movement of the probe head and flow measurements, (flow mapping).

3.3.2.3. Disc Brake Thermocouples

Various types of disc temperature measurement were examined. Rubbing type disc brake thermocouples were the preferred option, due to their cost, ease of use and availability, and are one of the most common methods of on-vehicle disc brake temperature measurement. The instrument consists of a K-type thermocouple, which is a silver-soldered to a flat piece of copper plate, and this plate is held firmly against the rotating disc by a steel spring. A diagram of the thermocouple is given in Figure 3.3.7. Further information on these thermocouples is given in Appendix A.2.

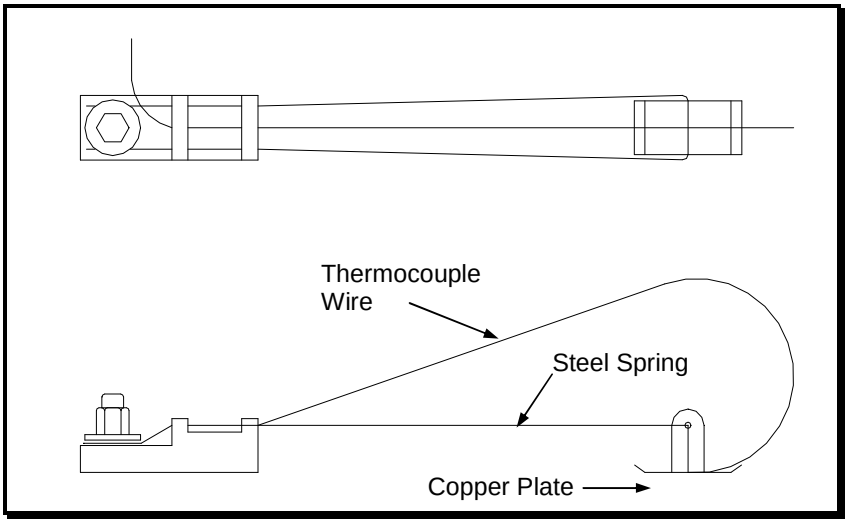

Figure 3.3.7 Diagram of Disc Brake Thermocouple

3.3.2.4. Infra-red Digital Thermal Imaging Camera

A Flir ThermaCam™ PM595 digital thermography camera (see Figure 3.3.8) was also used in the experiments. This device is capable of measuring temperatures ranging from –40 to 1500°C at distances of up to 1000 m. Output of the data is via high-resolution colour images, which can be analysed in real time or stored in memory for later use. The

images can also be transferred to PC for further analysis, using software supplied by the manufacturer. The salient details of the instrument are given in Table 3.3.4.

Flir ThermaCam™ PM595 Thermography Camera	
Object temperature measurement range	-40 ºC to +1500 ºC
Ambient operating temperature	–15 ºC to +50 ºC
Measurement Accuracy:	±2 ºC or ±2% across the range
Size:	220 x 133 x 140 mm
Weight:	2.3 kg, including battery

Table 3.3.4 Salient Details of the Digital Thermography Camera

Figure 3.3.8 Flir ThermaCam™ PM595 Digital Thermography Camera

3.3.2.5. Comparison of Disc Temperature Measurement Methods

In order to establish that reliable information could be obtained from rotating disc temperature measurement a series of tests was carried out (see Appendix A.2) in which the output from disc brake thermocouples was compared to a digital thermography camera. The results show excellent correlation between the two methods (Figure 3.3.9), in the heating phase, and good correlation in the cooling phase, with the thermocouple lagging by about 15 -20 seconds, most likely due to residual heat in the thermocouple.

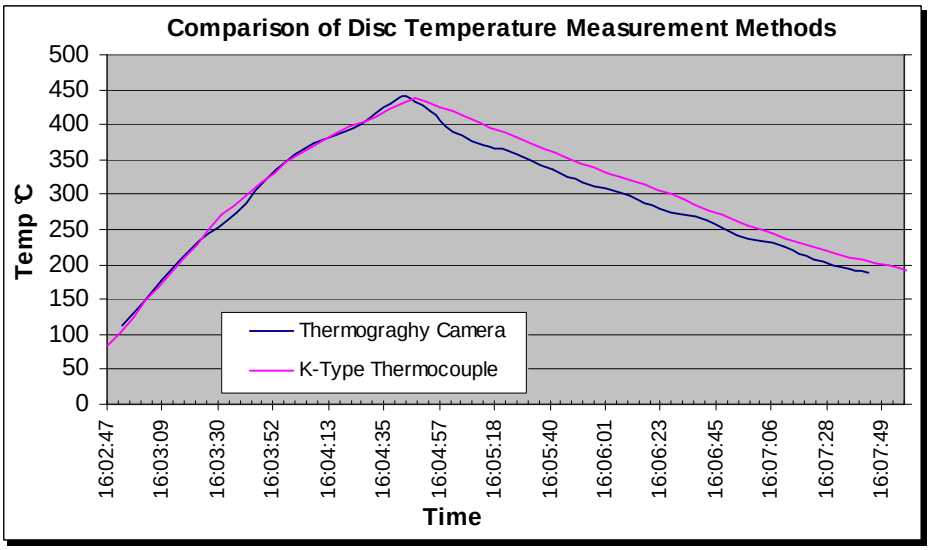

Figure 3.3.9 – Comparison of disc temperature measurement methods

3.3.2.6. Tachometer

The angular velocity of the test wheel was measured using an optical tachometer, and the output from the instrument was obtained directly from a digital panel meter.

3.3.2.7. Rotary Torque Sensor

The rotating type torque sensor used was a 01225 series supplied by Sensor Developments Inc. The sensor has a range from 0 to 271 Nm, at a maximum rotational speed of 5000 RPM. The device is factory calibrated, a copy of the calibration certificate is provided in Appendix A.3. The transducer is connected to a Unimeter digital panel meter, which provides the excitation voltage, as well as displaying the output in Nm directly.

3.3.2.8. Data Logger

A Fluke Hydra 2620A data logger was used to record the output from the disc brake thermocouples. This data logger has twenty analog input channels, any combination of dc voltage, ac voltage, thermocouple, resistance temperature devices, or frequency measurements can be connected to the input module without the need for additional signal conditioning. Thermocouple reference junction compensation is automatically performed. Output from the data logger is via an RS232 cable to a personal computer.

CHAPTER FOUR

4 VENTED ROTOR AIR FLOW MEASUREMENTS

4.1 Introduction

In this chapter the airflow through a vented rotor is examined. A brief description of the experimental procedure is given, which is followed by an analysis of the results. The airflow velocity through an internally vented rotor was measured at various rotational velocities in order to determine how well a simple straight vane, vented rotor operated as an air displacement device. Tests were developed to determine the nature and velocity of the flow through the rotor under various conditions. These conditions include the effect of the wheel, the vehicle body and the external flow (flow resulting from the forward motion of the vehicle). Airflow through the rotor was measured at rotational speeds corresponding to road velocities of between 40 and 100 km/h.

4.2 Experimental Set-up

The rotor test rig and the three-axis traverse with Cobra Probe attached were placed in the test section of the RMIT Wind Tunnel, as shown in Figure 4.2.1.

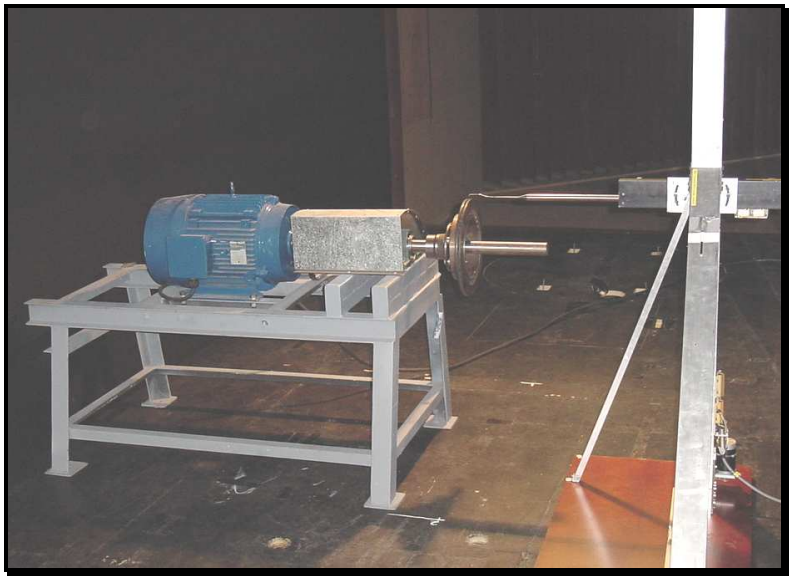

Figure 4.2.1 Rotor Test Rig and Three Traverse in Axis Position

The probe was positioned in the centre of the vane outlets at a distance of about 5 mm from the rotor. With the rotor spinning the probe head was adjusted until it was facing directly into the mean direction of local flow. This was achieved by rotating the probe head until the measured flow angle was approximately equal to zero. The optimum radial angle of the probe was found to be between 60 and 62.5° from the normal, see Figure 4.4.3. This angle was verified using a wool tuft to visualise the flow as can be seen in Figure 4.2.2.

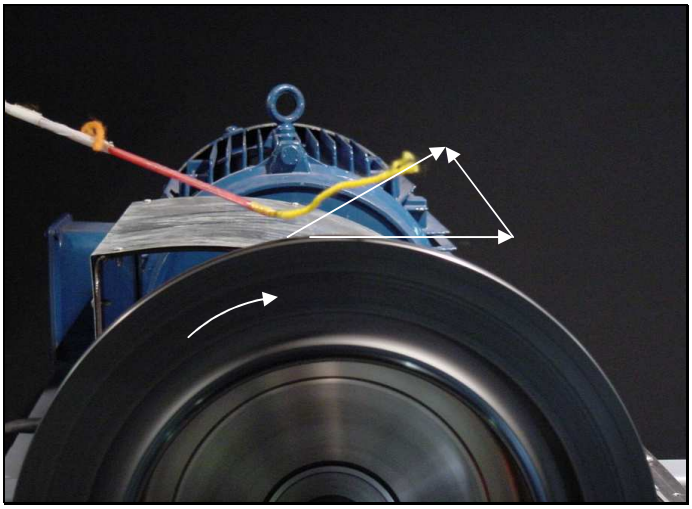

Figure 4.2.2 Wool tuft placed at vane outlet (Point 0), still air

In order to understand the development of the flow at the exit of the vanes, and to determine a suitable distance for the probe to measure this flow, a series of flow measurements were taken at 3, 5, and 10 mm from the vane outlets. The results of these tests can be found in Appendix B. From these results a final distance of 5 mm from the rotor was chosen, which was close enough to minimise effects of flow dispersion, and adequately distanced to prevent damage to the sensing element by accidental contact. Jerhamre and Bergstrom (2001) found only small differences in velocities when comparing measuring distances of 5 mm and 10 mm, however as observed in Appendix B, significant flow dispersion appears to occur at a distance of 10 mm. The final position and orientation of the probe can be seen in Figure 4.2.3.

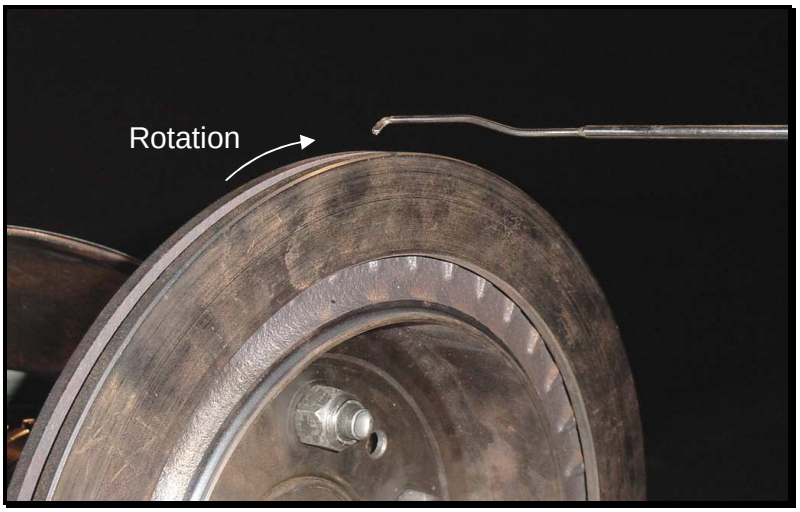

Figure 4.2.3 Position of Cobra Probe for Airflow Measurement

4.3 Experimental Procedure

Four test cases were developed, as outlined in Table 4.3.1. Case 1 involved measuring the airflow at the exit of the passages of a vented brake disc (303 mm in diameter) spinning in still air, this was to determine the relationship between vehicle speed and vent air flow. The rotational velocity of the disc was chosen as the equivalent rotational speeds for the vehicle travelling at road speeds of 40, 60, 80, and 100 km/hr. The relationship between brake disc rotational velocity and vehicle speed is outlined in Appendix C. By traversing the probe axially at 1 mm intervals from the inboard to the outboard edge of the disc, it was possible to obtain a good measurement of the flow field at the outlet of the vanes. The sampling frequency was set at 5000 Hz and the sampling time was 5.324 seconds, making a total of 26620 samples at each point. The various angle conventions adopted for describing the flow, as well as the probe traversing direction are outlined in Figure 4.4.3.

The measurement of airflow through the vented disc in still air is useful for determining its effectiveness as a centrifugal flow generator, and has been used to measure improvements made in vented rotor design see Hudson and Ruhl (1997); Daudi (1999). However, this condition is significantly different from the actual condition experienced by the disc in its normal operating environment. In order to determine the nature of the airflow through the disc in its normal operating condition, the next stage of the experiments was to examine the factors that influence airflow through the disc. The next test (case 2) repeated the above procedure with the disc surrounded by the wheel. Case 3 again used the wheel surrounding the disc but exposed to an external airflow, equivalent to the forward speed of

the vehicle. Finally in case 4 the flow was again measured through the disc in a representation of the on-road condition using a one-quarter car buck. In case 1 and 2 the vent airflow around the circumference of the brake disc was axi-symmetric as there was no external airflow acting upon it. Airflow measurements were therefore only required at one point, however for cases 3 and 4 this was not the case due to the interaction of the external airflow. Therefore flow measurements were taken at a number of points around the circumference of the disc including the top, bottom, front and back of the disc. A full experimental matrix is given in Table 4.3.1.

Experimental Matrix

Case No.	Description	Equivalent Vehicle Speed (km/h)	Measurement Positions
1	Isolated Disc Still Air	40, 60 , 80, 100	Top (of disc)
2	Still Air with Wheel On	40, 60 , 80, 100	Top
3	Moving Air with Wheel On	40, 60 , 80, 100	Top, Bottom Front Back
4	Car Buck Tests	40, 60 , 80, 100	Top, Bottom Front Back

Table 4.3.1 Experimental Matrix for Vented Disc Tests

4.4 Experimental Results

4.4.1 Case 1 – Airflow Through Isolated Brake Disc In Still Air

4.4.1.1. Time Averaged Results

The time-averaged velocity data collected from the isolated disc measurements are displayed graphically in Figure 4.4.1. The axial position is non-dimensionalised over the width of the disc, position 0 being the centre plane of the disc, and positions –1 and 1, are the inboard and outboard edges, respectively. The two vertical dotted lines represent the

boundaries of the internal flow passages. This chart shows the outlet flow velocity profiles from the disc at the various speeds under investigation.

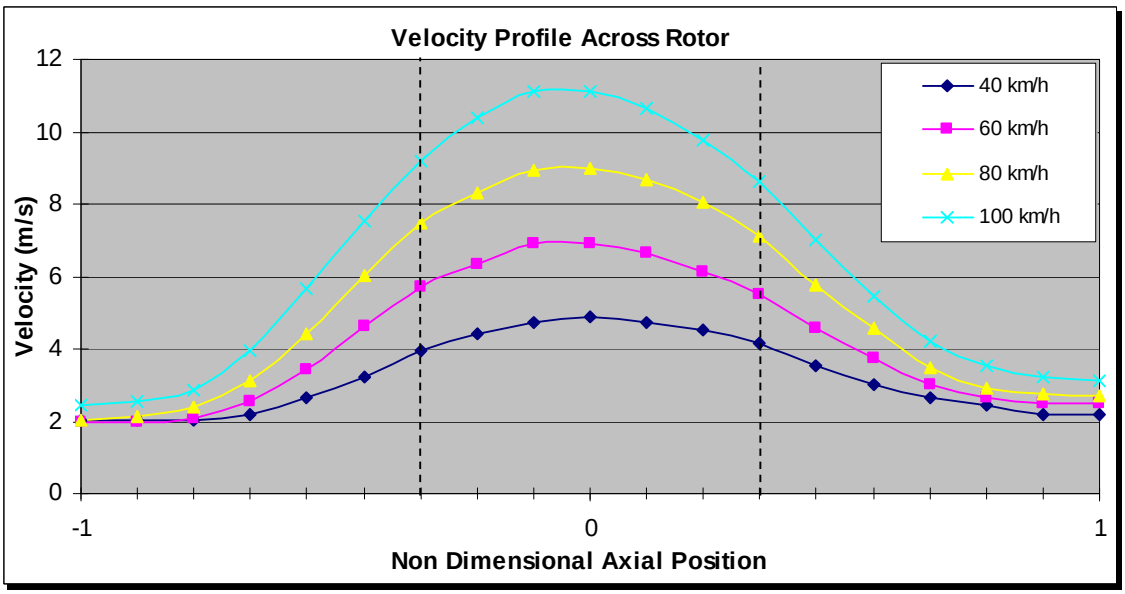

Figure 4.4.1 Velocity Profiles Across Disc

From this chart it can be seen that the point of maximum velocity through the disc does not coincide with the centre of the flow passage, this may be because airflow only enters the disc from the inboard side. Daudi (1998) found that by allowing air to enter from both inboard and outboard, airflow through the disc could be increased by 5% over traditional inboard only airflow. The velocity profiles are similar for all speeds, and appear to be proportional to the rotational velocity. Figure 4.4.2 shows the results when the measured velocities are shown in non-dimensional form. This is achieved by dividing the measured velocity by the peripheral velocity of the disc.

$$non\text{-}dimensional\ velocity = \frac{measured\ velocity}{\frac{2\pi r_o}{60} N} \qquad \text{Equation 4.4.1}$$

$$r_o = outer\ radius\ of\ rotor\ (m)$$
$$N = rotational\ speed\ of\ rotor\ (RPM)$$

The results appear to collapse onto a single line, particularly at higher speeds. At lower speeds there is some drift away from this line, particularly at the edges of the disc, which is attributed to minor Reynolds number effects and measurements errors at these low flow velocities.

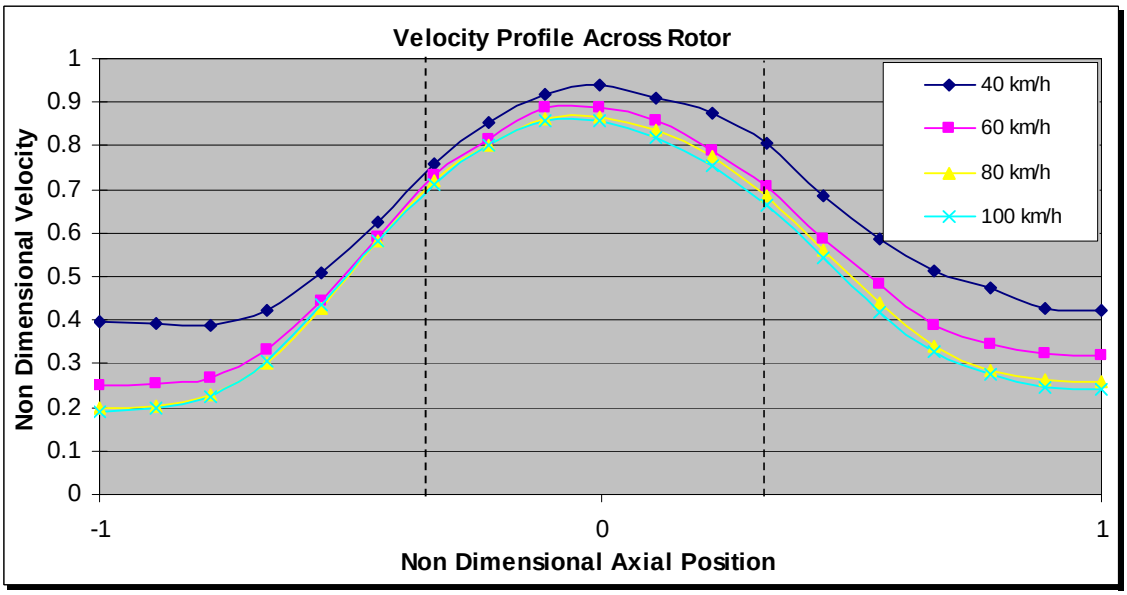

Figure 4.4.2 Non Dimensionalised Flow Through Disc

As discussed in Section 2.3.1, Limpert and Sisson have presented empirical equations for determining the flow through vented discs. Table 4.4.1 presents the measured values for flow through the disc, as well as the predicted flow rates using both Limpert's and Sisson's equations. When the average measured value is taken, which is the average of the flows as measured through the vent area, Sisson's equation produces results very close to the measured values (within 20% at all speeds). However, Limpert's equation yields values of about 40 - 50% lower than measured. Both Limpert and Sisson predict a linear relationship between rotational velocity and vent airflow, and Figure 4.4.2 appears to support this. It should be noted that the air velocity through the vane is very low in comparison to the vehicle velocity. Also shown in Table 4.4.1 is an estimation of the mass flow rate through the disc, which was calculated using the following formula:

$$\dot{m} = \rho_a A V_{ave} \qquad \textit{Equation 4.4.2}$$

$\dot{m} = mass\ \ flow\ rate\ (kg/s)$
$\rho_a = density\ of\ \ air\ (kg/m^3)$
$A = total\ outlet\ area\ of\ \ rotor\ (m^2)$
$V_{ave} = average\ velocity\ of\ \ air\ through\ vent\ \ at\ \ outlet\ (m/s)$

		Calculated		Measured		From Measured
Speed (km/h)	**(RPM)**	**Limpert (m/s)**	**Sisson (m/s)**	**Max. Measured (m/s)**	**Average (m/s)**	**Mass Flowrate kg/s**
100	816	6.82	8.89	11.11	10.12	0.0569
80	653	5.46	7.11	8.98	8.21	0.0462
60	490	4.09	5.34	6.90	6.30	0.0355
40	326	2.72	3.55	4.75	4.48	0.0252

Table 4.4.1 Measured Flow Through Disc Compared to Predictions from Formulae

Along with velocity measurements, the Cobra Probe is able to determine the angles of the flow stream relative to its head. For convenience, these angles have been transformed to angles relative to the disc and named radial angle and lateral angle, the convention adopted for these angles is given in Figure 4.4.3.

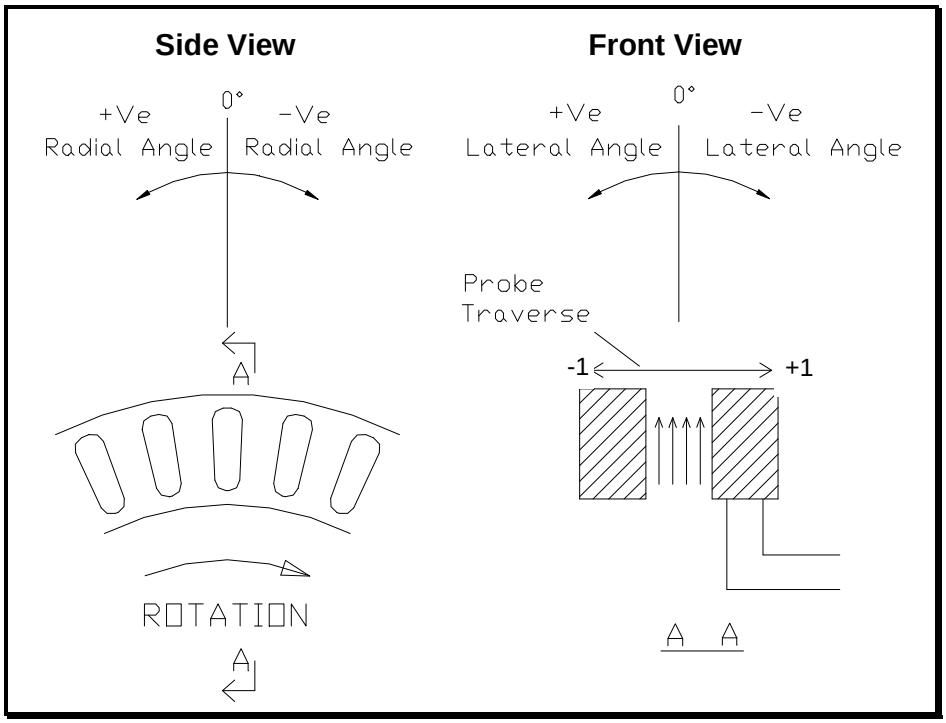

Figure 4.4.3 Airflow Angle Convention, for Air Flow Through Disc

The vector diagrams for the flow leaving the disc at an equivalent road speed of 100 km/h are shows in Figure 4.4.4. It can be seen that neither the flow angles nor the velocities are symmetrical about the centre of the vent. Also observed in this diagram is entrainment of the flow at the edges and diffusion at the centre. As well as radial angle, the lateral angle was measured along the width of the disc, this was found not to vary by more than a few

degrees from the inboard edge (point -1) to the outboard edge (point +1) see Figure 4.4.5. It can be seen that the patterns for all speeds are similar for both radial and lateral angles.

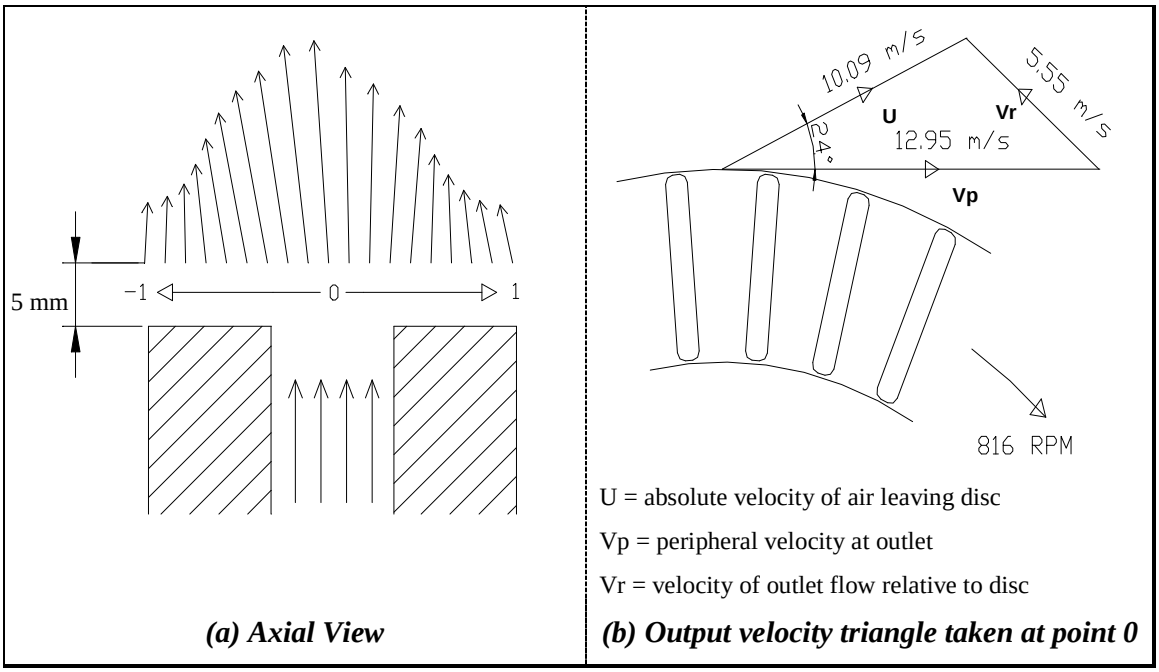

(a) Axial View ***(b) Output velocity triangle taken at point 0***

Figure 4.4.4 Flow Vectors for Vented Disc at 100 km/h Equivalent Road Speed

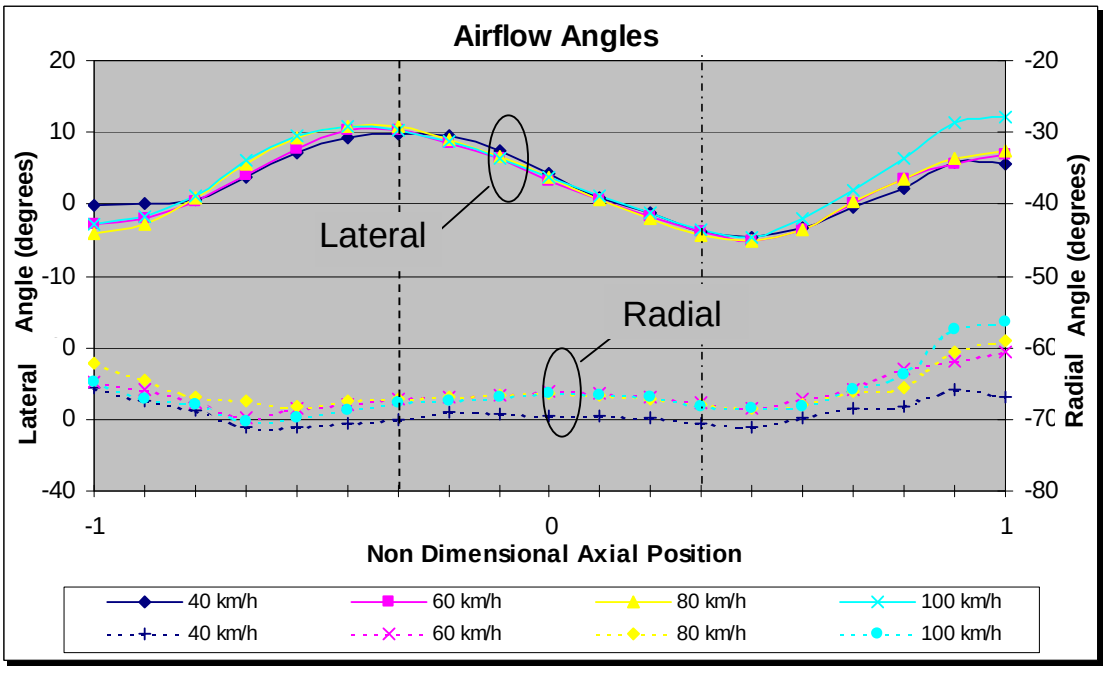

Figure 4.4.5 Measure Radial and Lateral Angles for Flow through the 303 mm Vented Disc

4.4.1.2. Real Time Results

In addition to time-averaged measurements, the Cobra probe allows measurement of real time and transient airflows. Figure 4.4.6 shows the velocity measurements for one revolution of the disc at an equivalent road speed of 100 km/h, (measured at the centre point of the vent outlet).

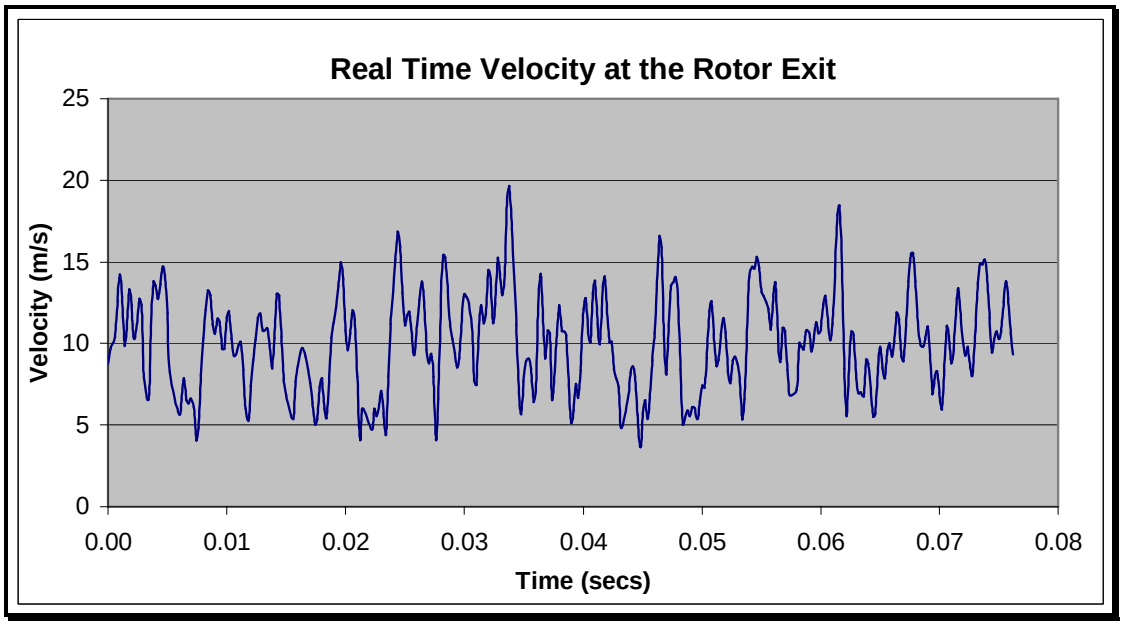

Figure 4.4.6 Airflow Velocity for One Revolution of Brake Disc

It is extremely difficult to obtain meaningful data from this type of trace, and it is more useful to look at the data in the frequency domain rather than the time domain. A Fast-Fourier Transform (FFT) was performed on the data using the Cobra Probe software, which allows a detailed analysis of the data in the frequency domain. Figure 4.4.7 shows the results of the FFT performed on the above data (100 km/h equivalent road speed). The frequency is displayed on the x-axis, and the root mean square of the velocity squared is shown on a decibel scale on the y-axis. The software filter cut-off frequency was 1500 Hz, this can be observed in the spectrum as a step change at 1500 Hz. A sharp spike can be observed in the spectrum at about 500 Hz. This is equivalent to the frequency of the vents in the disc passing the probe head. The disc contains 37 vents and at 100 km/h (816 RPM), thus the blade passing frequency is:

$$\frac{816}{60} \times 37 = 503.2\ Hz \qquad \textbf{Equation 4.4.3}$$

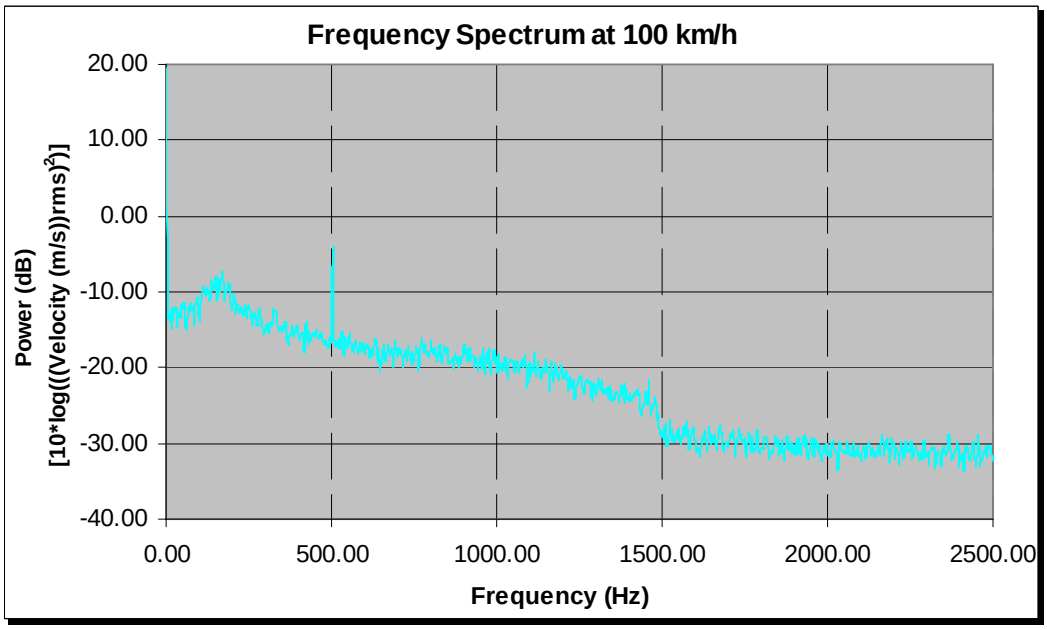

Figure 4.4.7 Frequency Spectrum at 100 km/h (816 RPM)

Also observed in the spectrum is a wider spike centred about 180 Hz, which is believed to be vortex shedding from the trailing edge of the internal vanes. In order to confirm that this was an actual measurement of a flow phenomenon and not a stray noise signal in the measurements, the spectrum was plotted at various points across the disc from the inboard edge (position -1) to the centre (position 0), in Figure 4.4.8. This chart clearly shows that this rise in power only occurs when the probe is in the flow stream, indicating that this is actually a phenomenon in the airflow from the vanes.

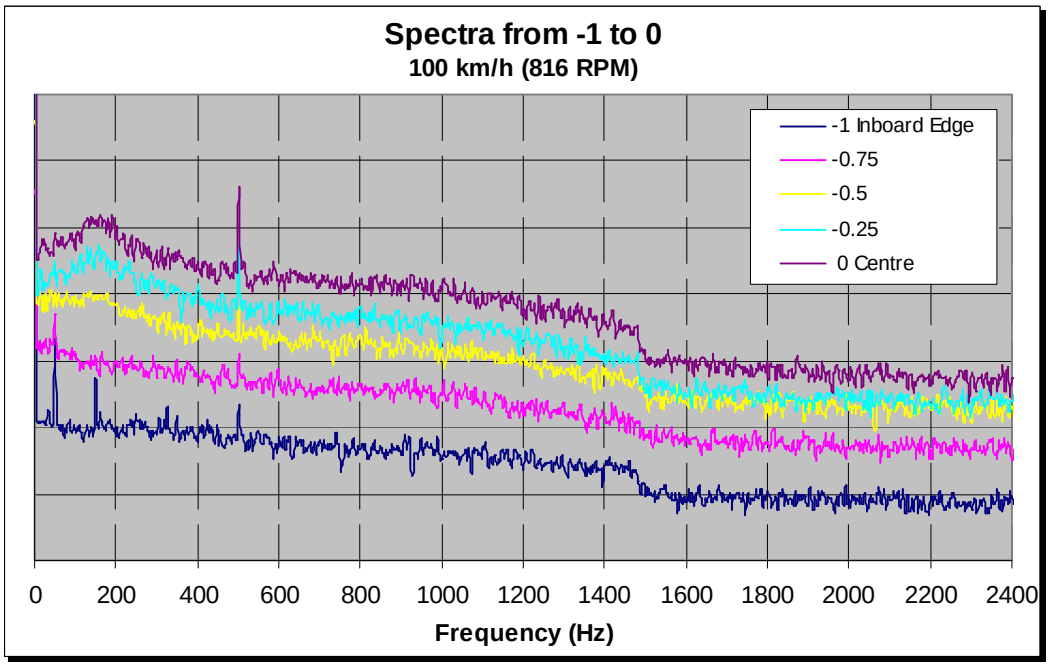

Figure 4.4.8 Spectra Recorded at 100 km/hr From Inboard Edge to Centre of Disc

Figure 4.4.9 shows the spectra for all speeds measured from 40 to 120 km/h, which are transposed in the y direction for comparison purposes.

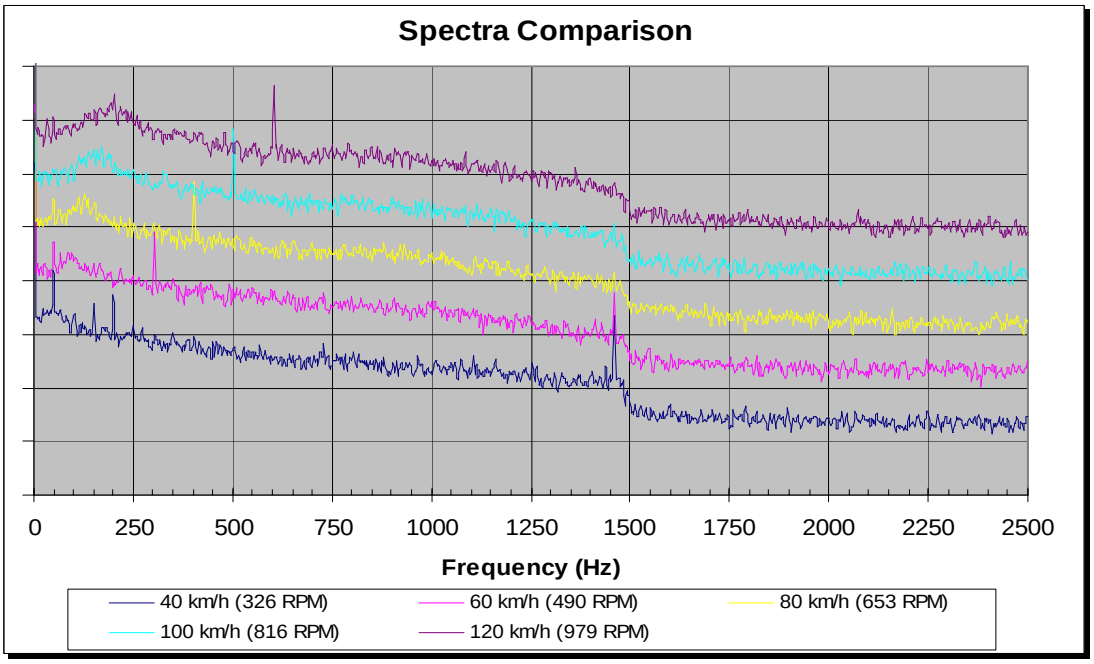

Figure 4.4.9 Spectra Comparison for Full Range of Speeds.

It can be seen that the blade passing and vortex shedding rise in the frequency plot are present at all speeds examined. According to Lawson (2001) vortex shedding will occur

at Reynolds numbers in the range $40 \leq \mathrm{Re} \leq 200000$, and with Strouhal numbers between 0.2 for (circular cylinder) and 0.08 for (rectangle). Equation 4.4.4 and Equation 4.4.5 were used to determine if the flow through the vanes was within the range for vortex shedding to occur. The results of these equations are outlined in Table 4.4.2, and show the combination of Reynolds and Strouhal numbers to be in the range that vortex shedding occurs.

$$\mathrm{Re} = \frac{V_{vent} D_o}{2\upsilon} \quad \textit{Sheridan et al. (1988)} \qquad \textbf{\textit{Equation 4.4.4}}$$

Where Re = Reynolds Number

V_{vent} = *air velocity through vent (m/s)*

D_o = *outer diameter of disc (0.303 m)*

υ = *kinematic viscosity* ($1.4 \times 10^{-5}\ m^2/s$)

$$St = \frac{f_r l}{V} \qquad \textbf{\textit{Equation 4.4.5}}$$

Where: St = *Strouhal number*

f_r = *frequency of shedding vortices* (Hz)

l = *characteristic length* (m)

V = *velocity* (m/s)

Speed (km/h)	RPM	V_{vent} (m/s)	*Re*	*l* (mm)	Measured Vortex Shedding Frequency (Hz)	Calculated Strouhal No.
100	816	10.12	85177	6	180	0.11
80	653	8.21	69101	6	125	0.09
60	490	6.30	53025	6	90	0.09
40	326	4.48	37707	6	50	0.08

Table 4.4.2 Vortex Shedding Frequencies

4.4.2 Case 2 – Airflow Through Brake Disc in Still Air with Wheel On

The results shown in Figure 4.4.11 are the airflow measurements through the disc with wheel in place (Figure 4.4.10) and no external airflow. The velocity profiles are similar to the free disc case for the inboard portion of the disc, however for the outboard portion of

the disc (wheel side) there appears to be significant airflow generated by the wheel. The maximum airflow velocity through the vane section appears similar in magnitude to the free disc case, although the profile is a little flatter. Non dimensional plots are not given as it is evident that results again collapse onto a single line.

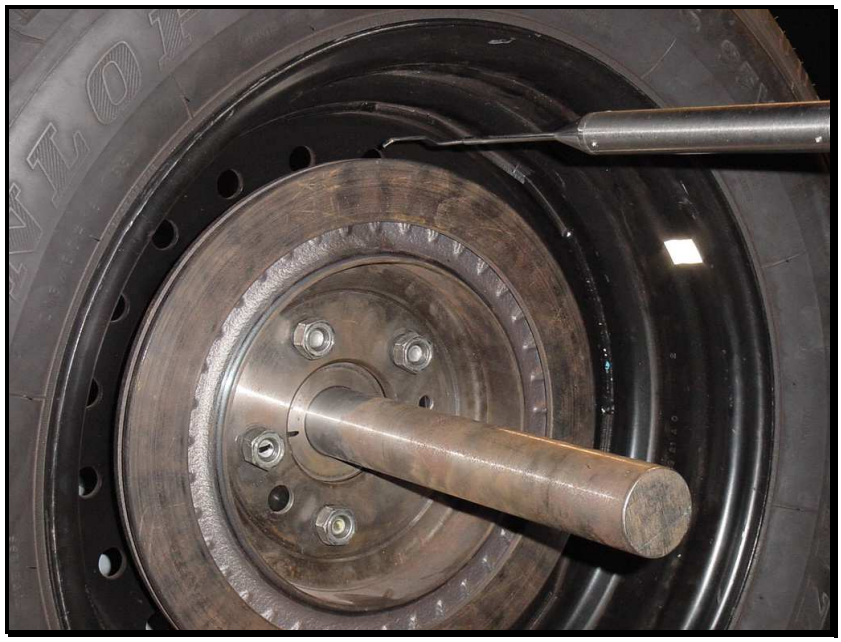

Figure 4.4.10 Airflow Measurements with Wheel in Place

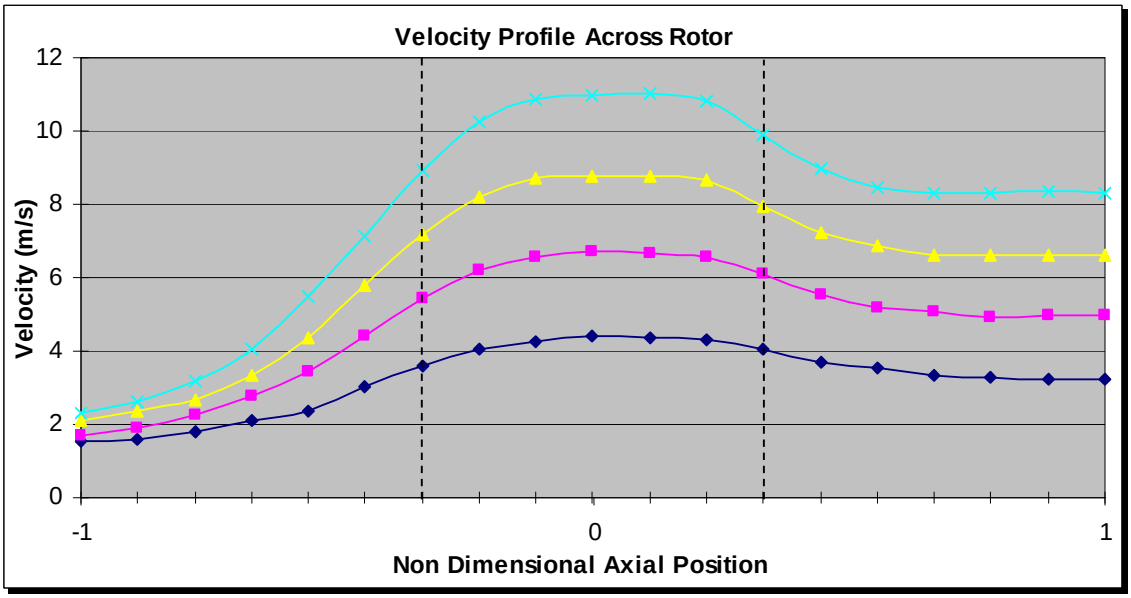

Figure 4.4.11 Velocity Profile Across Disc in Still Air (Wheel On)

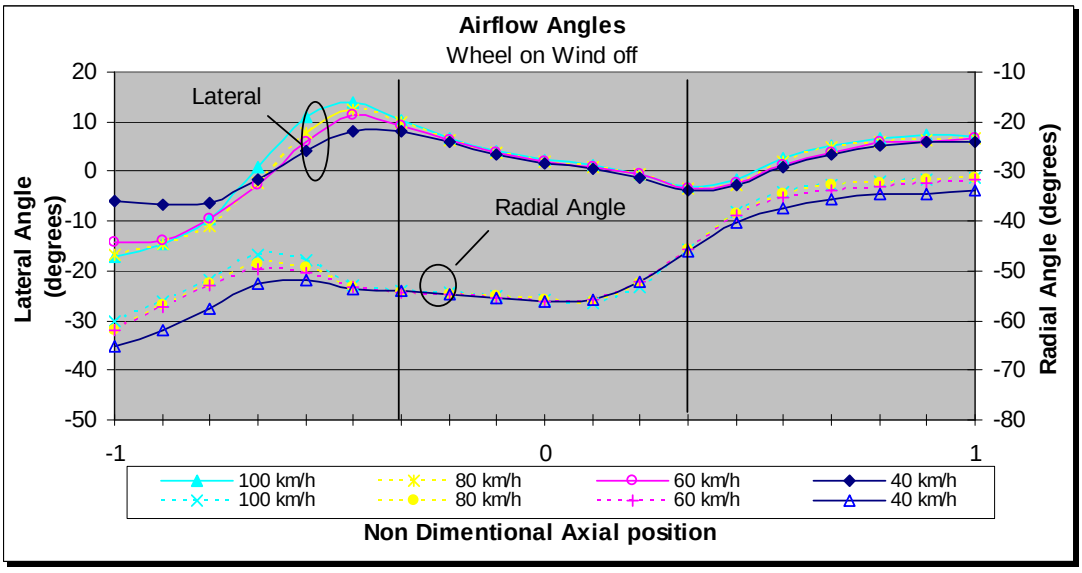

Figure 4.4.12 Measured Radial and Lateral Angles in Still Air (Wheel On)

The measured radial and lateral angles for this case are given in Figure 4.4.12. It can be seen from this chart that the lateral angle plot is similar to the free disc case, but reduced by about 10° towards the outboard edge indicating that airflow generated by the wheel at the outboard edge of the disc has the effect of forcing the vent airflow inwards. The radial angle is also reduced slightly particularly at the outboard edge, which also indicates the influence of airflow generated by the wheel. It should be noted that a standard wheel was used in the test which had an open area of 40cm^2; it is likely that a wheel with a larger vent area would have a significantly greater influence on the flow.

4.4.3 Case 3 – Airflow Through Brake Disc in Moving Air with Wheel On

Figure 4.4.13 shows the velocity profile across the disc for the wind on and wheel on condition, with the probe in the top position as in the previous set of experiments. The probe angle was kept at -60° in an attempt to determine if any flow was present. During this set of experiments it was noted that the data rejection rate of the probe for these measurements was also in excess of 30%, indicating that a significant portion of the flow was outside the ± 45° zone of acceptance of the probe head. Clearly from this chart the readings were affected by the external flow, and it is unknown if any internal flow was measured, as no discernible flow is observed through the centre portion of the disc. The flow profiles are however similar to each other for all speeds and proportional to the vehicle speed. The results from the angle measurements also indicate significant influence from the external flow when compared to the case 1, however very little variation is

observed from the inboard edge to the outboard edge indicating that the primary influence is external flow.

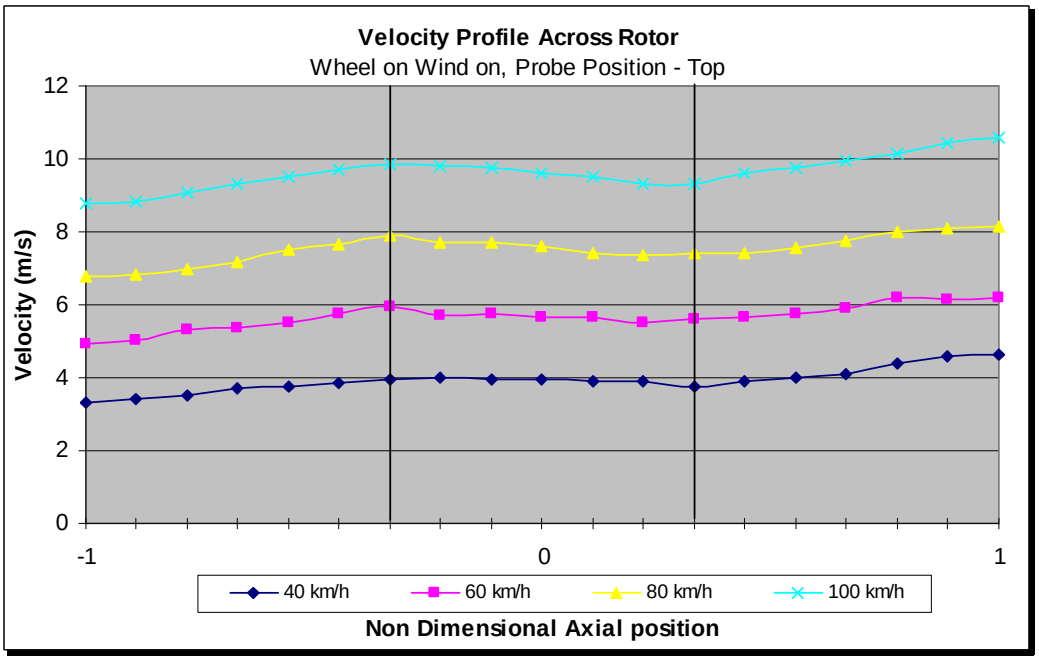

Figure 4.4.13 Velocity Profile Across Top of Brake Disc (case 3)

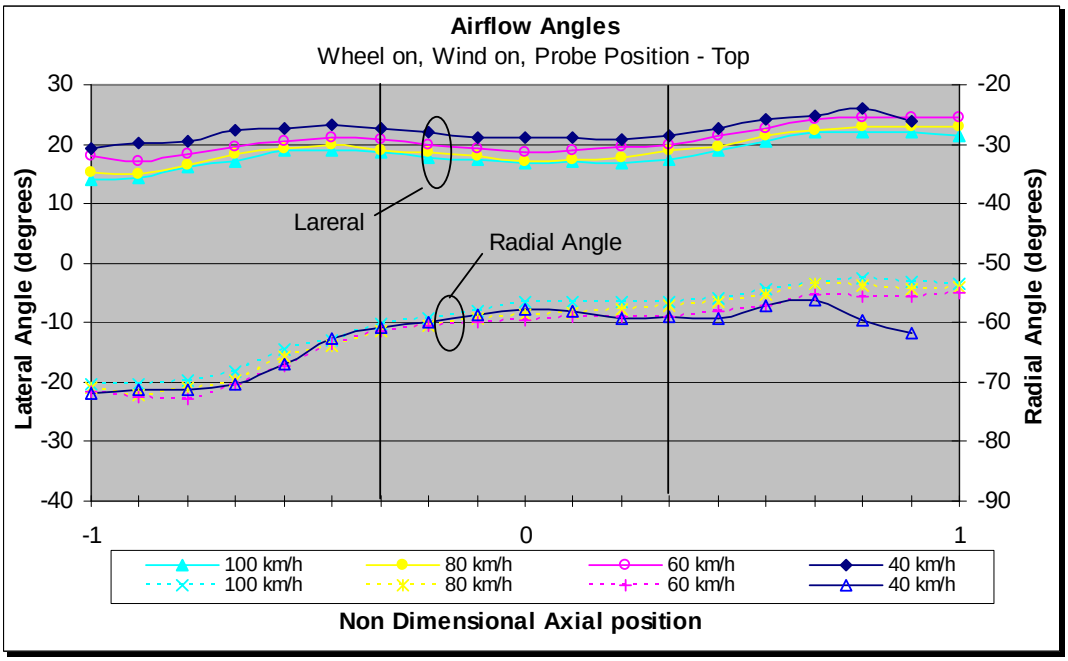

Figure 4.4.14 Radial and Lateral Angles, Case 3 probe position top

The results are also given for the measured flow at other points around the disc. Figure 4.4.15, Figure 4.4.17, and Figure 4.4.19 show the velocity profiles for the front, bottom

and back of the disc respectively. Apart from the flow measured at the front of the disc, it is not possible to see any evidence of internal flow through the vanes. It is likely that the outlet of the vanes at the front of the disc is within the wake of the front portion of the wheel and is therefore less affected by the external flow. This wake can be observed in Figure 4.4.21. Similarly for the angle measurements (given in Figure 4.4.16, Figure 4.4.18 and Figure 4.4.20), it is not possible to determine any effects on the airflow at the vent exit due to the influence of the external airflow.

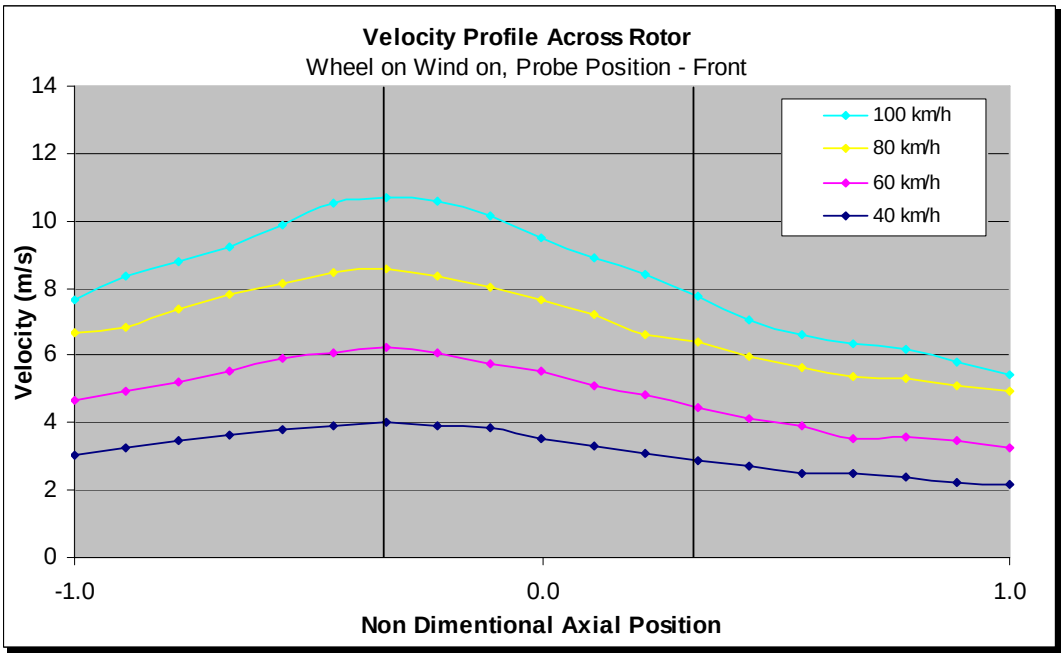

Figure 4.4.15 Velocity Profile Across Front of Disc (Case 3)

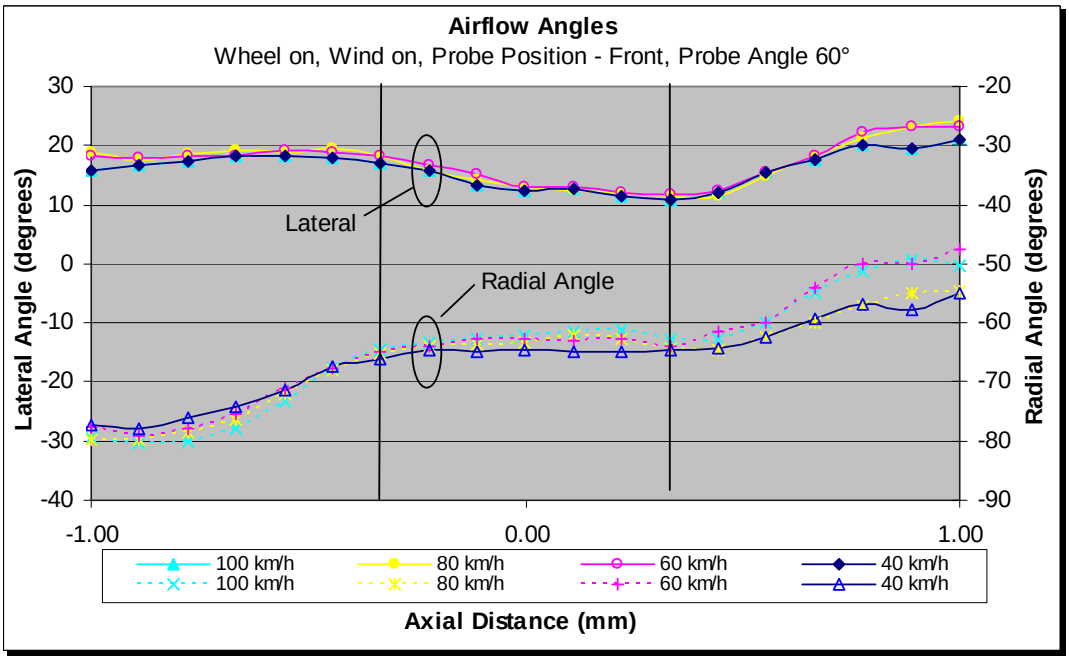

Figure 4.4.16 Radial and Lateral Angles, Case 3 probe position front

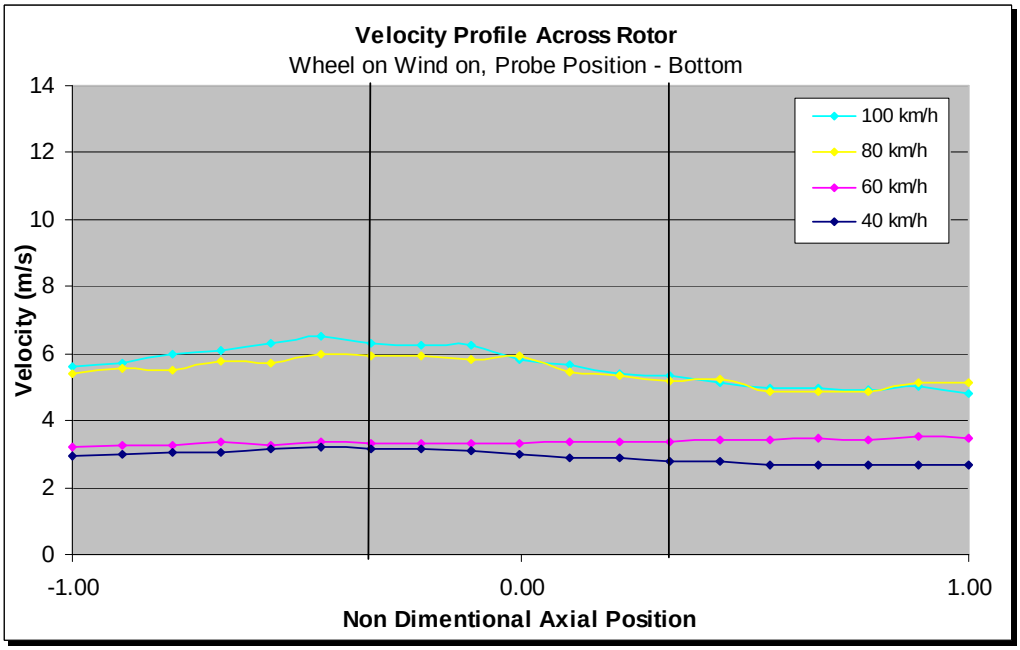

Figure 4.4.17 Velocity Profile Across Bottom of Disc (Case 3)

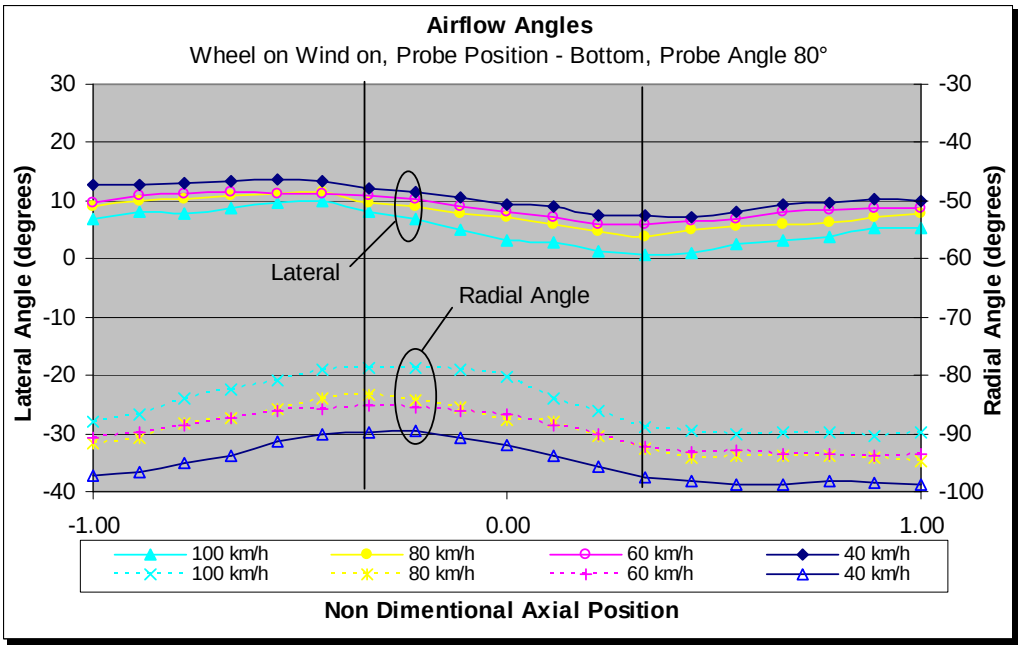

Figure 4.4.18 Radial and Lateral Angles, Case 3 probe position bottom

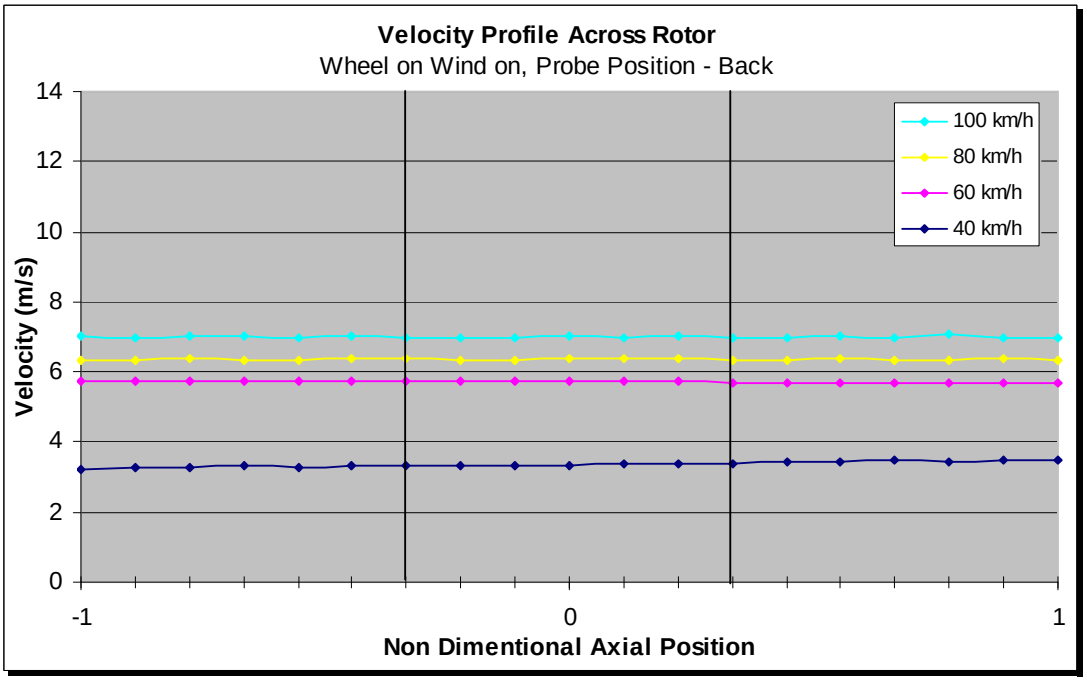

Figure 4.4.19 Velocity Profile Across Back of Disc (case 3)

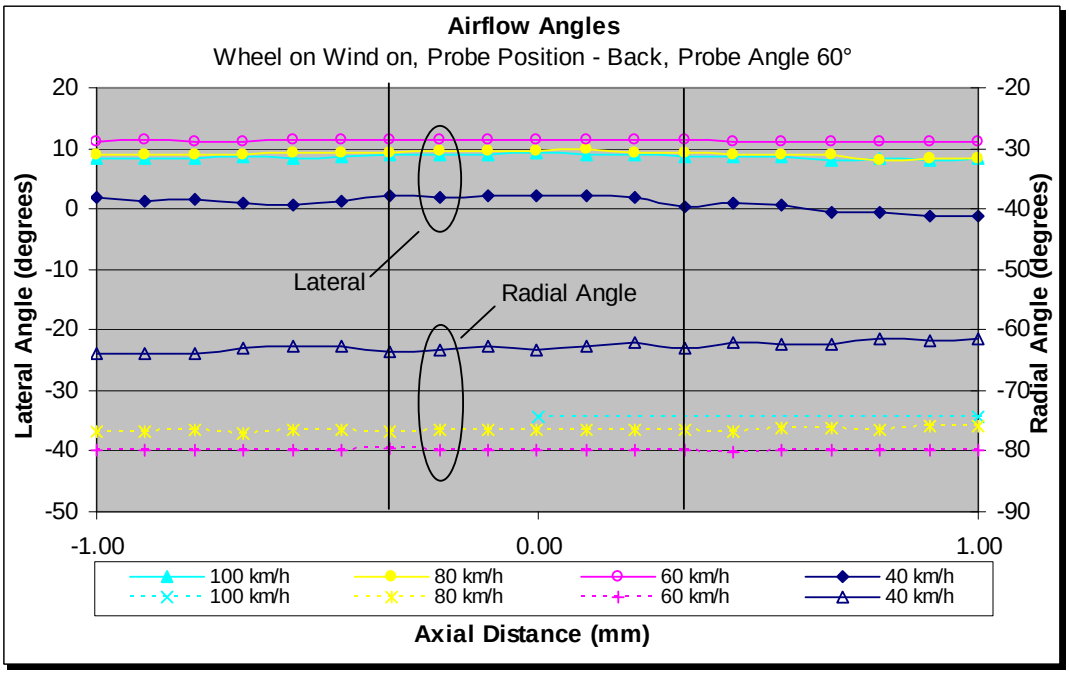

Figure 4.4.20 Radial and Lateral Angles, Case 3 probe position back

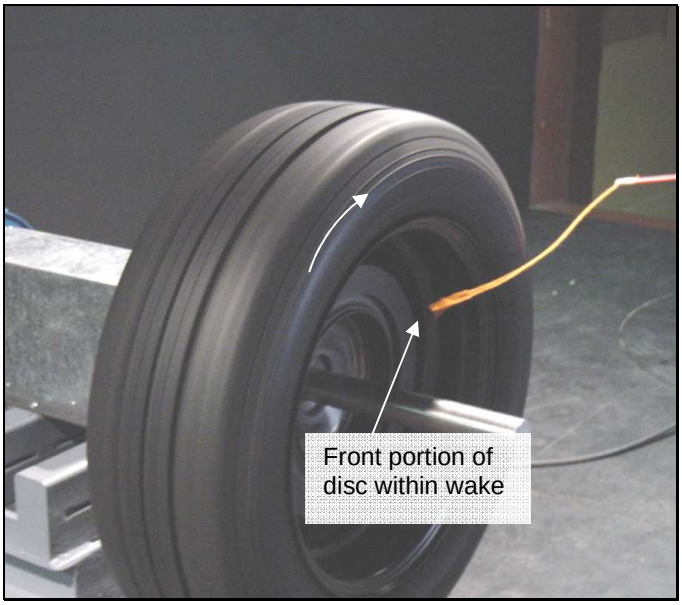

Figure 4.4.21 Wheel rotating with wind on

4.4.4 Case 4 – Airflow Through Brake Disc in Moving Air with Wheel and Quarter Car buck

In the previous tests it was difficult to determine if any airflow was being generated though the vanes of the disc in the wind on condition. As the external airflow was not

similar to the normal on-road condition, a further test was performed in a more representative simulation of the real world driving condition. In this test the test wheel was covered with a one-quarter car buck to represent the front right hand corner of the vehicle, as shown in Figure 4.4.22. This set-up within the RMIT wind tunnel could simulate the airflow conditions the brake rotor experienced under normal driving operation. The blockage area of the buck and associated equipment was approximately 20% (defined as projected frontal area of object divided by cross sectional area of test section). Although many corrections exist for blockage (e.g. Cooper (1992)), for this work the continuity equation was applied, and the upstream velocity was reduced by 20% to ensure the airflow around the test object approximated the equivalent on road condition.

Figure 4.4.22 Car Buck Used for Airflow Measurements

Figure 4.4.23 shows the velocity measurements for the flow measured at the top of the disc. Although the flow through the vanes appears to be affected by the external flow field, there is still evidence of flow through the vanes, particularly at higher speeds. The flow profiles are similar to the profiles recorded for the wheel on and without external air (Figure 4.4.11). It can also be seen that the peak measured flow are very similar to case 1 and 2.

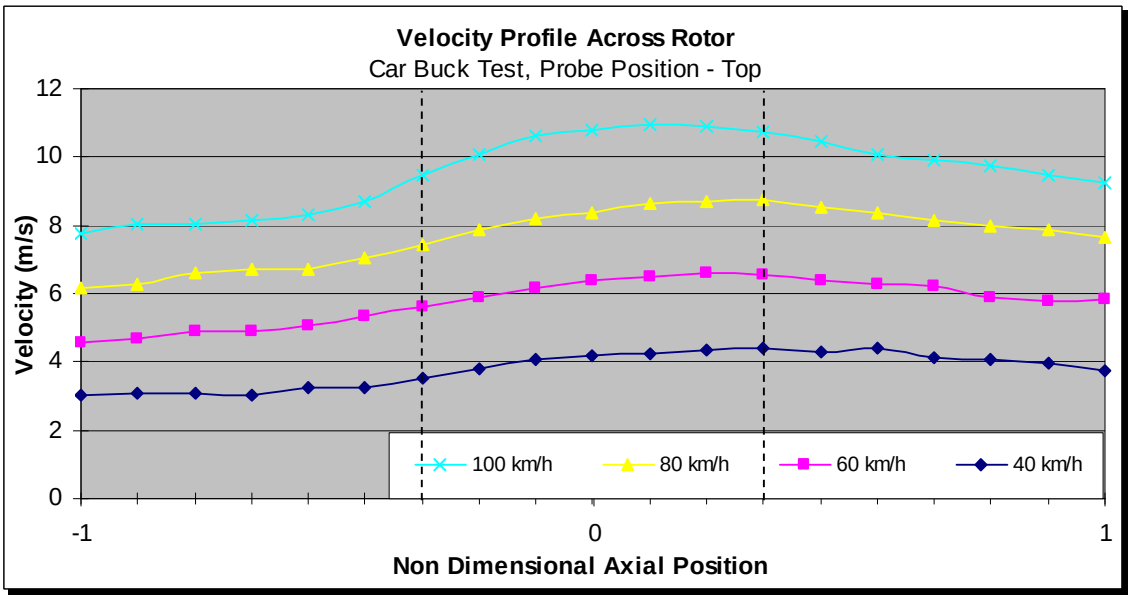

Figure 4.4.23 Velocity Profile Across Top of Disc (Case 4)

The charts shown in Figure 4.4.24 are the lateral and radial angles recorded at the top of the disc. The profiles are not significantly different for the case with the wheel on and still air Figure 4.4.24, and are consistent over the range of speeds tested.

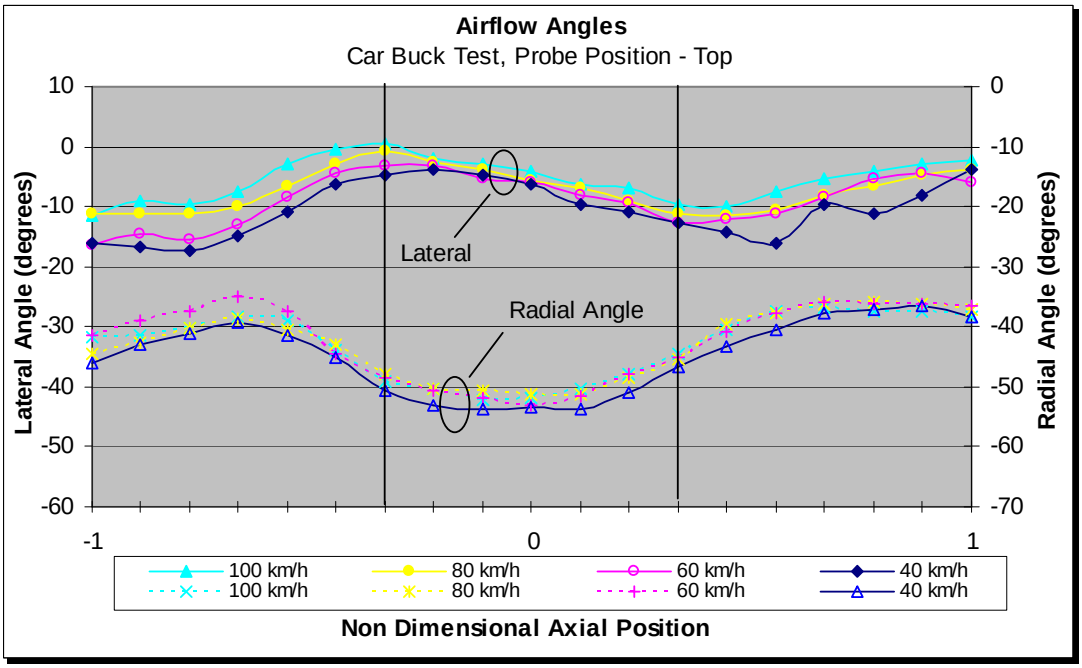

Figure 4.4.24 Radial and Lateral Angles, Case 4, Probe Position Top

The velocity plots for the front bottom and back of the disc are given in Figure 4.4.25, Figure 4.4.27 and Figure 4.4.29 respectively. From these plots it appears that no airflow

can be measured through the vanes from the front and bottom locations, although some flow is evident through the vanes at the back, particularly at higher speeds. The measured radial and lateral plots are given in Figure 4.4.26, Figure 4.4.28 and Figure 4.4.30; again it is difficult to establish any meaningful information of airflow from the vane exits due to the influence of external flow.

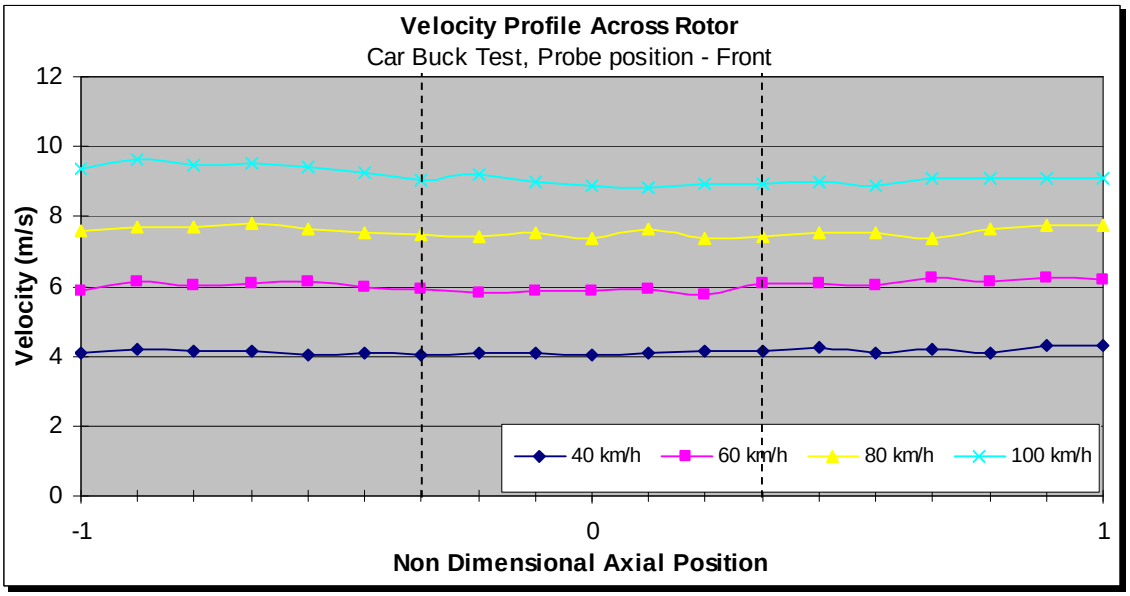

Figure 4.4.25 Across Front of Disc - Car Buck Test

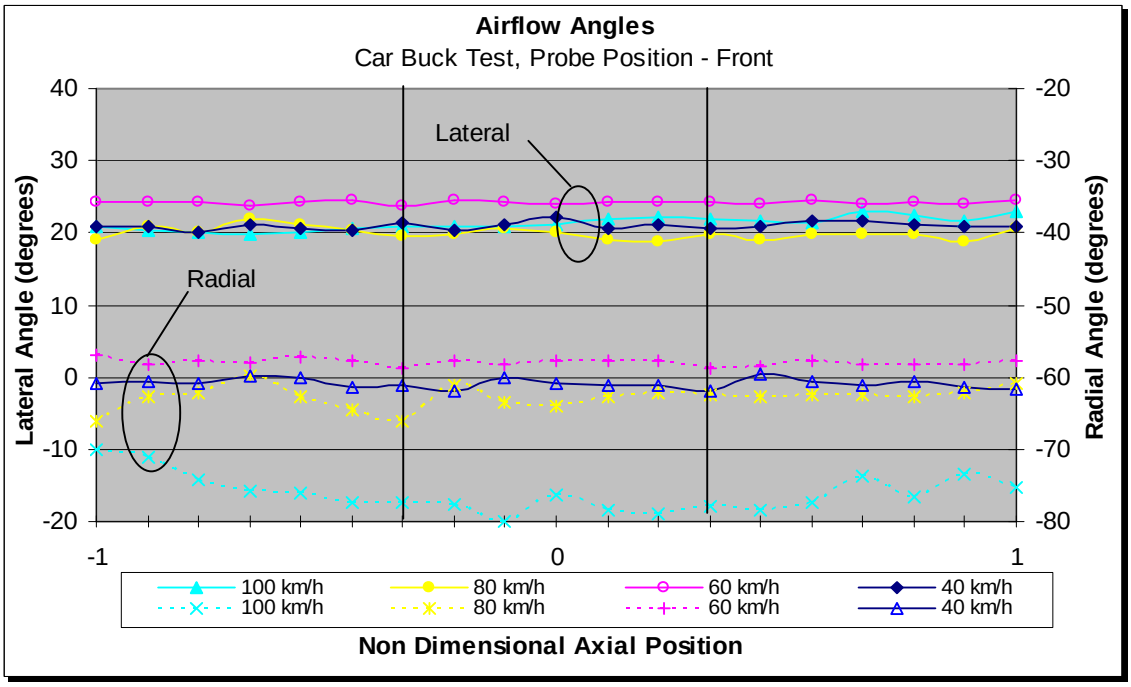

Figure 4.4.26 Radial and Lateral Angles, Case 4, Probe Position Front

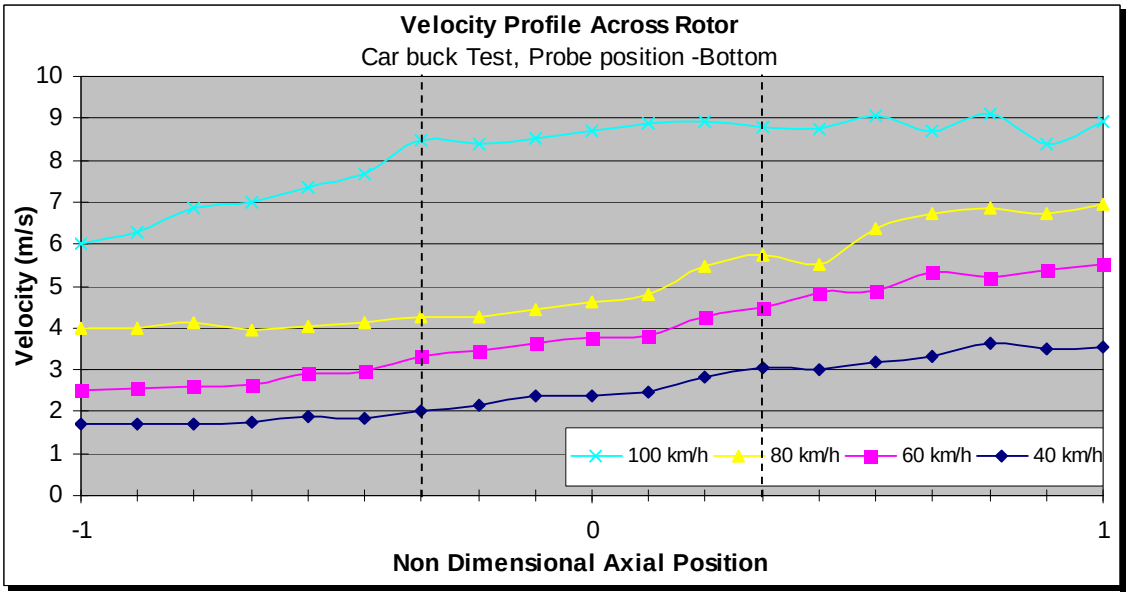

Figure 4.4.27 Across Bottom of Disc - Car Buck Test

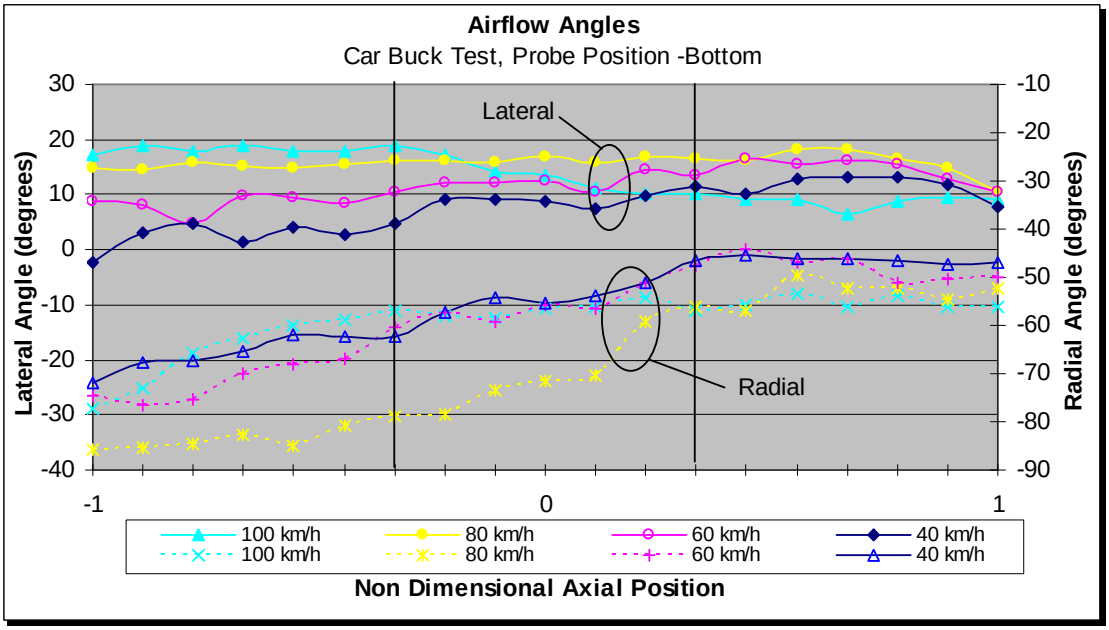

Figure 4.4.28 Radial and Lateral Angles, Case 4, Probe Position Bottom

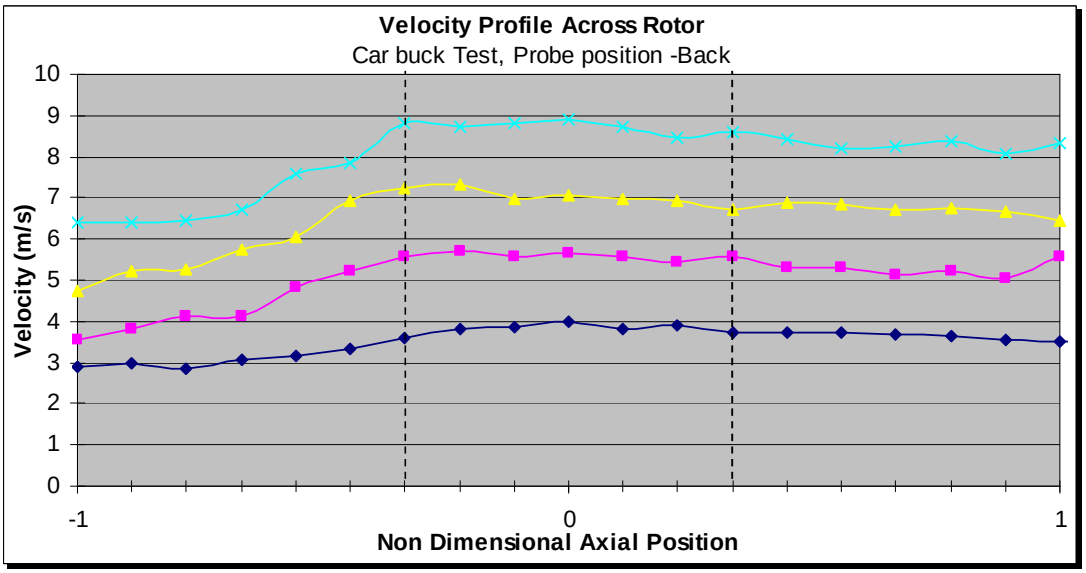

Figure 4.4.29 Across Back of Disc - Car Buck Test

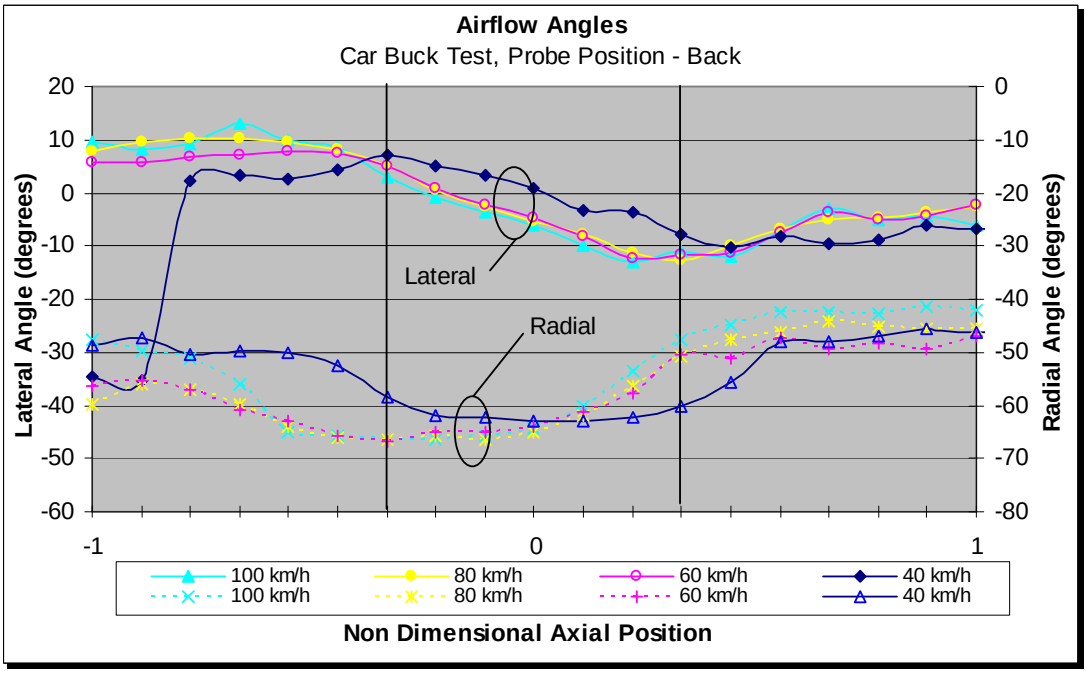

Figure 4.4.30 Radial and Lateral Angles, Case 4, Probe Position Back

4.5 Discussion of Results

Much work has been done to develop vented discs that displace more air for a given rotational speed, however previous research in this area has generally examined the airflow in discs in still air only. The results outlined in the still air tests (section 4.4.1)

appears to agree with earlier work by Limpert (1975); Sisson (1978); Hudson and Ruhl (1997) when predicting the expected flow through vented discs. However from the frequency analysis it appears that there is also some other flow disturbance existing through the vanes of the disc, possibly vortex shedding. Kubota et al. (2000) also found disturbances in the flow as show in Figure 4.5.1. It should therefore be possible to further increase the vent flow by reducing these disturbances and allow the cooling air to flow through the vents more smoothly.

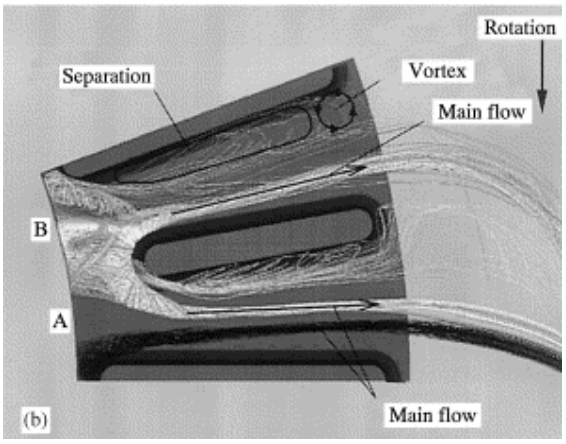

Figure 4.5.1 Visualisation of Flow within the Disc (Kubota et al. 2000)

When factors that influence the airflow in the region of the brake rotor were introduced to the tests, it became clear that the disc vent flow is severely influenced by the presence of the wheel vehicle and externally imposed flow (from the forward movement of the vehicle). Nothing was found in the public literature that experimentally determined flow through the disc vents in a representative road condition. It was not known how much or if any flow occurs through the disc vanes during normal operation, or how this flow was influenced by vehicle velocity. Therefore it may be questionable to attempt to gain more airflow through vented discs if no airflow exists in its normal operating condition. The presence of the wheel alone around the disc appears to influence this flow as shown in case 2. Figure 4.5.2 illustrates how the various interactions affect the flow through the disc at a vehicle speed of 100 km/h. Clearly all these interactions have an effect on the flow, the greatest being the external flow, as illustrated in case 3.

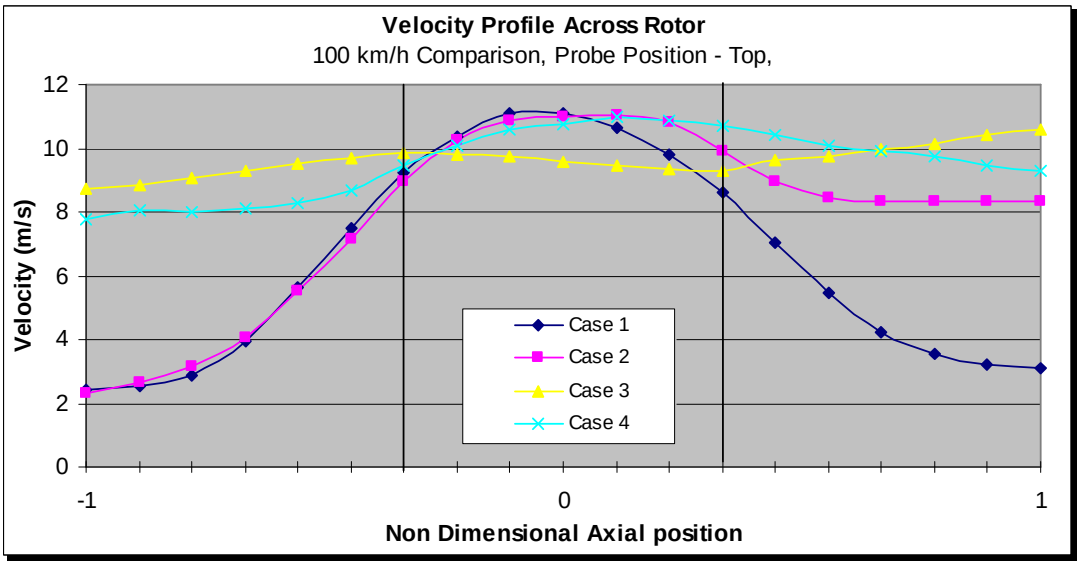

Figure 4.5.2 Comparison of Airflow Through Vented Disc at 100 km/hr (Cases 1-4, probe position Top)

As observed in Figure 4.5.2 (case 4) the effect of external flow on the flow through the vents is significantly reduced by shielding from the vehicle body, and the flow in the vented part of the disc is similar to the wheel and disc test (case 2). It is interesting to note that the maximum measured vent velocity is similar for cases 1, 2, and 4, suggesting that measuring the flow through a disc in still air may give an indication of the flow in normal operation. It can therefore be concluded that although the flow through the vents is affected by external airflow, some airflow still occurs through segments of the disc, even at higher speeds. Therefore a measurable improvement in cooling could be found by improving the flow through vented discs, as found by Zhang (1997) and Daudi (1999) and others.

In Figure 4.5.3 and Figure 4.5.4 the lateral and radial angle are also compared at 100km/hr across the four cases. Again apart from case 3 the lateral profiles are very similar, for the radial angles cases 2 and 4 are very similar particularly at the outboard portion of the rotor where the influence of the wheel is most apparent.

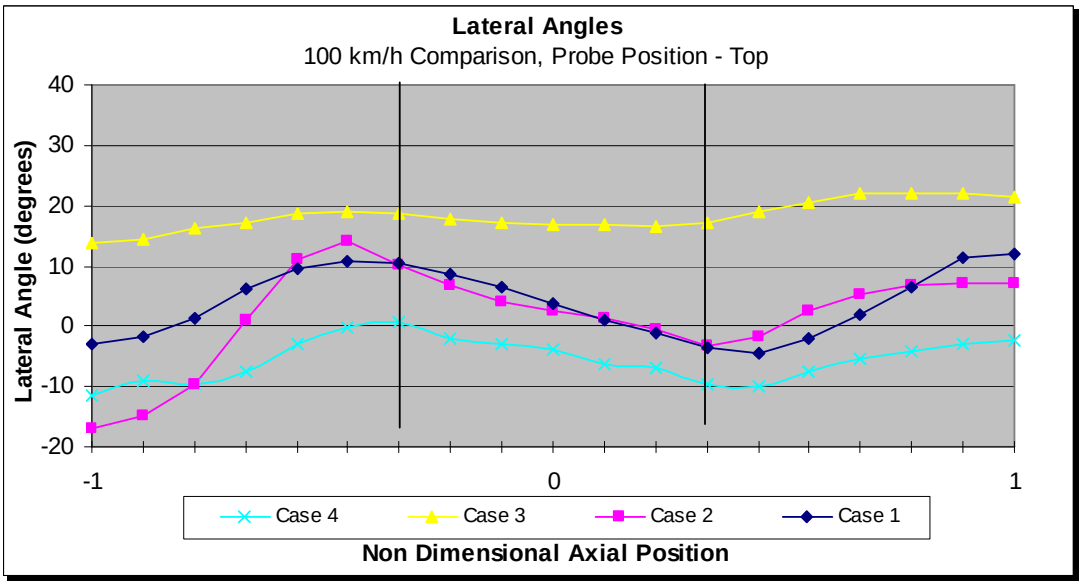

Figure 4.5.3 Comparison of Lateral Angles at 100 km/hr (Cases 1-4, probe position Top)

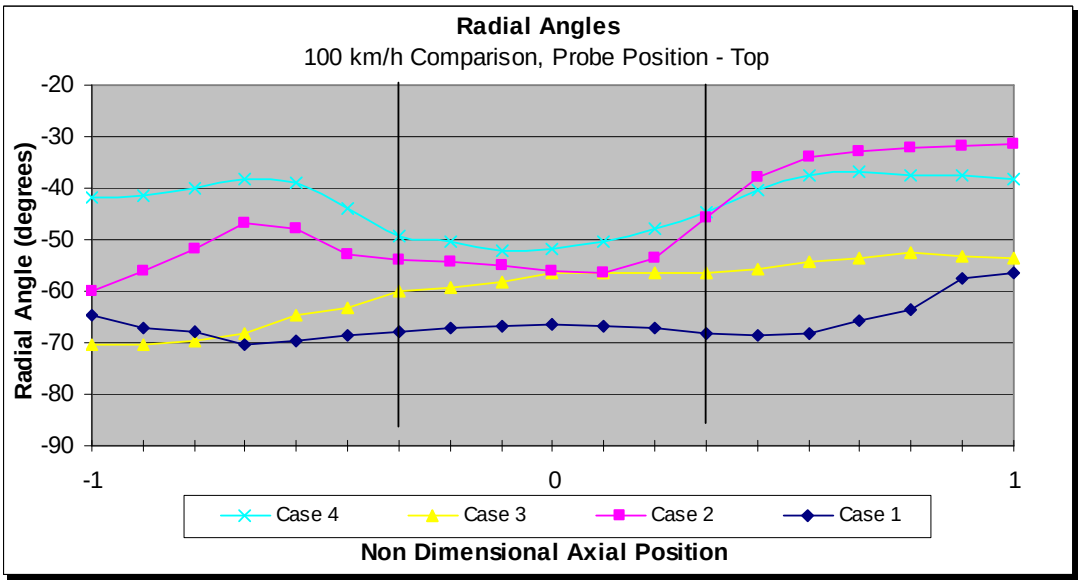

Figure 4.5.4 Comparison of Radial Angles at 100 km/hr (Cases 1-4, probe position Top)

The results also highlight a contradiction, in the effect of the body shielding created by the vehicle body improves the conditions for the vented disc to operate, (compare case 3 with case 4). This also has the effect of reducing the airflow around the outer surfaces or the disc reducing the overall cooling air interacting with the disc. There may therefore be a greater gain in cooling by increasing the airflow into the region of the brake disc, than

what is gained by vented discs, although this will negatively impact on the vehicles aerodynamic drag. It is likely that the vent area of the wheel will also play a significant role and should also be considered. Vented rotors may well have the best use in vehicles where the external flow is restricted in the area around the brake rotor, including low drag hybrid or electric vehicles.

CHAPTER FIVE

5 ON-VEHICLE TESTS

5.1 Introduction

In the previous chapter, tests were conducted on the airflow through a vented brake disc in order to obtain an understanding of factors that influence this airflow. However, as this airflow is designed to improve the thermal performance of the braking system, any evaluation must also incorporate some measure of thermal performance. In the series of tests described in this Chapter, the thermal performance of various brake discs were examined, and a range of parameters that affect the cooling of brakes were evaluated. These parameters include; the size and type of the brake disc chosen, the effects of wheel type (both material and vent area), as well as the cooling performance at various road speeds. All vehicle brake testing was conducted in the RMIT Industrial Wind Tunnel, and used the brake test facility. Full details of the equipment and experimental procedure are given in Chapter 3.

5.2 Experimental Set-up and Blockage Correction

As the test section of the RMIT Industrial Wind Tunnel is limited in size, the presence of a full-size vehicle produces a very high blockage ratio, therefore careful consideration was given to ensure the local flow simulated in the wind tunnel matched the on-road condition. Typical blockage ratios for full-scale automotive wind tunnels are between 5 and 10%, although blockage ratios of up to 20% have been used, (Hucho 1998). The blockage ratio for the vehicle being tested within the RMIT Wind Tunnel is approximately 30%. Therefore matching the upstream flow in the wind tunnel to the equivalent road speed would not provide a true representation of the flow field over the vehicle. A simple solution would have been to use the continuity equation to correct the up stream wind velocity to obtain the required flow velocity around the vehicle. However this would not

factor in such things as boundary layer effects on the tunnel wall and floor, or local accelerations around the side or top of the vehicle. It was decided that it was not possible or necessary to simulate the flow over the entire vehicle, and the flow was only simulated accurately in the region of the brake disc.

In order to get a more accurate representation of the flow field in the region of the rear brake a series of road tests were conducted where the actual local airflow velocity was measured relative to the vehicle. The airflow was measured using a pitot static tube connected to a differential pressure transducer, for calibration of the transducer see Appendix A.4. The pitot static tube was attached to the vehicle (800 mm forward of the rear axle, 200 mm above the ground and 80 mm out from the rear wheel) as shown in Figure 5.2.1.

Figure 5.2.1 Local Velocity Measurement Using a Pitot Static Tube

The vehicle was driven at a series of set speeds 40, 60, 80, 100, and 120 km/hr, under calm on-road conditions. The differential pressure (P_1-P_2) values taken from the pitot-static tube were recorded at these speeds. The tests were repeated a number of times driving the vehicle in both north and south directions, to reduce errors and any effects of

atmospheric winds. The results of this test are summarised in Figure 5.2.2, and full details are given in Appendix D.

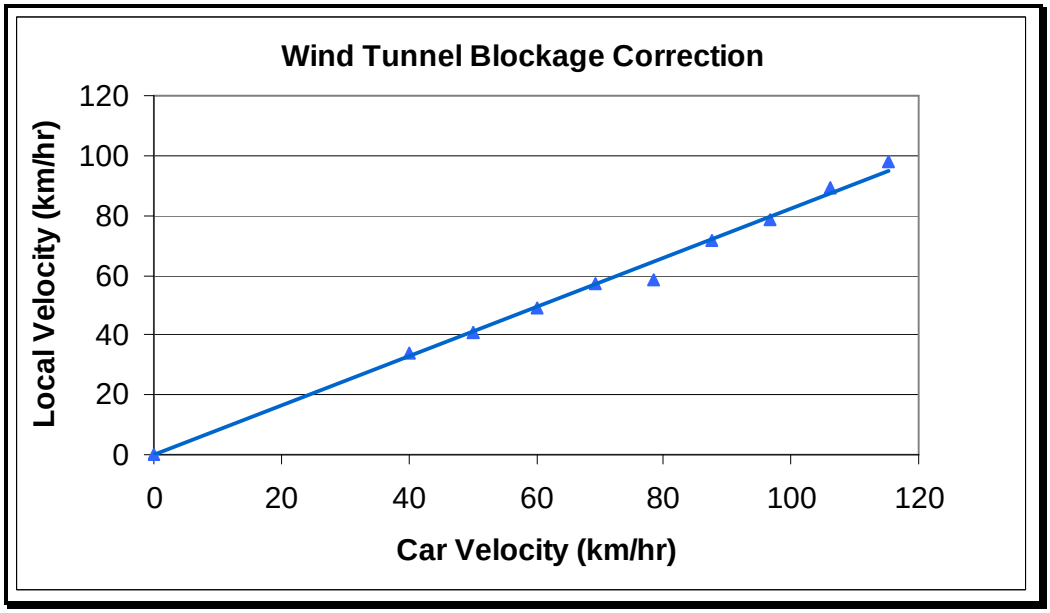

Figure 5.2.2 Wind Tunnel Blockage Correction

When performing the wind tunnel tests the pitot tube was retained and the local flow speed was matched with the recorded on-road measurements for the particular vehicle velocity required. In this way a close simulation of the local flow field was obtained in the wind tunnel. Exact representation was not possible, mainly due to the absence of a rolling road, however the rotation of the wheel at the correct relative speed provided wheel ventilation similar to the on-road characteristic.

5.2.1 Vehicle Set-up

The test vehicle was placed in the Wind Tunnel with its rear right wheel positioned in the brake test rig as shown in Figure 3.3.3. The test wheel brake line was disconnected from the vehicle and connected to the external brake applicator to enable actuation of the brake externally. In order to protect the vehicle's transmission the drive shaft was disconnected at the differential. The vehicle was anchored to the floor to prevent any movement during testing.

The experimental instrumentation included either one or two disc brake thermocouples, positioned on the centre of the rubbing path of the disc as shown in Figure 5.2.3, an

optical tachometer to determine rotational velocity of the wheel, and a torque transducer to determine brake load. The brake load and rotational velocity were displayed on dedicated displays, while the outputs from the thermocouples were logged on the Fluke Hydra data acquisition unit. Calibration reports for all instrumentation are given in Appendix A.

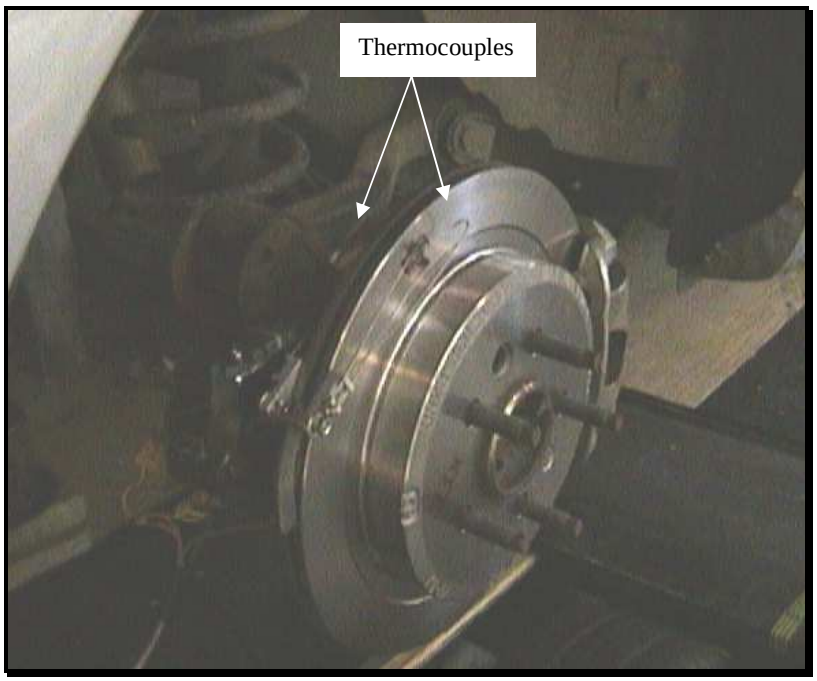

Figure 5.2.3 Position of Thermocouples on Disc

As this phase of the testing was carried out to evaluate the thermal performance of the braking system it was important that all the tests were performed under similar initial conditions. Prior to any testing, the braking system was put through a number of heating and cooling cycles. This ensured that the residual heat in the brake and thermally linked components was similar for the start of each test.

5.3 Contribution of Wheel to Brake Disc Cooling

This set of experiments was designed to determine the effect the wheel has on the cooling of the brake disc. The tests were conducted at an equivalent road speed of 50 km/h with an appropriate wind velocity to account for blockage. In order to evaluate the thermal storage properties of the wheel and aerodynamics effects of airflow through the wheel

three different wheels were tested. The parameters changed included; wheel material, size and vent area. The combination of experiments undertaken is outlined in Table 5.3.1.

Brake Disc Cooling Test

Disc Type	Velocity (km/hr)	Wheel	RPM	Modifications
287 mm Solid	50	Std. 15" Steel	424	
287 mm Solid	50	Std. 15" Steel	424	Open Area Blocked
287 mm Solid	50	15" Alloy	424	
287 mm Solid	50	15" Alloy	424	Open Area Blocked
287 mm Solid	50	Std. 15" Steel	424	Hubcap on
287 mm Solid	50	Std. 15" Steel	424	Hubcap on Holes Blocked
287 mm Solid	50	16" Steel	408	Open Area Blocked
287 mm Solid	50	16" Steel	408	Open Area Blocked
287 mm Solid	50	15" Steel	408	Elongated Holes

Table 5.3.1 Wheel Tests Undertaken

5.3.1 Test Procedure

These tests were performed by rotating the wheel at a constant RPM as shown in Table 5.3.1, (equivalent to a road speed of 50 km/h) while applying a brake load of approximately 75 Nm to heat the disc to 500°C. Once the required temperature was reached, the wind tunnel was set to the equivalent road speed, and the brake load was released. The disc temperature was recorded in 3-second intervals until its temperature dropped below 100°C.

5.3.2 Test Results

The effects of the parameters were analysed by observing the cooling (both rate and total time) of the disc from a temperature of 470°C to 100°C. Figure 5.3.1 shows the cooling of the 287 mm brake disc, with various combinations of wheel. The temperature shown was measured by a single disc brake thermocouple on the outboard surface of the disc.

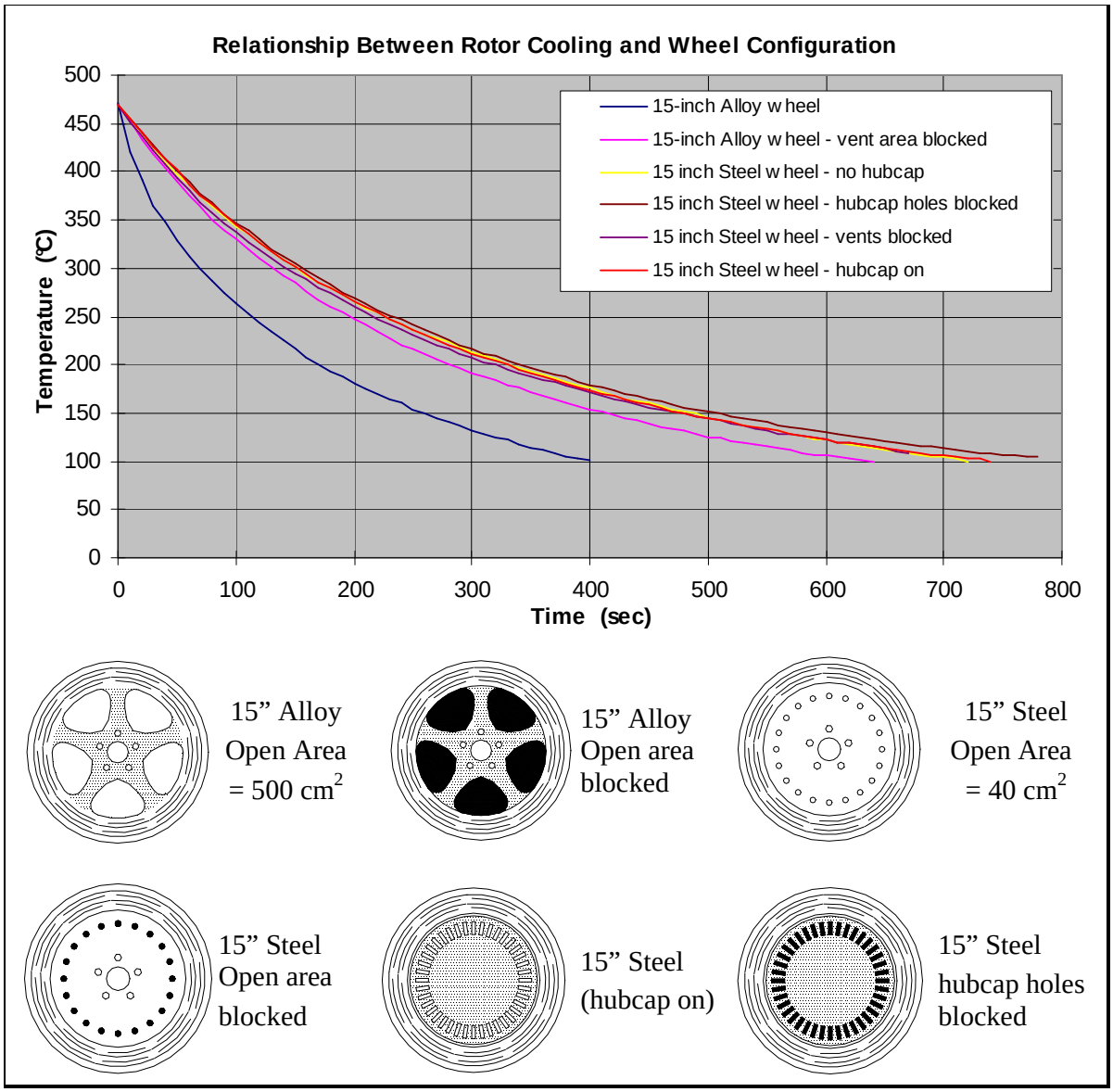

Figure 5.3.1 Wheel Type Effect on Disc Cooling

Clearly from this chart it can be seen that the best cooling is achieved by using an alloy wheel with a open area of 500 cm^2. However when the test is repeated with the open area of the alloy wheel blocked, almost all the cooling advantage over the steel wheel is lost. This would indicate that the larger influence on disc cooling is the increased open area and not the thermal capacitance of the wheel material. The increased open area of the alloy wheel allows more airflow around the outboard surface of the disc, as well as flow through the wheel. It is also likely that heat is conducted away from the disc into the wheel more effectively with an alloy wheel. The wheel is then in turn cooled by airflow through the larger open area, which does not happen when the open area is blocked. It is

also noted that the cooling curves for the various combinations of steel wheels are very similar. The open area of the standard 15" steel wheel is only 40 cm^2, blocking these holes makes very little change in cooling[3]. It would also appear from this graph that the inclusion of the plastic wheel cover slightly increases the overall cooling time, but is not of major significance.

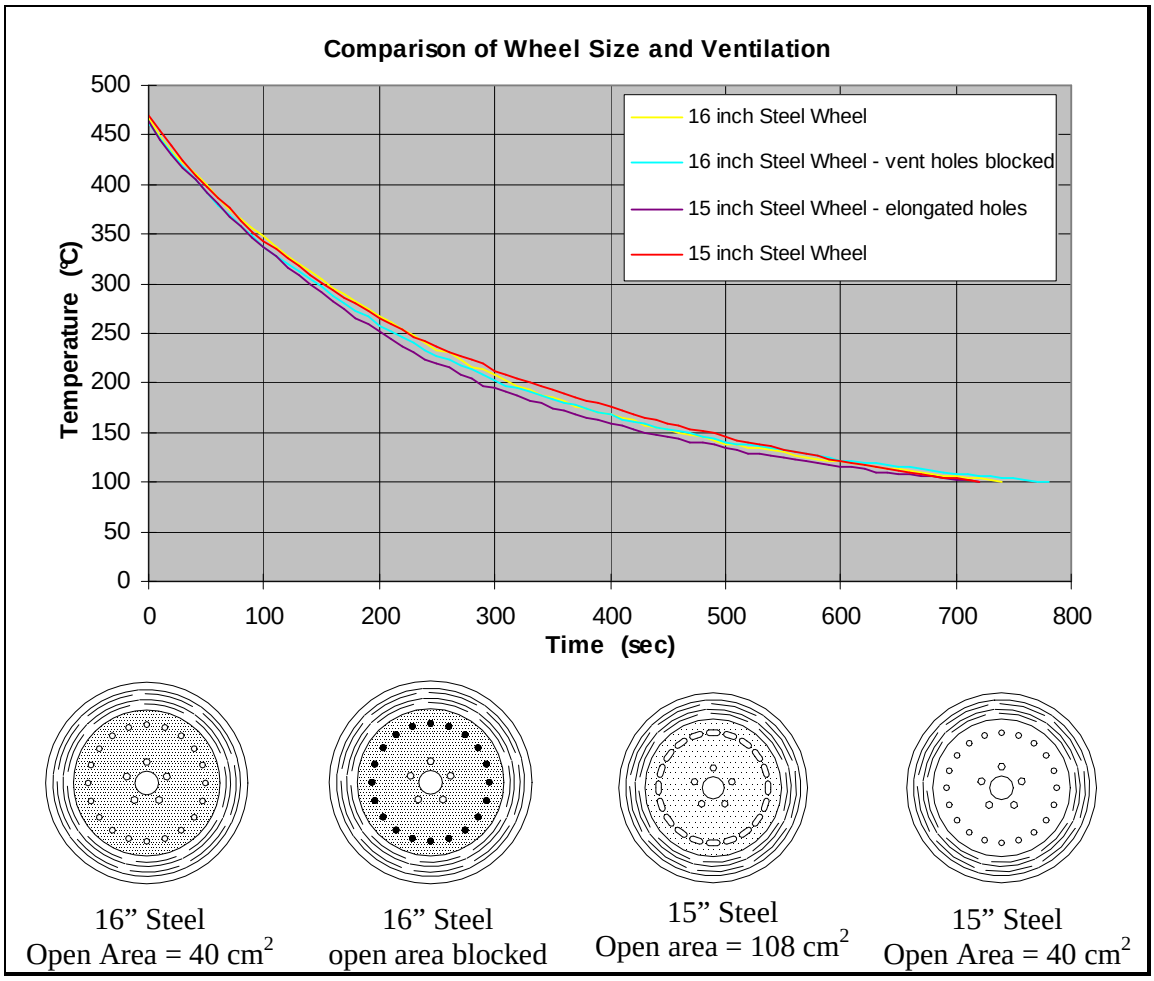

Figure 5.3.2 Wheel Size and Open Area Effect on Disc Cooling

Figure 5.3.2 shows the standard 15" wheel (open area = 40 cm^2) compared to a wheel that has its open area increased to 108 cm^2 by elongating the vent holes. The chart also shows the cooling time for a larger 16" diameter wheel, both with vent holes open and blocked. As can be seen this small increase in open area appears to increase the cooling rate at higher temperatures, although there is little effect on the overall cooling time. The result

[3] Garrett, D. and W. Munson (1983). Cooling of brakes-a conflict of interests. Braking of Road Vehicles, University of Technology, Loughborough, The institute of Mechanical Engineers. recommended a minimum vent area for a medium size family car be 70 cm^2.

of using a larger diameter wheel has little impact on cooling rate or time. A larger wheel may also mean a larger rolling diameter, which will decrease the rotational velocity of the wheel, reducing any possible airflow created by the rotation of the wheel. This should be considered when using vented discs, as vent airflow was found to be proportional to rotational velocity see Figure 4.4.2.

5.4 50 Nm Constant Load Test

The objective of this test was to determine the influence of the disc (both size and type) on the thermal performance of the braking system. The thermal characteristics of three different brake discs were measured under a continued constant speed braking condition, simulating a down hill driving event.

5.4.1 Test Procedure

The wind tunnel and brake rig were set to an equivalent road speed of 60 km/hr. A 50 Nm brake load was applied and kept constant for a ten-minute period. This is equivalent to the brake load on the rear wheel of a one tonne vehicle descending a 1 in 10 slope, at a constant speed of 60 km/h, see Appendix E. The temperature of the disc was recorded throughout this period. The procedure was repeated for three discs, the 303 mm vented disc, an equivalent 303 mm solid disc and a smaller 287 mm solid disc. Table 5.4.1 shows the tests undertaken.

Constant Load Test			
Disc Type	**Velocity**	**Wheel**	**Open Area**
303 mm Vented	60 km/h	Std. 15”	40 cm^2
303 mm Solid	60 km/h	Std. 15”	40 cm^2
287 mm Solid	60 km/h	Std. 15”	40 cm^2

Table 5.4.1 Brake Discs Used in Constant Load Test.

5.4.2 Test Results

Figure 5.4.1 shows the measured temperature response of the discs in this test, which is an average of the inboard and outboard disc surface temperatures.

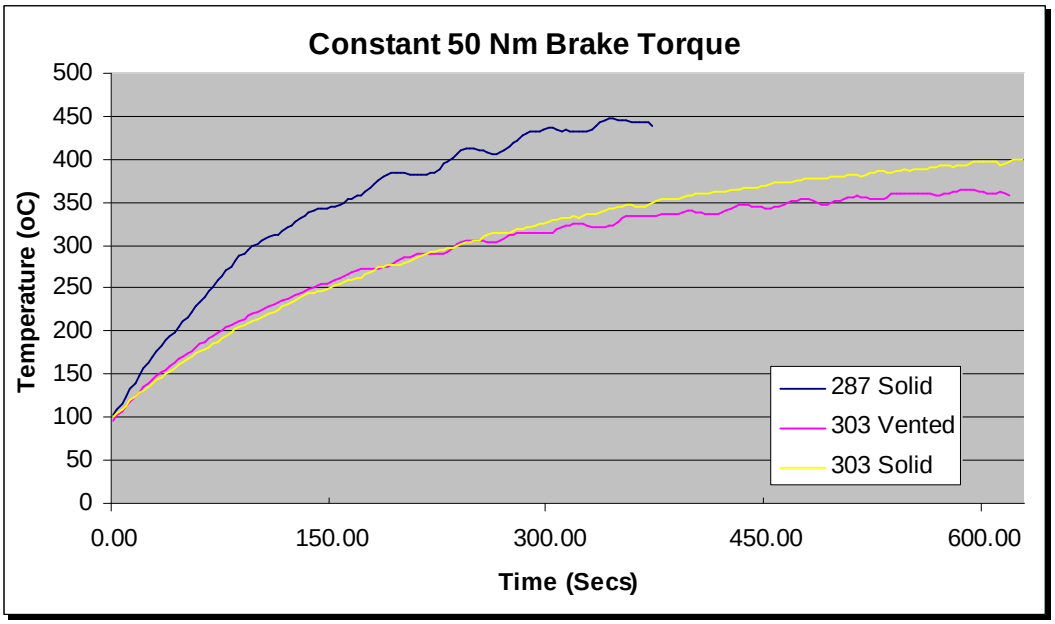

Figure 5.4.1 Temperature Response of Brake Discs Under Constant Brake Load at 60 km/h.

It can be seen Figure 5.4.1 that both 303 mm discs (solid and vented) appear to follow very similar curves, particularly at lower temperatures. Both these discs are similar in mass and therefore have similar thermal storage capacities, and can absorb more thermal energy than the smaller 287 mm disc. At temperatures above 250°C the temperature of the solid 303 mm disc begins to rise faster than the equivalent vented disc. As convective heat transfer is dependent on both surface area and temperature difference, the extra surface area (combined with the airflow through the vents) in the vented disc enables it to dissipated heat more effectively at higher temperatures. Clearly in this type of braking situation the larger 303 mm discs offers much better thermal performance than the smaller 287 mm disc. It would also appear that in such a braking operation the thermal capacity of the disc is the major factor in determining the time to reach critical temperature. The uneven nature of the 287 mm curve at high temperatures is due to a cycle of thermal expansion of the disc and fluid creating increased braking (as the external brake applicator was not a constant pressure device), which is then corrected by reducing the brake load slightly, and the process is repeated.

When comparing these three discs, an examination of the rate of temperature rise alone can be misleading, as the thermal capacity, and hence the mass of the disc will determine the time at which the brakes will reach a critical temperature. Table 5.4.2 shows the projected times to reach a critical temperature of 500°C if this braking operation were allowed to continue.

Brake Disc	Mass (kg)	Curve Function	Time to Critical Temp (mins)
287 Solid	5.14	$y = 78.263x^{0.3708}$	7.43
303 Solid	7.34	$y = 68.835x^{0.3326}$	19.42
303 Vented	7.75	$y = 77.476x^{0.2994}$	24.94

Table 5.4.2 Comparison of Time for Brake Discs to Reach Critical Temperatures

From the above table it appears that there is a significant advantage in using a vented disc over a solid disc in this type of braking operation, with the vented disc taking about 30% more time to reach the critical temperature than the equivalent solid disc. At the end of such a braking cycle the dissipation rate of this heat is vital to ensure that the brakes are capable of satisfactory performance when required again.

5.5 Brake Disc Cooling Tests

In these tests various parameters that effect the cooling performance of brake discs were examined, these parameters included the disc, size and type; the velocity of the vehicle; and the contribution of the wheel on disc cooling.

5.5.1 Test procedure

The procedure for these tests is similar to the procedure outlined in section 5.3.1. However in these tests the wheel was unchanged, while the velocity and disc was changed. Thermocouples were placed on both inboard and outboard disc surfaces. Table 5.5.1 shows a matrix of the tests undertaken.

Brake Disc Cooling Test			
Disc Type	**Velocity (km/hr)**	**Wheel**	**RPM**
287 mm Solid	40	Std. 15” Steel	339
287 mm Solid	60	Std. 15” Steel	509
287 mm Solid	80	Std. 15” Steel	679
303 mm Solid	40	Std. 16” Steel	326
303 mm Solid	60	Std. 16” Steel	490
303 mm Solid	80	Std. 16” Steel	653
303 mm Vented	40	Std. 16” Steel	326
303 mm Vented	60	Std. 16” Steel	490
303 mm Vented	80	Std. 16” Steel	653

Table 5.5.1 Experimental Matrix for Disc Cooling Tests

5.5.2 Experimental Results

The cooling curves shown in Figure 5.5.1 are for the above brake discs, cooling from a temperature of 470°C to 100°C at a constant speed of 60 km/h. The temperatures shown are an average of the inboard and outboard disc surface temperatures.

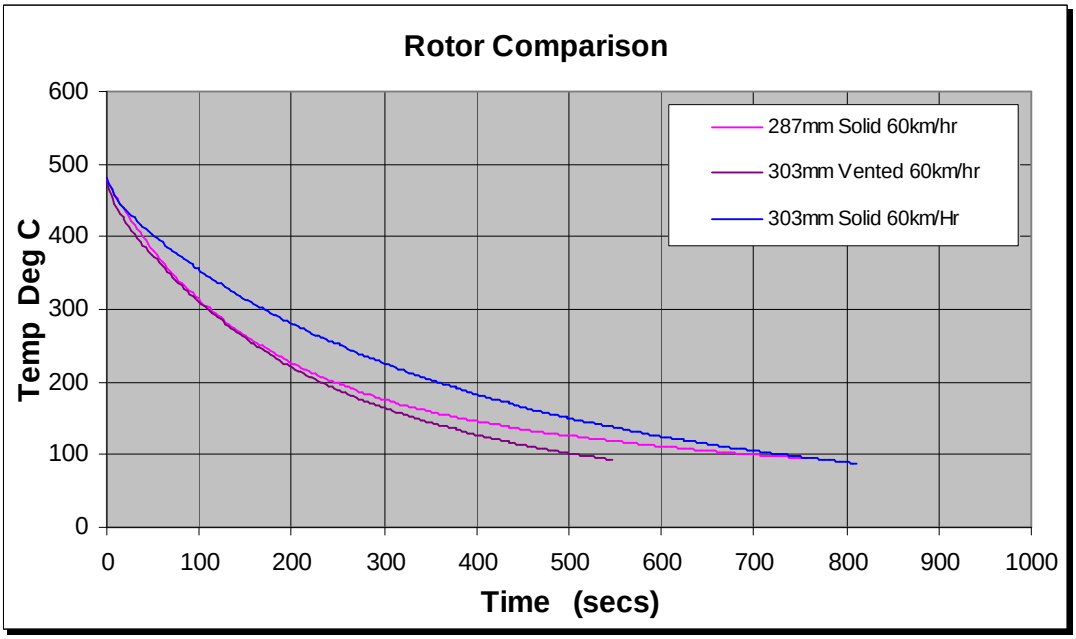

Figure 5.5.1 Disc comparison at 60km/h

It can be seen from these cooling curves that although the total cooling time for both solid discs are similar; at higher temperatures the cooling rate of the smaller (287 mm) disc cools is much greater that larger solid disc. At higher temperatures the cooling rate of the 287 mm solid and the 303 mm vented discs are similar, and it is only at temperatures below 280°C that the vented disc begins to cool more rapidly. Comparing the two 303 mm discs, the vented disc appears superior in both cooling rate and overall cooling time, however at lower temperatures <200°C, their cooling rate appears to be similar, supporting the findings of section 5.4.2, that additional cooling from the vented disc is greatest at higher temperatures. Although cooling from the same temperature, the quantity of heat stored or dissipated by each disc is not equal; the discs with the greater mass will have the greater thermal energy stored. Therefore although the curves appear very similar for both solid discs, the quantity of heat dissipated by the large (303 mm) disc is about 40% greater, see Table 5.5.2. On examination of this table the heat dissipation of the vented disc is even greater when the rate of heat dissipation rate is examined.

The quantity of heat lost from the disc during the cooling period is given by the following formula:

$$Q = MC_P\Delta T \qquad \textbf{- Equation 5.5.1}$$

Where:

Q = *heat lost by rotor* (J)

C_P = *specific heat capacity cast iron.* $(0.42\frac{kJ}{kgK})$

M = mass of rotor (kg)

ΔT = temperature change in rotor (K)

Disc Type	Mass (kg)	Heat Dissipation (J)	Average Rate of Heat Dissipation (kW) (at 60 km/h)
303 Solid	7.34	1171464	1.604 kW
303 Vented	7.75	1236900	2.356 kW
287 Solid	5.14	820344	1.155 kW

Table 5.5.2 Comparison of Heat Dissipation from Discs

In Figure 5.5.2 and Figure 5.5.3 the curves for 40 km/h and 80 km/h are presented respectively. It can be seen from these graphs that similar profiles occur as for the 60 km/h case already shown.

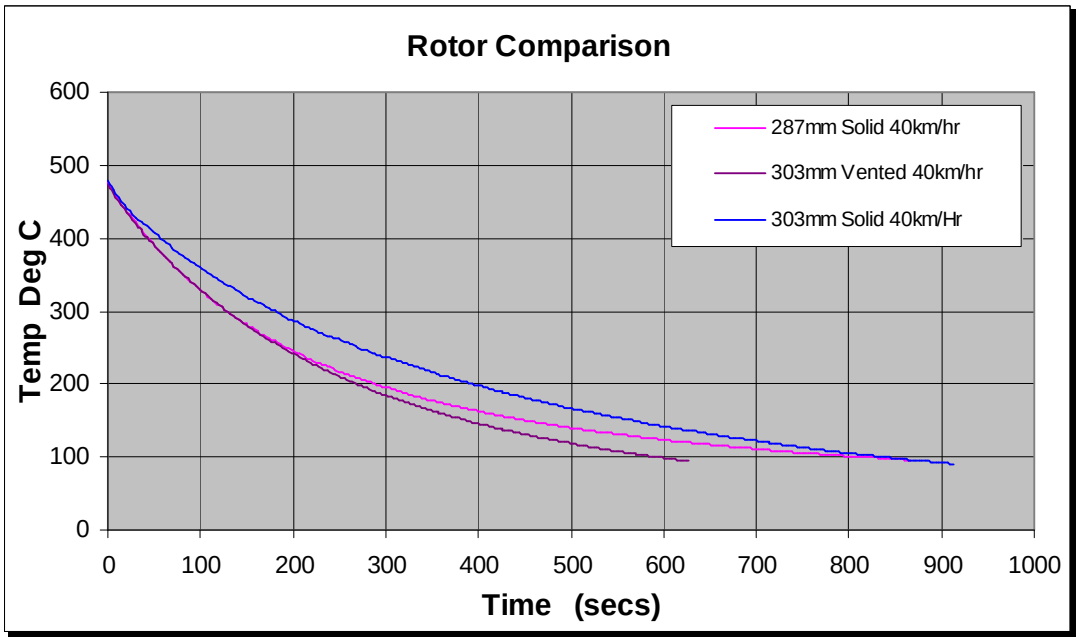

Figure 5.5.2 Disc comparison at 40km/h

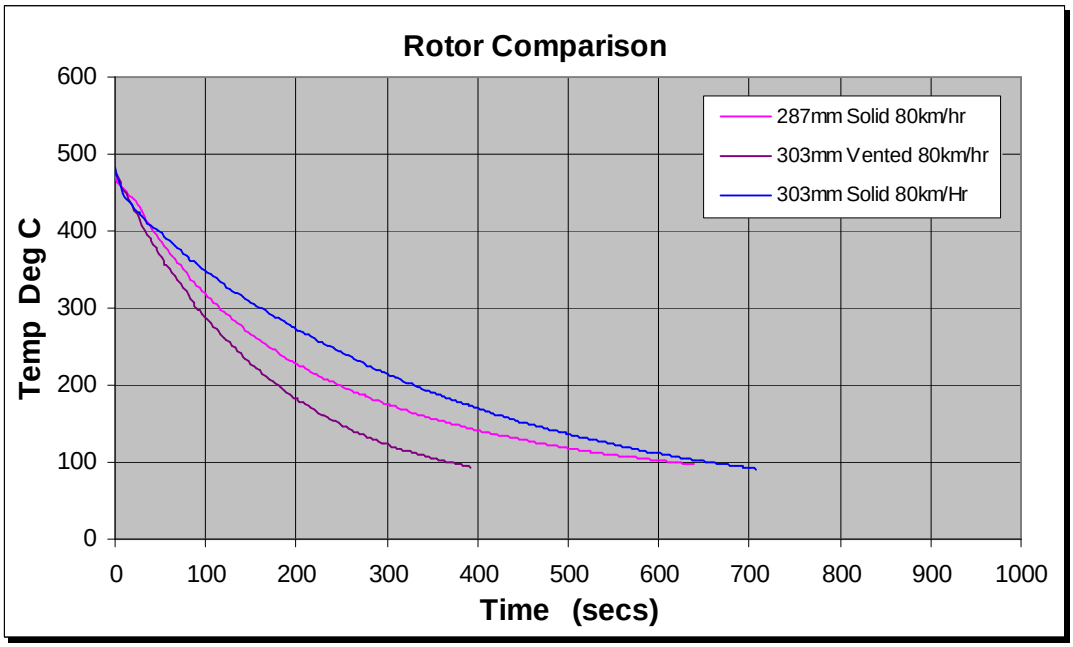

Figure 5.5.3 Disc comparison at 80km/h

Clearly from these charts the vented disc offers considerable improvements in overall cooling time from 480°C to 100°C (approx. 40%) over both solid discs at all speeds. It can also be seen that, the overall cooling time reduces with increasing velocity. This can

be seen more clearly in Figure 5.5.4, where overall cooling time is plotted against vehicle velocity.

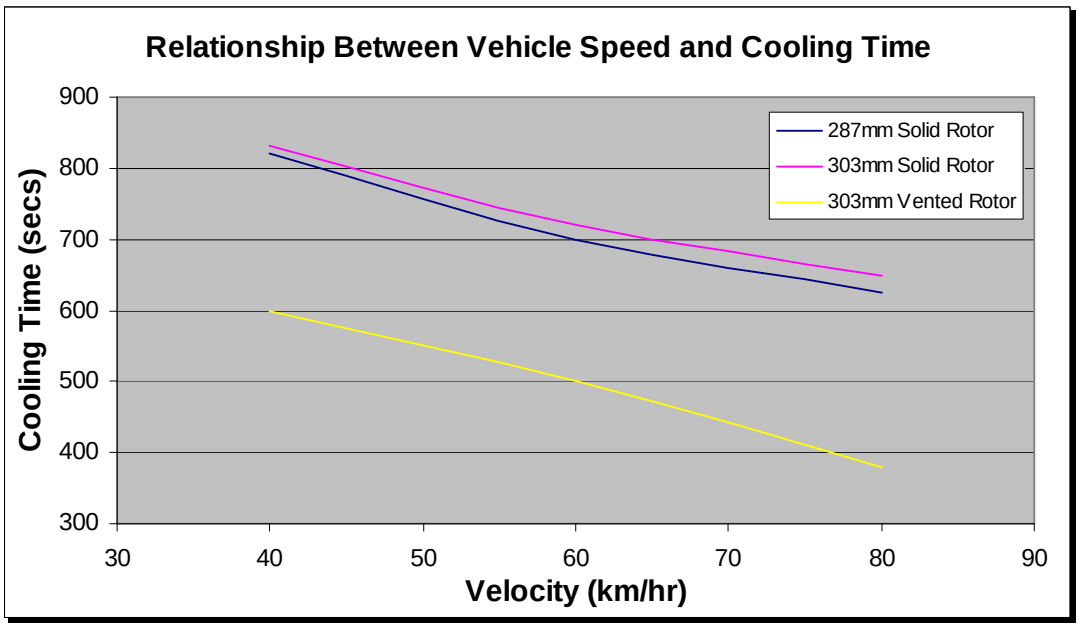

Figure 5.5.4 Relationship between cooling time and vehicle speed.

The overall cooling time from 480°C to 100°C is shown in Figure 5.5.4 for all three discs at the speeds examined. The chart shows that an increase in speed of 20 km/h of the vehicle will decrease the overall cooling time by about 20%. The cooling time for both solid discs are very similar, and reduce proportionally with speed. The overall cooling time for the smaller 287 mm disc is slightly quicker, although with less heat dissipation. It is interesting to note that the vented disc provides superior cooling at all speeds, and does not appear to be affected by the external airflow. Performance of the vented disc appears to slightly improve at higher speeds, contrary to what is suggested by some of the literature. However it should be remembered that these tests were performed on the rear wheel of a vehicle, where the external flow has already had significant interaction with the vehicle, before reaching the brake disc. This may not be the same for vented discs operating on the front of vehicles, as airflow may be directed into the wheel cavity.

5.5.3 Temperature Distributions in Brake Disc

5.5.3.1. Axial Temperature Differences

The disc temperatures given above are an average of the inboard and outboard disc surface temperatures. However, it was found that there could be significant temperature difference (axial and radial thermal gradients) between these two disc surfaces. These temperature differences can result in uneven thermal expansion, which may to lead thermal cracks or deformation of the disc. The following charts (Figure 5.5.5, Figure 5.5.6, and Figure 5.5.7) present the temperature difference between the inboard and outboard surfaces as a function of average disc temperature.

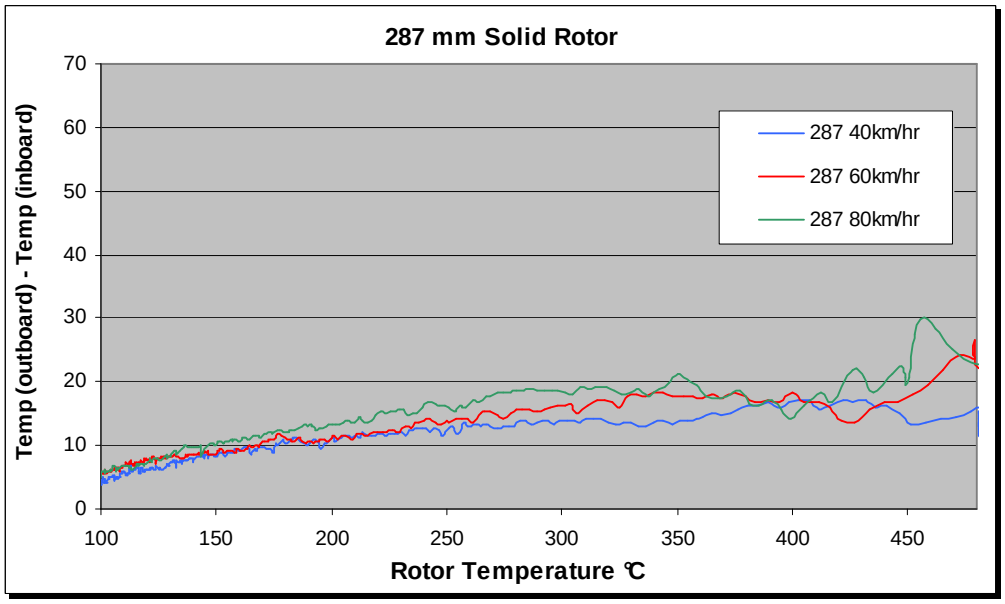

Figure 5.5.5 Surface Temperature Differences on 287 mm Solid Disc

From Figure 5.5.5 it can be seen that the outboard disc surface has a consistently higher temperatures than the inboard disc surface. This temperature difference is slightly greater at elevated disc temperatures and higher velocities, with a maximum temperature difference of 30°C recorded at a disc temperature of 460°C. It appears that greater cooling may be achieved on the inboard disc surface as a result of airflow entering the wheel cavity from underneath the car body, whereas the outboard surface is shielded by the wheel and receives much less airflow. As this test was performed using a wheel with a vent area of only 40 cm^2, therefore it is likely that very little airflow is achieved around

the outboard surface of the disc. This supports earlier findings that suggested superior cooling was provided with greater wheel ventilation.

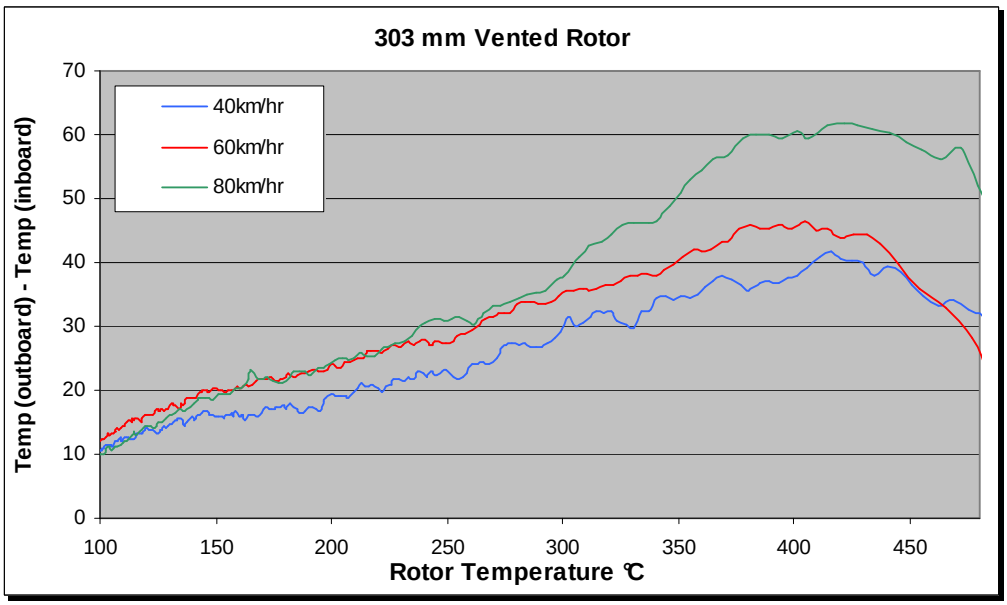

Figure 5.5.6 Surface Temperature Differences on 303mm Vented Disc

Figure 5.5.6 shows the measurements from the 303 mm vented disc. The temperature differences are more significant with the maximum difference found to be about 60°C, again temperature differences are found to be greater at higher velocities and temperatures, with a peak temperature difference appearing at about 425°C. At disc temperatures above 425°C the temperature differences in the disc surfaces appear to reduce, which may be as a result of conduction and radiation effects at high temperatures.

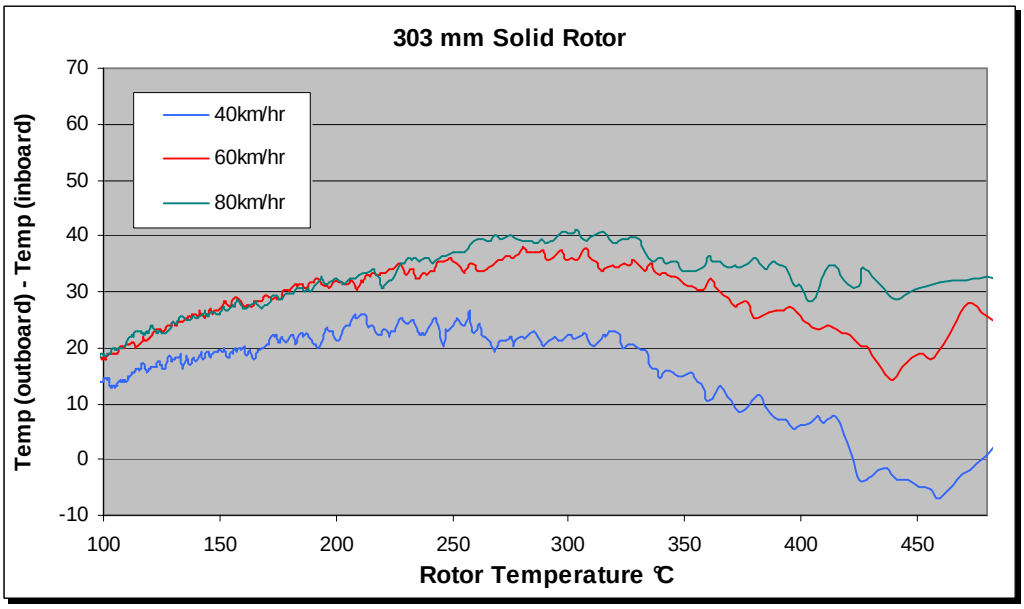

Figure 5.5.7 Surface Temperature Differences on 303 mm Solid Disc

The pattern is similar for the 303 mm solid disc with the outboard side rising to a maximum of 40°C higher than the inboard at about 300°C Figure 5.5.7. However for the 40 km/h case the inboard disc temperature actually exceeds the outboard temperature by about 8°C at a disc temperature of 450°C. It is likely that a more uniform temperature distribution exists in solid discs, as heat flow is not interrupted by air gaps that are present in vented discs.

The results of these plots appear to confirm earlier results, which indicate that larger vent areas in the wheel significantly improve cooling, as temperatures are almost consistently higher on the disc surface facing the wheel. The highest temperature difference recorded between the inboard and outboard surface was only 60°C, which would only cause an approximate 0.2 mm difference in diameter from inboard to outboard surface[4]. This is not large enough to cause any significant thermal deformation.

---

[4] $\Delta D = D \times \alpha_{cast\ iron} \theta$

Where: D = *Outer diameter of rotor (303 mm)*
α = *Thermal Expansion co-efficient of cast iron (12 x 10^{-6} K^{-1})*
θ = *Temperature Change (60 K)*
Therefore:

$$\Delta D = 303 \times 12 \times 10^{-6} \times 60$$
$$= 0.22mm$$

5.5.3.2. Radial Temperature Differences on Disc Surfaces

In Figure 5.5.8 a sequence of thermograms are presented, which provide a visual display of the thermal behaviour of a disc under load. These images were captured with the wheel rotating and with a brake load being applied gradually. Approximate temperatures of the disc can be estimated from the scale on the side of each image. An emissivity value of 0.64 was used (polished cast iron), which is similar to the rubbing surface of a brake disc; therefore temperatures can only obtained on the disc surface; however the images may be used to qualitatively observe the flow of heat in the surrounding components. General details about each image are given at the side; this includes the emissivity, ambient temperature and the temperature at two points on the disc, SP1, and SP2.

These two points were placed specifically to measure radial thermal gradients on the disc. For ease of understanding a photograph of the area in the thermal is given Figure 5.5.9.

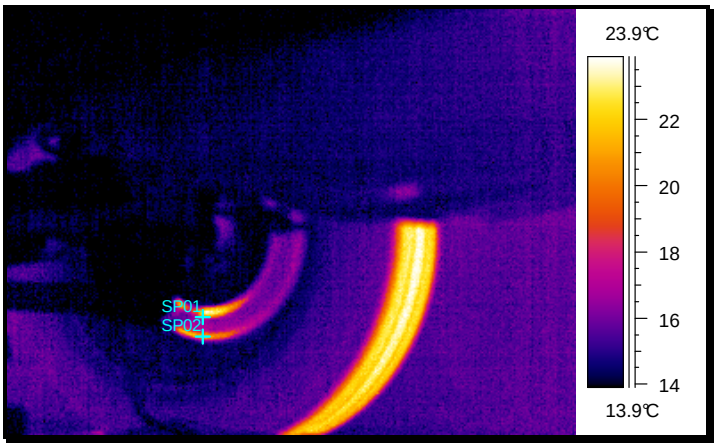

Object Parameter	Value
Emissivity	0.64
Object distance	2.0 m
Ambient temperature	14.7°C

Temperatures	
SP01	18.7°C
SP02	21.0°C

Image (a)

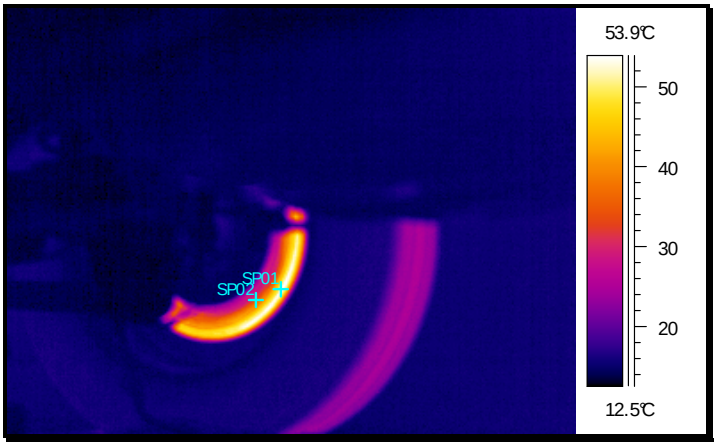

Object Parameter	Value
Emissivity	0.64
Object distance	2.0 m
Ambient temperature	14.7°C

Temperatures	
SP01	53.9°C
SP02	33.8°C

Image (b)

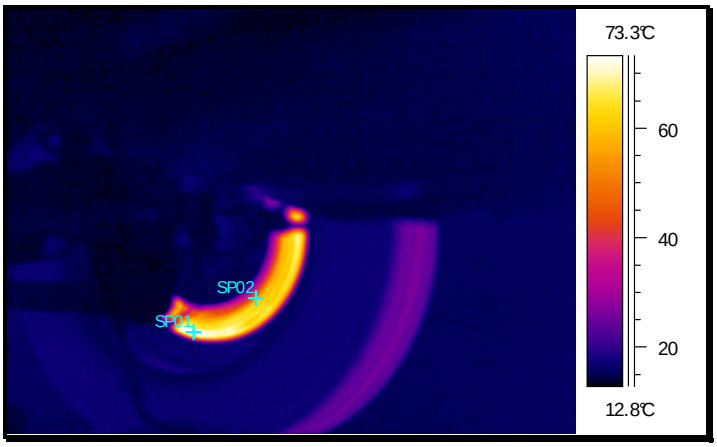

Object Parameter	Value
Emissivity	0.64
Object distance	2.0 m
Ambient temperature	14.7°C

Temperatures

SP01	73.3°C
SP02	54.2°C

Image (c)

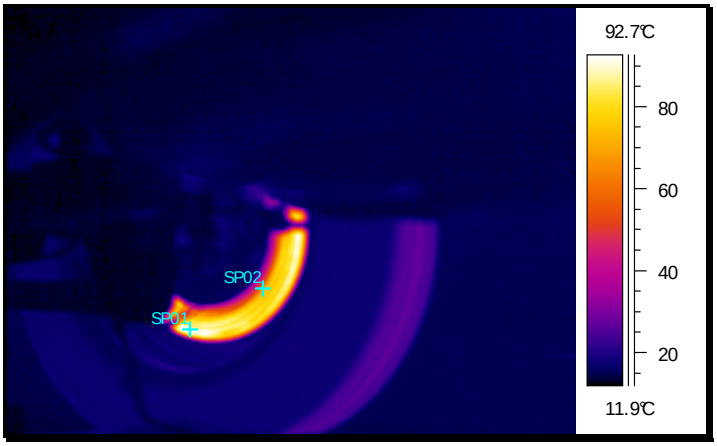

Object parameter	Value
Emissivity	0.64
Object distance	2.0 m
Ambient temperature	14.7°C

Temperatures

SP01 = 92.9°C
SP02 = 68.7°C

Image (d)

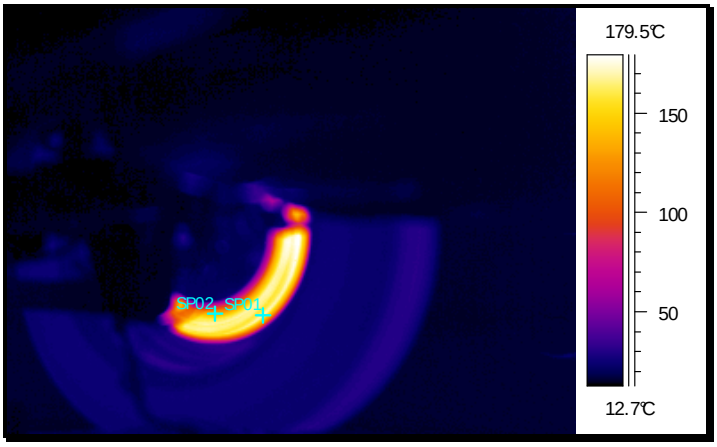

Object Parameter	Value
Emissivity	0.64
Object distance	2.0 m
Ambient temperature	14.7°C

Temperatures

SP01 = 169.5°C
SP02 = 134.5°C

Image (e)

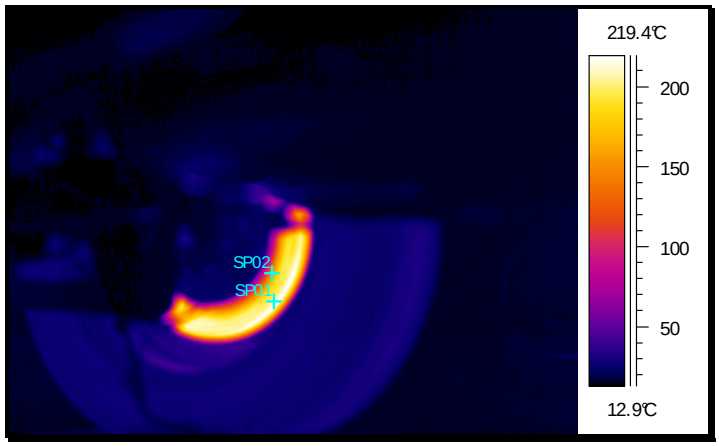

Object Parameter	Value
Emissivity	0.64
Object distance	2.0 m
Ambient temperature	14.7°C

Temperatures
SP01 = 209.6°C
SP02 = 153.9°C

Image (f)

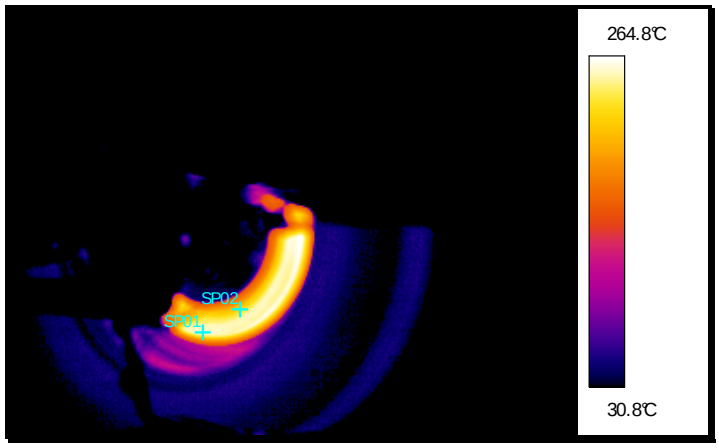

Object Parameter	Value
Emissivity	0.64
Object distance	2.0 m
Ambient temperature	14.7°C

Temperatures
SP01 = 248.6°C
SP02 = 205.9°C

Image (g)

Figure 5.5.8 Thermograms of 287 mm Solid Disc Under Braking

Figure 5.5.9 Area Shown in Thermal Image

Image (a) clearly shows two distinct hot spots on the lower outer edge and inner edge of the disc, as the maximum temperature recorded is only 23°C it's not considered significant. On images (b) (c) and (d), the temperature appears greater at the outer radius of the disc; SP1 and SP2 show temperature differences of approximately 20°C. The images (e), (f) and (g) are taken at higher temperatures, and although the temperature differences on the thermograms are less visually obvious, SP1 and SP2 indicate larger thermal gradients, up to 56°C. There also appears to be some circumferential temperature differences on the disc, this can be observed on the thermograms as a bright spot on the disc. As it was not possible to obtain an image of the entire disc this could not be verified. Also observed on all the images is a cooler ring on the inner radius of the disc, this is a slightly misleading temperature indication as it outside the rubbing path of the brake, and will therefore have a different emissivity value. Heating of the inner surface of the wheel can also be seen in image (g).

5.6 Discussion of Results

It appears from the above results that one of the major influences on the cooling of a brake is the open area of the wheel. The significant reduction in cooling time as a result of using an alloy wheel is due to the large vent area, most of this advantage is lost when airflow through the vent area is prevented. A measurable increase in cooling can also be observed when the open area of a standard wheel is increased from 40 cm^2 to 108 cm^2, indicating the importance of open area to the cooling of brake discs. This supports earlier research by Garrett and Munson (1983) who believed that the vent area should be at least 70 cm^2, for a standard mid size vehicle. However vehicle drag increases with increased wheel vent area, so a compromise may need to be reached between minimum aerodynamic drag and sufficient brake cooling.

The significance of the size and type of disc employed can also be observed in the results. The size and hence mass of the disc will govern its thermal storage capability. Larger discs with greater thermal storage will therefore absorb more energy and will therefore provide more braking before critical temperatures are reached. However larger discs will have a slower cooling rate, which may be of concern during repeated braking operations. In all tests undertaken vented discs offered superior cooling both in terms of overall cooling time and rate of cooling. In the case of the equivalent downhill test, the initial rate

of disc heating appears to be governed by the thermal capacity of the disc, however at higher temperatures the vented disc offers superior performance. In the cooling tests, the extra cooling of the vented disc over a solid disc is more pronounced at higher temperatures. Therefore in braking situations where maximum temperatures are a problem, a solution may be found by switching from solid to vented discs. Interestingly, the cooling capability of the vented disc was evident at all speeds and was not unduly influenced be the external airflow. This may indicate that either airflow still occurs through the vents at higher speeds, or the extra cooling is provided by the additional surface area as suggested by Limpert (1975).

The axial temperature distribution measured also indicates that an insufficient vent area in the wheel may inhibit disc cooling. In almost all cases the temperature of the outboard disc surface was higher than the inboard disc surface. The temperature differences were even greater on the vented disc, as the air vents limit the heat conduction within the disc. Axial temperature differences were also observed, although only the inboard face of the disc was examined. It should be remembered that many aerodynamic cooling aids, such as used in motor racing only provide cooling to one side of the disc, this additional cooling could create temperature differences large enough to distort the disc.

CHAPTER SIX

6 DISCUSSION AND CONCLUSIONS

The objective of this work was to apply similar aerodynamic techniques to the area of brake cooling that have been previously applied to other areas of the vehicle, and hence determine the major aerodynamic factors that influence disc brake cooling. To achieve this, two separate experimental areas of research were developed together with a detailed survey of the previously published material. This chapter brings together all the major findings of the research, and examines how these results build on the previous research and knowledge in this area. The research questions are addressed and the conclusions of the work are developed. Recommendations on how further research could be undertaken to advance the field are also given.

6.1 Discussion

The experiments were performed to gain a thorough understanding of interaction of aerodynamics on disc brake cooling. The parameters evaluated were vehicle velocity, wheel type (both material and ventilation) and rotor type (solid and vented). Air speed velocity and its associated Reynolds number are a major influence in aerodynamics, this research found the vehicle velocity to be the single biggest influence on heat dissipation from brake discs. For all types of test undertaken, the higher the speed the faster the rate of cooling as the airflow into the wheel cavity is increased. At higher speeds greater rotation of the wheel can also force more airflow through the rotor vanes (if any) and through the open area of the wheel. However, it was also found that airflow into the wheel cavity severely disrupts airflow from the vanes, although some flow is evident through the vanes at certain segments of the rotor. Interestingly at higher speeds the relative cooling advantage of vented rotors over solid rotors was slightly greater in the thermal tests. It is possible that at higher speeds the flow through the vanes may be less affected by external flow due to a wake effect of the wheel and other components, but due to the turbulent nature of the flow in this region, it was not possible to determine this in the airflow measurements. However the effect of braking is to reduce the vehicles

velocity which means that improvements in braking cannot be dependent on vehicle speed. The second largest influence was found to be wheel ventilation. In tests where disc cooling is measured under constant 50 km/hr speeds the fastest rate of disc brake cooling was found to be achieved using an alloy wheel with a very large open area. When the test was repeated with this open area blocked, the overall cooling time was increase by about 75%, which made the cooling pattern similar to a standard steel wheel with minimal ventilation. It is interesting to note that in cooling test from 480 to 100°C, a vented rotor took longer to cool at 60km/hr with a standard wheel than a solid rotor at 50 km/hr with an alloy wheel and a large open area ratio, indicating that the additional cooling must therefore be as a result of airflow through the wheel. This is also supported by airflow measurements also which show that the flow generated by the rotation of the wheel to be significant, even in the absence of external flow (sections 4.4.3 and 4.4.4).

The next most influential factor was disc type, both size and type. In general vented discs performed best in all tests, the actual size and hence mass of the disc was also found to be a significant factor. In heating tests (during braking) the initial rate of heating is a function of the thermal storage capacity of the rotor, it was also found that the thermal performance of a solid and an equivalent sized vented rotor was similar. As braking continues and the temperature rises the rotors' ability to dissipate heat becomes more important and the vented rotor showed superior cooling capability. In cooling tests (after braking) it was found that the vented rotors dissipated heat more quickly than a similar sized solid rotor. The relative cooling advantage of vented discs over solid discs was found to be even greater at higher speeds, (section 5.5.4). However in the airflow measurements it was found that there was a direct relationship between flow through the rotor and vehicle speed (see Figure 4.4.2). A significant amount of work in this area has focused upon improving the quantity of air flow through a vented rotor, in order to improve its cooling capabilities. Researchers including Hudson and Ruhl (1997) and Zhang (1997) found that measurable increases in airflow could be achieved though modifications to the design of the rotor. However given that the maximum measured flow through the rotor vents (obtained in still air conditions) is very low relative to the vehicles velocity, and due to the extremely turbulent nature of the results of flow measurements in the tests, it is unlikely that these small increases in flow would be translated to significantly improved cooling of disc brakes. However the results do show that the

overall cooling time for vented rotors was shorter in all situations tested, and at worst the cooling of a vented rotor was similar to its equivalent solid rotor. One disadvantage of vented discs over solid was found to be greater axial temperature differences, particularly at higher temperatures, although the results shown in section 5.5.3 has shown these effects to be minimal. However this may not be the case in more severe braking applications, and axial temperature differences could lead to thermal distortion of the rotor, and its associated problems.

6.2 Conclusions

The main contribution factors to effective automobile brake cooling were found to be vehicle velocity, wheel material, wheel vent area, the thermal storage capacity of the rotor, and rotor type (solid or vented).

- The contribution of the wheel to rotor cooling is considerable; it can not only affect the airflow pattern through a vented rotor, but can improve heat dissipation by conducting heat away from the brake components. Wheel ventilation plays a significant role in brake disc cooling, the larger the open area the greater the cooling effect, (and the greater its contribution to the vehicles drag, (Hucho 1998)). Alloy wheels have much better thermal conduction and storage capabilities than steel wheels, and combined with a usually larger open area will significantly increase the heat dissipation from the brake rotors.

- Vented discs offer superior cooling over equivalent sized solid rotors, approximately 40+% improvements in all the situations tested. Cooling airflow through the internal vanes is affected by external flow, however some airflow can still be measured through some segments of the rotor for most cases tested. It was previously believed that little airflow through vented rotors occurred at high speed due to external air trying to enter the outlet of the vanes, however it is evident that this is not the case, both from the airflow measurements and from cooling tests. Frequency analysis of the flow through a vented rotor showed that there were significant flow disturbances occurring, (vortex shedding), Kubota et al. (2000) also found similar disturbances in this flow. It should therefore be possible to further increase this flow by reducing these disturbances through more aerodynamic shaping of the vanes in the rotor.

However any thermal improvements found may be minimal as other aerodynamic influences may be greater.

- It has been shown that increasing the airflow in the vicinity of the brake will improve its cooling capability, therefore any local aerodynamic aids such as air deflectors will contribute to improved cooling, although these are not widely adopted as they may have a negative influence on aerodynamic drag, and will be most effective at higher speeds and not during braking applications.

- Flow through vented rotors is significantly reduced by air entering the region of the rotor due to the forward movement of the vehicle. However flow will still occur through segments of the rotor even at higher speeds.

- Improvement in vehicle brake cooling can be achieved through improved aerodynamics; however like other areas of vehicle aerodynamics it can not be determined in isolation, as other concerns such as vehicle drag weight all need to be examined.

6.3 Recommendations for Further Research

To further this research a more detailed analysis of the flow in the vicinity of the brake rotor is required; however the physical measurement of this airflow in the vicinity is extremely difficult. As an alternative CFD modelling techniques could be used to study the flow in and around the brake disc, both for solid and vented discs. Thermal effects could also be included in the model to determine rates of disc cooling and heating, thus combining the research conducted in Chapters 4 and 5 of this thesis. CFD modelling would also be capable of determining the relationship between improved brake cooling and vehicle drag, without the need for physical testing. However accuracy of any CFD modelling is dependent on the validity of the boundary conditions for the control volume chosen. In this case the boundary conditions would first need to be defined at positions where the flow condition could be measured, (or reasonably approximated from experimental measurements), such as the inlet and outlet of the wheel arch. Validation of the CFD would also involve further experimental work.

REFERENCES

Axon, L., K. Garry, et al. (1999). "The influence of Ground Condition on the Flow Around a Wheel Located Within a Wheelhouse Cavity." SAE: 149-158.

Baker, A. K. (1986). Vehicle braking. London, Pentech Press.

Blazek, J. (2001) Computational Fluid Dynamics - Principles and Applications, Elsevier 2001.

Bleier, F. P. (1997). Fan Handbook - Selection, Application and Design, McGraw-Hill.

Commonwealth Department of Industry, S. a. R. (2001). Key Automotive Statistics 2001**:** 21.

Cooper, K. R. (1992). Bluff-Body Aerodynamics as Applied to Vehicles. Second International Colloquium on Bluff Body Aerodynamics (BBAA II), Melbourne Australia.

Daudi, A. R. (1998). Hayes high Airflow Design Rotor for Improved Thermal Cooling and Coning., SAE.

Daudi, A. R. (1999). 72 Curved Fin Rotor Design Reduces Maximum Rotor Temperature, SAE.

Daudi, A. R. (1999). 72 Curved Fins and Air Director Idea Increases Airflow through Brake Rotors. International Congress and Exposition, Detroit, Michigan, SAE.

Day, A. J. (1988). "An Analysis of Speed Temperature, and Performance Characteristics of Automotive Drum Brakes." Journal of Tribology **110**: 298 - 303.

Day, A. J. and T. P. Newcomb (1984). "The Dissipation of Frictional Energy From the Interface of an Annular Disk Brake." Proceedings Institute of Mechanical Engineers 198(11): 201-209.

Dinwiddie, R. B. and K. Lee (1998). IR-camera methods for automotive brake system studies. Conference; 20th, Orlando, Florida, SPIE.

Eisengraber, R., J. Grochowicz, et al. (1999). Comparison of Different Methods for the Determination of thr Friction Temperature of Disc Brakes. International Congress and Exposition, Detroit, Michigan, SAE.

Fabijanic, J. (1996). "An Experimental Investigation of Wheel-Well Flows." SAE: 161-172.

Garrett, D. and W. Munson (1983). Cooling of brakes-a conflict of interests. Braking of Road Vehicles, University of Technology, Loughborough, The institute of Mechanical Engineers.

Hooper, J. D. and A. R. Musgrove (1995). "Pressure Probe Measurements of Reynolds Stresses and Static Pressure Fluctuations in Developed Pipe Flow." Twelfth Australasian Fluid Mechanics Conference. Sydney, Australia - Dec 10-15,1995.

Hooper, J. D. and A. R. Musgrove (1997). "Reynolds Stress, Mean Velocity, and Dynamic Static Pressure Measurement by a Four-Hole Pressure Probe." Experimental Thermal and Fluid Science 15(4): 375-383.

Hucho, W.-H. (1998). Aerodynamics of Road Vehicles, SAE.

Hudson, M. D. and R. L. Ruhl (1997). Ventilated Brake Rotor Air Flow Investigation. International Congress and Exposition, Detroit, Michigan, SAE.

Hunter, J. E., S. S.Cartier, et al. (1998). Brake Fluid Vaporization as a Contributing Factor in Motor Vehicle Collisions. International Congress and Exposition, Detroit, Michigan, SAE.

Idogaki, T., H. Kawai, et al. (1987). Measuring System of Transient Temperature Distributions on the Brake Disk Rotor. International Congress and Exposition, Detroit, Michigan, SAE.

Incropera, F. P. and D. P. DeWitt (1996). Fundamentals of Heat and Mass Transfer, Wiley.

Jerhamre, A. and C. Bergstrom (2001). Numerical Study of Brake Disc Cooling Accounting for Both Aerodynamic Drag Force and Cooling Efficiency. SAE 2001 World Congress, Detroit, Michigan.

Jones, R. A., P. L. Cormier., et al. (1995). "Modeling the Cooling of an Automotive Brake Rotor." SAE: 327-332.

Kao, T. K., J. W. Richmond, et al. (2000). "Brake disc hot spotting and thermal judder: an experimental and finite element study." International Journal of Vehicle Design **23**(3/4): 276-296.

Kruger, L. K., K. Boss, et al. (1995). Brake Test Rig for operating Load Simulation, SAE.

Krusemann, R. and G. Schmidt (1995). Analysis and optimisation of Disk Brake Cooling via Computational Fluid Dynamics. International Congress and Exposition, Detroit, Michigan, SAE.

Kubota, M., T. Hamabe, et al. (2000). "Development of a lightweight brake disc rotor: a design approach for achieving an optimum thermal, vibration and weight balance." JSAE Review **21**(3): 349-355.

Lawson, T. (2001). Building aerodynamics. London, Imperial College Press.

Limpert, R. (1975). Cooling analysis of Disc Brake Rotors. Truck Meeting, Philadelphia, Pa., SAE.

Limpert, R. (1975). The Thermal Performance of Automotive Disc Brakes. Automobile Engineering Meeting, Detroit Michigan, SAE.

Limpert, R. (1999). Brake design and safety. Warrendale, Pa., Society of Automotive Engineers.

Little, E., T.-K. Kao, et al. (1998). "A Dynamometer Investigation of Thermal Judder." 81-89.

Noyes, R. N. and P. T. Vickers (1969). Prediction of Surface Temperatures in Passenger Car Disc Brakes.

Rusnak, R. M., H. W. Schwartz, et al. (1970). A Comparision by Thermal Analysis of Rotor Alloys for Automobile Disc Brakes, SAE 700137.

Sheridan, D. C., J. A. Kutchney, et al. (1988). Approaches to the Thermal Modeling of Disc Brakes. International Congress and Exposition, Detroit, Michigan, SAE.

Sisson, A. E. (1978). Thermal Analysis of Vented Brake Rotors. Congress and Exposition, Cobo Hall, Detroit, SAE.

Watkins, S., P. Mousley, et al. (2002). Measurement of Fluctuating Flows Using Multi-Hole Probes. Ninth International Congress on Sound and Vibration, Orlando, Florida , USA.

Watkins, S (2001). Industrial and Vehicle Aerodynamics. Course Notes, School of Aerospace, Mechanical and Manufacturing Engineering.

Westbrook, M. H. (2001). The electric car : development and future of battery, hybrid and fuel-cell cars. London, Institution of Electrical Engineers.

Woodward, A. J., T. Hodges, et al. (1993). Advanced measurement systems for routine assesement of brake performance. Braking of Road Vehicles, Institute of Mechanical Engineers, Birdcage Walk, London, IMechE.

Zhang, J. J. (1995). A methodological Process for Optimising Brake Cooling and Simulation of Brake Rotor Flow Field. 13th Annual Brake Colloquium and Engineering Display, Philadelphia, Pennsylvania, SAE.

Zhang, J. J. (1997). “A High Aerodynamic Performance Brake Rotor Design Method for Improved Brake Cooling.”.

APPENDIX A

CALIBRATION OF INSTRUMENTS

A.1 - CALIBRATION OF COBRA PROBE

The cobra uses four pressure taps to calculate all outputs including velocity and local static pressure; flow angles, and turbulence characteristics; therefore Static pressure calibration of the cobra Probe was performed on a regular basis during the course of the experiments. Static calibration was achieved by applying a known pressure (measured using an inclined tube manometer) to the cobra probe's pressure transducer, and comparing this pressure to the displayed output. If a difference occurs the correct pressure is inputted. This procedure is repeated throughout the expected range of the measurements, in this case 0 to 1000 Pa, approximately equal to 0 - 40 m/s.

A secondary calibration was also performed to ensure accurate readings were obtained from the Cobra Probe. Both the Cobra Probe and a pitot static tube were placed in RMIT wind tunnel and exposed to the same free stream velocity. The results of from both instruments were recorded and are presented in Table A.1 (i). As can be seen the results were found to be extremely similar.

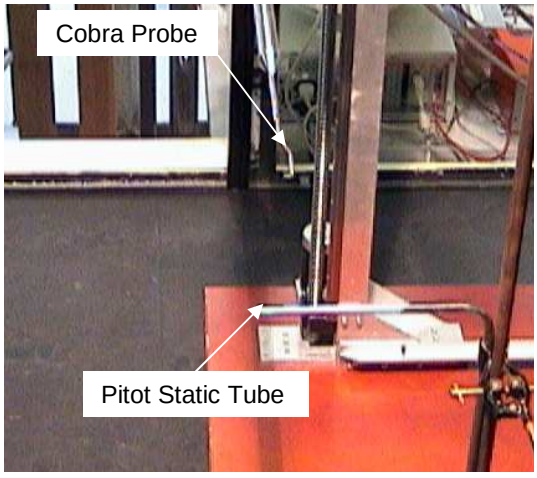

Figure A.1 (i)

Manometer		Cobra Probe
Pt-Ps (Pa)	Vel. m/s	m/s
63.38	10.28	10.19
38.94	8.06	8.25
20.42	5.83	5.92
6.67	3.33	3.12
0.00	0.00	0.01

Table A.1 (i)

A.2 - CALIBRATION OF DISC BRAKE THERMOCOUPLE

In order to establish the accuracy of the thermocouples in measuring rotating disc temperature a comparison was performed between the temperature measurements obtained from the rubbing type thermocouple and a digital thermography camera. The experiments were carried on an open wheel racing car "Formula SAE" rather than the test vehicle in order to have a direct line of sight to the point of temperature measurement see figure A.2(i) .

Equipment used

Formula SAE racing car
RMIT Brake Test Rig
K-Type Rubbing Thermocouple
Flir Digital Thermography Camera
Fluke Data Logger with PC
ThermoCam Reporter Software

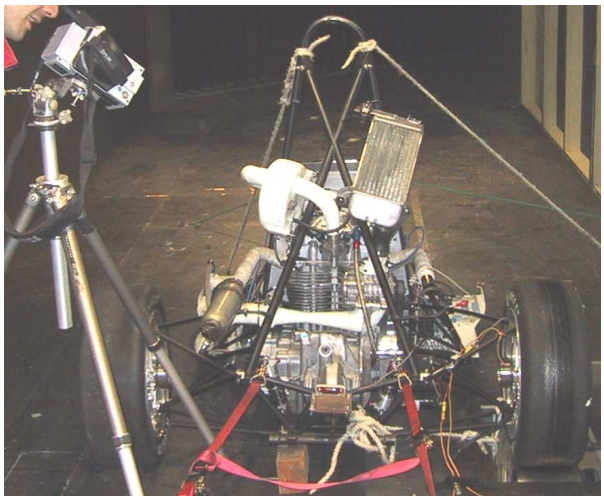

Figure A.2 (i)– Experimental Set-up

Experimental set-up

The right rear wheel of the racing car was placed in the brake test rig (described in section 3.3.1.3) and the brake was connected to the external applicator. The rubbing thermocouple and thermography camera were positioned to measure the temperature on inside surface of the rotor, as shown in figure A.2(vi). Data from the thermocouple was recorded on the PC via the Fluke data logger, information from the thermography camera was recorded and stored within it's own memory. The internal clocks on the thermography camera and the PC were synchronised so that temperatures at a particular instant in time could be compared.

Procedure

The tests were performed by rotating the wheel at a constant speed approximately equal to 50km/hr road speed. A gradual brake load was applied and the temperatures were recorded at 5 and 15 second intervals from the thermocouple and thermography camera respectively. The procedure was continued until a temperature of about 450°C was reached, at which point the brake load was released. Continual recording of the temperatures occurred until the rotor temperature dropped to about 200°C. Output from the thermocouple was obtained directly from the PC in a temperature scale; however output from the thermograhy camera was in the form of a thermal image (thermograph). Figure A.2(iii) shows a typical thermograph taken from this test. The thermal image provides a qualitative view of the temperature distribution. For comparison an equivalent photograph is provided in figure A.2(vii). The thermal image can also be analysed for quantitative data using a PC with specialist software "ThermoCam Reporter 2000". The temperature was measured at two points on the rotor approximately 180° apart, (SP01 and SP02) and an average was taken as the rotor temperature[5]. The results for both thermocouple and thermal imaging camera were charted and can be seen graphically in figure A.2(iv).

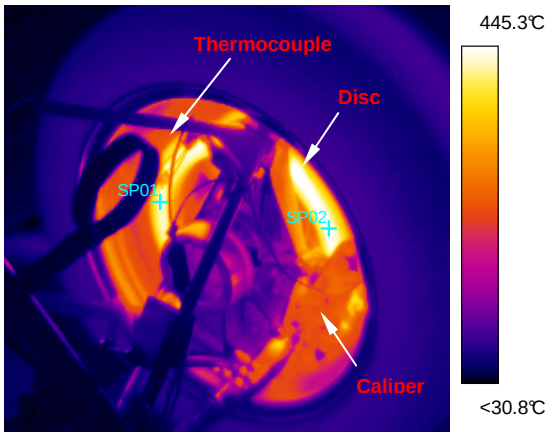

File name	**Time**
Seq067.img	4:04:44 PM

Object parameter	**Value**
Emissivity	0.79
Object distance	1.6 m
Ambient temperature	19.1°C
Label	Value
SP01	418.2°C
SP02	437.6°C

Figure A.2 (iii) – Typical thermograph and data of taken during test.

[5] The emissivity of the brake rotor (carbon steel) was obtained prior to the test by keeping the rotor at a constant temperature, the emissivity variable was then adjusted until the a matching temperature was recorded. The final value was found to be 0.79 which in the range of published data of mildly burnished carbon steel.

Results

From figure A.2(iv) it can be seen that the results from both the thermocouple and the thermography camera are very similar, particularly during the heating phase of the test. Both reach a similar peak temperature, although the thermocouple lags the thermogragh by about 10 seconds.

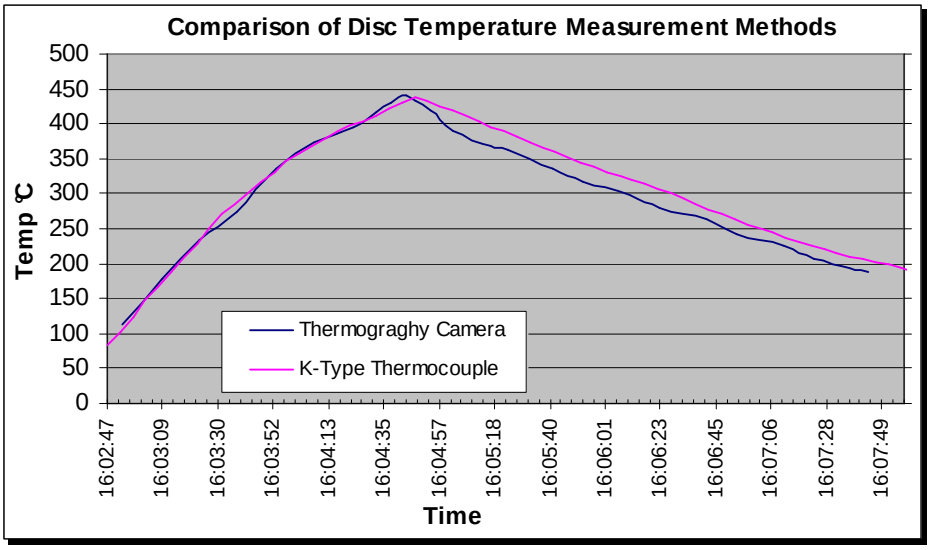

Figure A.2 (iv) – Comparison of disc temperature measurement methods

Once the peak temperature is reached response of the thermograghy camera is about 20 – 25° lower than the thermocouple. It is believed that the response of the thermocouple is slower in cooling than heating due to residual heat its rubbing components. This is consistent with Limpert, 1975 who believed that rubbing thermocouples yielded results of about 17° higher than actual temperatures, mainly due to friction generated by the sliding component. It must also be remembered that thermocouple will yield temperatures that are an average of several rotations of the wheel, whereas temperatures obtained from the thermogram are at an instant in time. The emissivity value (0.79) may not be constant due to temperature effects and brake pad residue on the surface under examination. From this test it was decided that an acceptable level of accuracy could be obtained for rubbing type thermocouples for use in the experimental stages of this research.

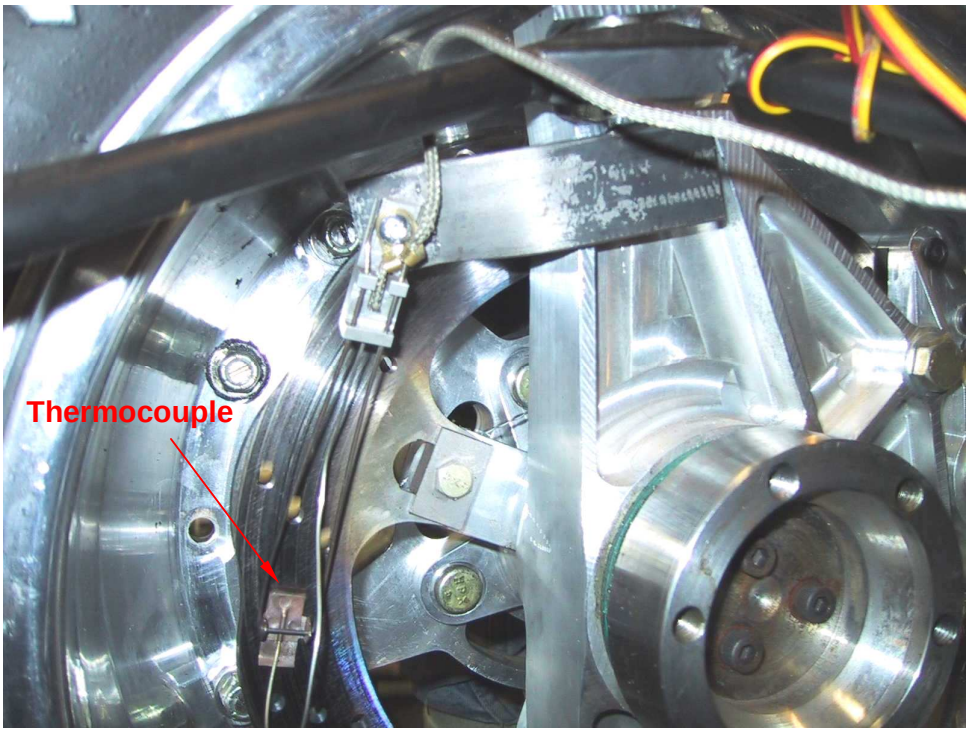

Figure A.2 (vi) Close up view of thermocouple in position

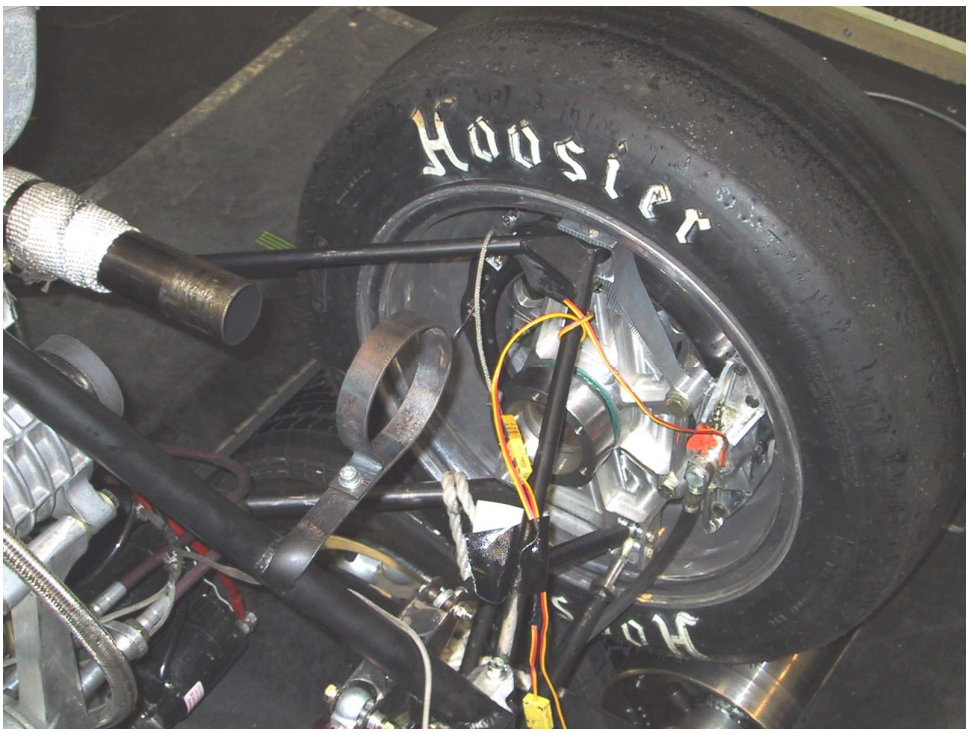

Figure A.2 (vii) – Photograph of view shown in thermal image

Experimental Data

Thermal Camera Data			
Time	**SP01 ℃**	**SP02 ℃**	**Average ℃**
4:02:53 PM	101.4	126.5	113.95
4:03:08 PM	167.3	185.9	176.6
4:03:23 PM	219.4	246.4	232.9
4:03:38 PM	265.8	281.5	273.65
4:03:53 PM	332.6	340.4	336.5
4:04:08 PM	351.0	395.7	373.35
4:04:23 PM	390.0	400.9	395.45
4:04:32 PM	396.2	438.7	417.45
4:04:38 PM	412.5	449.6	431.05
4:04:44 PM	418.2	445.2	431.7
4:04:47 PM	412.0	454.7	433.35
4:04:53 PM	399.0	439.7	419.35
4:05:02 PM	384.9	395.9	390.4
4:05:17 PM	361.4	373.3	367.35
4:05:23 PM	350.0	375.5	362.75
4:05:41 PM	329.9	340.0	334.95
4:05:53 PM	306.8	330.2	318.5
4:06:11 PM	285.6	310.3	297.95
4:06:23 PM	276.0	284.9	280.45
4:06:41 PM	262.5	265	263.75
4:06:53 PM	236.8	248.2	242.5
4:07:11 PM	218.9	231.5	225.2
4:07:23 PM	201.1	213.3	207.2
4:07:37 PM	189.2	199.1	194.15
4:07:44 PM	181.5	196	188.75

Thermocouple Data			
Time	**Temp ℃**	**Time**	**Temp ℃**
4:02:37 PM	79.9	4:06:02 PM	331.6
4:02:42 PM	79.4	4:06:07 PM	325.8
4:02:47 PM	83.5	4:06:12 PM	319.5
4:02:52 PM	102.8	4:06:17 PM	313.7
4:02:57 PM	123.7	4:06:22 PM	307.7
4:03:02 PM	146.9	4:06:27 PM	300.2
4:03:07 PM	168	4:06:32 PM	294.2
4:03:12 PM	189.5	4:06:37 PM	286
4:03:17 PM	210.2	4:06:42 PM	277.1
4:03:22 PM	229.7	4:06:47 PM	270.2
4:03:27 PM	249.8	4:06:52 PM	262.7
4:03:32 PM	270.4	4:06:57 PM	256.2
4:03:37 PM	284.9	4:07:02 PM	249.4
4:03:42 PM	299.9	4:07:07 PM	243.7
4:03:47 PM	316	4:07:12 PM	237.5
4:03:52 PM	331.3	4:07:17 PM	232.1
4:03:57 PM	346.8	4:07:22 PM	226.8
4:04:02 PM	356.5	4:07:27 PM	221.5
4:04:07 PM	368.1	4:07:32 PM	216.2
4:04:12 PM	379.8	4:07:37 PM	210.8
4:04:17 PM	390.4	4:07:42 PM	206.3
4:04:22 PM	397.5	4:07:47 PM	202.1
4:04:27 PM	404.2	4:07:52 PM	197.6
4:04:32 PM	412.6	4:07:57 PM	193.3
4:04:37 PM	421.2	4:08:02 PM	189
4:04:42 PM	431.2	4:08:07 PM	184.6
4:04:47 PM	437.7	4:08:12 PM	180.2
4:04:52 PM	433.5	4:08:17 PM	176.9
4:04:57 PM	426	4:08:22 PM	173.1
4:05:02 PM	418.5	4:08:27 PM	169.6
4:05:07 PM	410.8	4:08:31 PM	166.3
4:05:12 PM	403.7	4:08:37 PM	162.5
4:05:17 PM	395.9	4:08:42 PM	159.2
4:05:22 PM	388.7	4:08:47 PM	155.6
4:05:27 PM	380.8	4:08:52 PM	152.9
4:05:32 PM	373.3	4:08:57 PM	146.6
4:05:37 PM	365.6	4:09:02 PM	145.4
4:05:42 PM	358.9	4:09:07 PM	142.8
4:05:47 PM	352	4:09:12 PM	139.7
4:05:52 PM	344.6	4:09:17 PM	136.6
4:05:57 PM	337.9		

Table A.2 (i) – Experimental Data

A.3 – TORQUE TRANSDUCER CALIBRATION CERTIFICATE

SENSOR DEVELOPMENTS INC.
BOX 290
Lake Orion, MI 48361
(248) 391-3000

CALIBRATION DATA SHEET

Description: CW
SDI Mod. No. 01225 — FS Capacity: 271 NM — Customer: HARE
SDI Serial No.: 167329 — Date: 11-21-2000 — Cus. Mod. No.:
SDI Job No.: 12814 — Operator: BG — Customer P/N:
Ambient Temp.: 72 F — Humidity: 19 %

LOAD	OUTPUTS (mV/V)				DEVIATIONS		
	ASCENDING	DESCENDING	AVERAGE	BF/0	N/L	HYS	BF/0
0	0.0000	0.0000	0.0000	0.0000	0.00	0.00	0.00
27	0.3318	0.3312	0.3315	0.3317	0.00	-0.02	-0.00
54	0.6635	0.6625	0.6630	0.6633	0.01	-0.03	-0.01
81	0.9952	0.9939	0.9946	0.9950	0.01	-0.04	-0.01
108	1.3269	1.3254	1.3262	1.3266	0.01	-0.04	-0.01
136	1.6586	1.6570	1.6578	1.6583	0.01	-0.05	-0.01
163	1.9902	1.9887	1.9895	1.9899	0.01	-0.04	-0.01
190	2.3218	2.3205	2.3212	2.3216	0.01	-0.04	-0.01
217	2.6534	2.6525	2.6529	2.6532	0.01	-0.03	-0.00
244	2.9850	2.9845	2.9847	2.9849	0.00	-0.02	0.00
271	3.3166	3.3166	3.3166	3.3165	-0.00	-0.00	0.01

Shunt Cal Data:

Value (OHMS)	Across	Produces Simulated Signal of: mV/V	NM(Term)	(BF/0)
60 K OHMS	- EXCITE & - SIGNAL	4.1267	337.2	337.2
120 K OHMS	- EXCITE & - SIGNAL	2.0754	169.6	169.6
60 K OHMS	+ EXCITE & - SIGNAL	-4.1514	-339.2	-339.2
120 K OHMS	+ EXCITE & - SIGNAL	-2.0866	-170.5	-170.5

Load may be computed using the following equation: Load = (K1 + K2*Output)*Output
where Load is in NM & Output is in mV/V

CURVE	K1	K2
Ascending	81.6836	0.00811
Descending	81.8366	-0.03801
Average	81.7601	-0.01495
Terminal	81.6836	0.00000
Best Fit/0	81.7126	0.00000

Bridge Resistance (OHMS):

Excitation 1644.3
Signal 1002.5

Status of Tolerance:

In (X)
Out ( )

This report shall not be reproduced except in full, without the written approval of Sensor Developments, Inc. This instrument has been calibrated using references traceable to national or international standards. This instrument was calibrated with an accuracy ratio of greater than or equal to 4:1 unless otherwise stated. This calibration was performed in conformance with the SDI Quality Manual revision 5 and ANSI/NCSL Z-540-1.

Technician — 11-21-00 Date

Approved By — 11-21-00 Date

A.4 - CALIBRATION OF DIFFERENTIAL PRESSURE TRANSDUCER

The differential pressure transducer was calibrated against an inclined tube manometer. A pitot static tube was placed in the RMIT Industrial Wind Tunnel, and connected in series to an inclined tube manometer and the differential pressure transducer. As the air velocity in the tunnel was increased, the output from the pressure transducer (mV) and manometer readings (mm H_20) were recorded simultaneously. The results given in table A.4(i) are averaged over three tests.

Calibrations Readings	
Transducer	**Manometer**
volts	**h (mm)**
0.104	1
0.29	6
0.371	7
0.529	12
0.622	13
0.793	21
1.004	24
1.263	32
1.475	35
1.823	45

Table A.4(i) – Calibration data from differential pressure transducer

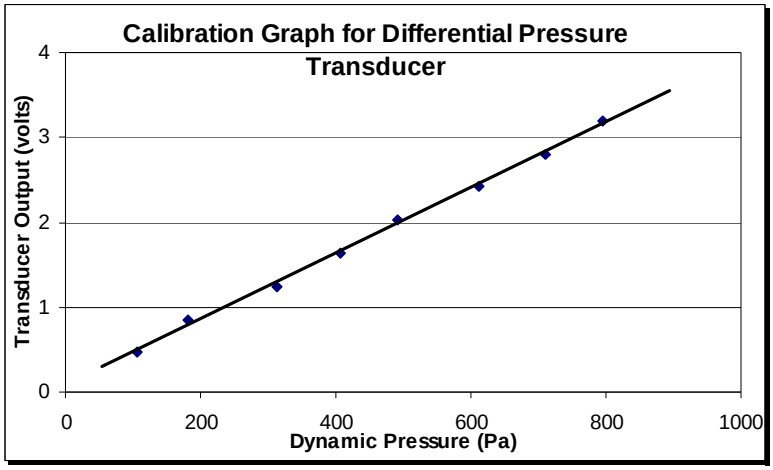

Figure A.4(i) – Calibration graph for differential pressure transducer

APPENDIX B

OPTIMAL DISTANCE BETWEEN VENT OUTLET AND PROBE HEAD

The distance the Cobra Probe is positioned from the perimeter of the rotor will have a direct bearing on the accuracy of the results. Hudson (1997) used a distance of 10 mm when measuring vent velocity at the perimeter of a vented brake rotor. However it was decided to perform a series of tests in order to determine how sensitive the results were to the distance between the probe head to the vent outlet. Flow measurements were taken at distances of 3 mm, 5 mm, 10 mm, and 15 mm. From these results (shown below) it was found that the closer the probe was placed to the rotor the less the flow dispersed. Little difference was observed between distances of 3, and 5 mm, while at further distances there appeared to be significant differences. A final distance of 5 mm was chosen, as it was close enough to the rotor to minimise errors, but far enough to reduced the possibility of accidental contact. The results also showed that comparison between tests could only be made if the probe distances were the same for all tests.

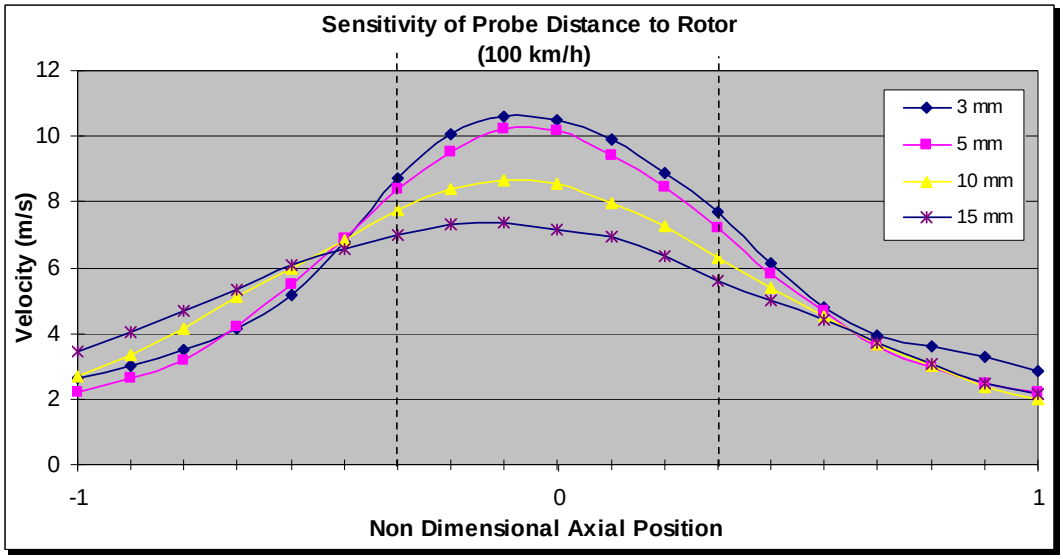

Figure B(i) – Relationship between probe head distance and accuracy of results

APPENDIX C

RELATIONSHIP BETWEEN BRAKE ROTOR ROTATIONAL VELOCITY AND EXTERNAL AIR-STREAM.

The wind velocity a vehicle experiences as it travels through the atmosphere is equal but opposite to its velocity, excluding the effects of atmospheric winds. The rotational velocity of the wheel is directly proportional to the vehicle speed, and is governed by the expression: $\omega = \frac{V}{r}$

Where: V = velocity of vehicle (m/s)
R = rolling radius of wheel (m) (0.65 m)
ϖ = angular velocity of wheel/rotor (rad s^{-1})

And

$$N = \frac{\omega \times 60}{2\pi}$$

Where: V = velocity of vehicle (m/s)
R = rolling radius of wheel (m) (0.65 m)
ϖ = rotational velocity of wheel/rotor (RPM)

Therefore there is a direct linear relationship between the vehicle velocity and the rotational speed of the wheel and hence the rotor.

Vehicle Speed (km/hr)	Vehicle Speed (V) (m/s)	N (RPM)	Wind Tunnel Velocity (m/s)
120	33.33	979	33.33
100	27.78	816	27.78
80	22.22	653	22.22
60	16.67	490	16.67
40	11.11	326	11.11

Table D.(i) Relationship between brake rotor rotational velocity and external air-stream

APPENDIX D

BLOCKAGE CORRECTION

Date of Test: 20/05/2001

Test Vehicle: Ford Falcon AU

Equipment Used: Pitot Static Tube

Differential Pressure Transducer, (voltage output).

Raw Data		
Vehicle Speed (km/hr)	Driving Direction North (volts)	South (volts)
0	**0.104**	**0.104**
40	**0.297**	**0.284**
50	**0.357**	**0.384**
60	**0.547**	**0.512**
70	**0.578**	**0.665**
80	**0.891**	**0.695**
90	**0.995**	**1.014**
100	**1.321**	**1.205**
110	**1.423**	**1.526**
120	**1.826**	**1.820**

Table D (i) – Raw data taken from on-road tests.

The output from the differential pressure transducer was converted to dynamic pressure (Pa) using the calibration graph given in Figure A.1. The local air stream velocities were then obtained using the following equation:

$$\Delta P = \tfrac{1}{2}\rho V^2$$

Where, ΔP is the differential pressure across the pitot static tube, (Pa).

ρ is the density of air (kg/m^3).

V is the local air stream velocity (m/s).

Calculated Data

Corrected Vehicle Speed (km/hr)	Average (volts)	(From fig A.1) Dynamic Pressure Pa	local Velocity m/sec	km/hr
0	**0.104**	**7.04**	**0**	**0**
40	**0.290**	**56.15**	**9.4**	**33.76**
50	**0.371**	**71.50**	**11.4**	**41.13**
60	**0.529**	**119.77**	**13.6**	**48.94**
70	**0.622**	**127.83**	**15.8**	**56.89**
80	**0.793**	**207.54**	**16.2**	**58.32**
90	**1.004**	**233.86**	**20.0**	**71.83**
100	**1.263**	**316.93**	**21.9**	**78.78**
110	**1.475**	**343.01**	**24.8**	**89.30**
120	**1.823**	**445.68**	**27.2**	**97.93**

Table D (ii) – Local air stream velocity measurements at equivalent road speeds.

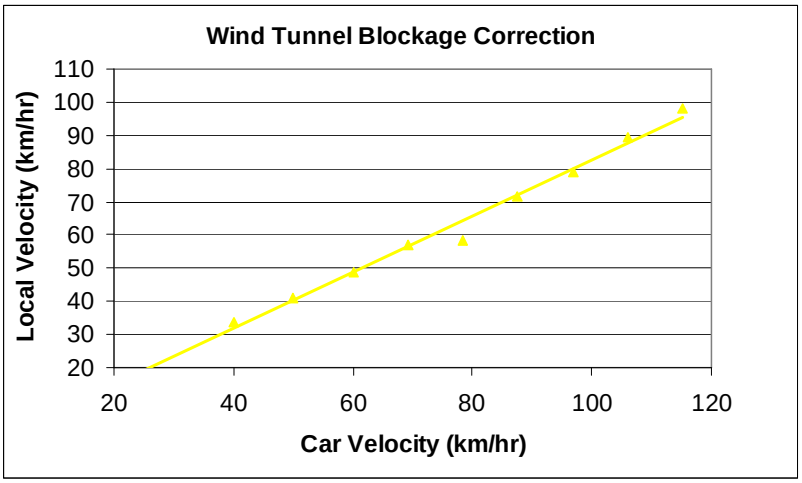

Figure D(i) - Relationship between local flow to freestream velocity.

APPENDIX E

BRAKING TORQUE REQUIRED FOR A ONE TONNE VEHICLE DECENDING A 1 IN 5 SLOPE AT A CONSTANT SPEED OF 60 KM/H

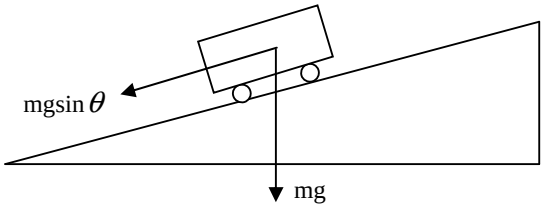

Mass = 1000 kg.

Velocity of Vehicle = 60 km/hr.

Rolling diameter of tyre = 0.65m.

Slope of decent = 10°.

For continued braking at constant speed the power required is given by the formula:

$$P_b = mgV \sin\theta \quad \textit{- Limpert (1999)}$$

Where: P_b (W) is the braking power required to keep the vehicle at constant velocity.

mg is the weight of the vehicle (N).

V is the velocity of the vehicle (m/s).

θ is the angle of decent.

$$P_b = 1000 \times 9.8 \times 60 \left(\frac{1000}{3600} \right) \sin\theta$$

Assuming a 70/30 front to rear brake distribution. The brake power required for 1 rear wheel is

$$P_b = \frac{1}{2} \left(1000 \times 9.8 \times 60 \left(\frac{1000}{3600} \right) \sin\theta \right) 0.3$$

$$P_b = 3836 \quad watts$$

$$\omega = \frac{V}{r} = \frac{60 \diagup 3.6}{0.325} = 51.28 \; rad \; s^{-1}$$

$$Torque = \frac{P_b}{\omega} = \frac{3836}{51.28} \quad = 74.8 \; Nm$$

APPENDIX F

Paper Number - 03B-193

Aerodynamic Testing of a Vented Disc Brake

Arthur Stephens, Simon Watkins and Chris Dixon

Vehicle Aerodynamics Group
Dept of Mechanical & Manufacturing Engineering
RMIT University, Melbourne,
Australia

Copyright © 2001 Society of Automotive Engineers, Inc.

ABSTRACT

Many attempts have been made to improve automotive brake cooling by increasing the pumping action of vented brake rotors, both experimentally and using computational fluid dynamics. Testing of these improvements has occurred by measuring the airflow at the outlet of a rotating brake rotor in still air, however this is a vastly different environment to the actual working condition of the rotor. Airflow around the rotor, as a result of the forward movement of the vehicle, will have a considerable effect on its pumping ability. In this paper a comparison is made between the measured airflow through a straight-vane vented disc: (1) isolated disc still air; (2) disc in still air with the wheel on; (3) disc in moving air with the wheel on; and (4) on road simulation using a ¼ car. Both time-averaged and real-time measurements are presented. In the still air tests results showed a linear relationship between rotational velocity and airflow through the disc. Spectral analysis indicated the possibility of vortex shedding occurring behind the vanes. For tests (3) and (4) vent airflow was a function of both rotational speed of the rotor and angular position around the rotor, with the volume flowrate of air significantly lower than that measured in still air tests.

INTRODUCTION

One of the most important components in a road vehicle is its braking system. Apart from a few exceptions such as regenerative braking in electric and hybrid vehicles, no viable substitute has been found for friction braking systems. As long as such systems are employed, the effective dissipation of thermal energy from the brake drum or disc will be a concern to brake designers and engineers. Most of the heat dissipated from brake rotors is by convection to the atmosphere and therefore sufficient cooling air must interact with the rotor to provide satisfactory heat dissipation. The modern trend of streamlined low drag vehicles has resulted in a reduction in the cooling air available to the braking system as well as such things as the engine, exhaust, differential, etc. With this in mind, much work has been done to improve the cooling capabilities of brake rotors and in particular to increase the cooling airflow to brake rotors, both computationally and experimentally, including [1, 2]. A significant portion of this previous work involved attempts to improve the airflow through vented disc rotors. The measurement of airflow through the rotor vents is usually conducted on isolated rotors operating in still air, a condition that is axi-symmetric and vastly different from its normal operation. In normal operation the airflow in the region of a brake rotor is not axi-symmetric, extremely complex and turbulent, mainly due to air entering the wheel cavity from the forward movement of the vehicle. It is therefore not known how much flow under "real" operating conditions occurs through a vented rotor on a vehicle. It has also been suggested that it is the extra surface area in a vented disc that produces the largest gain in cooling and not the flow generated [3].

The objective of this work is to compare measured flow through an isolated vented rotor operating in still air to the measured flow in normal operation conditions. A series of experiments were developed to measure the flow through a rotating vented rotor under various conditions, including: (1) the isolated disc in still air; (2) the disc in still air with the wheel on; (3) the disc in moving air with the wheel on; and (4) an on road simulation using a ¼ car.

EXPERIMENTS

The experiments were conducted in the RMIT Industrial Wind Tunnel, a rotor test bench was used to spin the rotor and airflow measurements were taken with a high frequency dynamic Cobra probe. This probe has a multifaceted head that contains four pressure taps, which can measure flow fields within a range of ±45°. Any flow measured outside this zone of acceptance is automatically rejected. The probe is capable of mean and time-varying values of: velocity (3-components); pitch and yaw angles; local static pressure; turbulence intensity and all six components of Reynolds stresses. Further information on the Cobra probe can be found in references [4, 5]. The vented brake disc used in the experiments was a cast iron 303 mm rotor containing 37 vents.

The rotational velocity of the disc was chosen as the equivalent rotational speeds for the vehicle travelling at road speeds of 40, 60, 80, and 100 km/hr. The probe head was positioned to face directly into the mean angle of outlet flow (-60°), see Figure 1. By traversing the probe axially at 1 mm intervals from the inboard to the outboard

edge of the disc, it was possible to obtain a good description of the flow field at the outlet of the vanes. The sampling frequency was 5000 Hz and the sampling time was 5 seconds, making more than 25000 samples at each point.

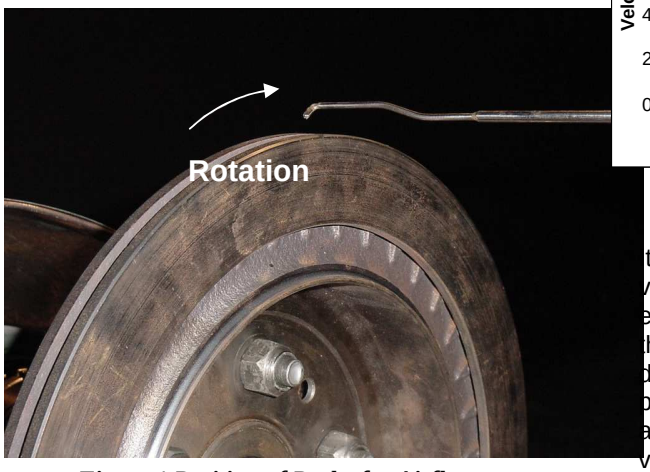

Figure 1 Position of Probe for Airflow Measurement

RESULTS

CASE 1 ISOLATED ROTOR IN STILL AIR

Time Averaged Results

The time-averaged velocity data collected from the isolated disc measurements are displayed graphically in Figure 2. The axial position is non-dimensionalised over the width of the disc, point 0 being the centre point of the disc, and –1 and 1, are the inboard and outboard edges, respectively (Figure 4Figure 4.4.3). The two vertical dotted lines represent the boundaries of the internal flow passages. This chart shows the outlet airflow velocity profiles from the disc at the various speeds under investigation, and a jet of air is evident which is entraining the surrounding flow.

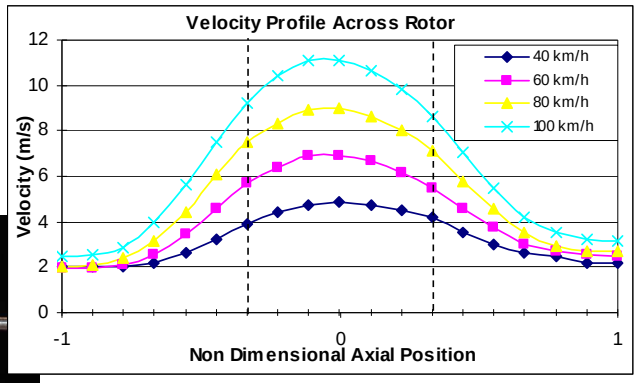

Figure 2 Velocity Profiles Across Disc

It can be seen that the point of maximum velocity through the disc does not coincide exactly with the centre of the flow passage, this may be because airflow only enters the disc from the inboard side. The flow velocity profiles are similar for all speeds, and appear to be proportional to the rotational velocity. Figure 3 shows the results when the measured velocities are shown in non-dimensional form.

The results appear to collapse onto a single line, particularly at higher speeds. At lower speeds there is some drift away from this line, particularly at the edges of the disc, which is attributed to minor Reynolds number effects and measurements errors at these low flow velocities.

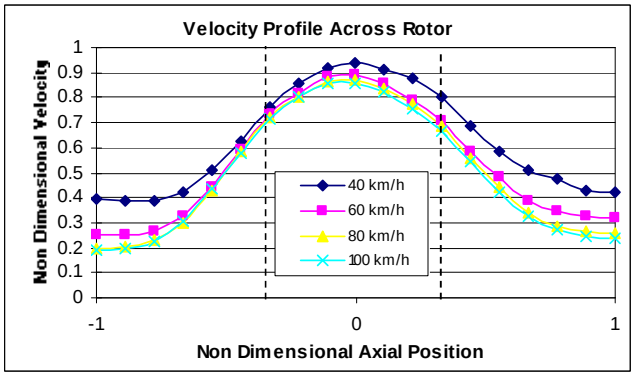

Figure 3 Non Dimensionalised Flow Through Disc

Previously Sisson [6] and Limpert [7] have independently developed empirical equations to predict the flow through vented rotors. The following table shows the results expected from both equations as well as the measured values. Sisson's equation produces results very close to the measured values (within 20% at all speeds). However, Limpert's equation yields values

of about 40 - 50%s lower than measured. Both Limpert and Sisson predict a linear relationship between rotational velocity and vent airflow, and Figure 3 appears to support this.

		Calculated		Measured		From Measured
Speed (km/h)	RPM	Limpert (m/s)	Sisson (m/s)	Max. Measured (m/s)	Average (m/s)	Mass Flowrate kg/s
100	816	6.82	8.89	11.11	10.12	0.0569
80	653	5.46	7.11	8.98	8.21	0.0462
60	490	4.09	5.34	6.90	6.30	0.0355
40	326	2.72	3.55	4.75	4.48	0.0252

Table 3 Measured and Predicted Flow Through Disc

The Cobra probe is also able to determine the angles of the flow stream relative to its head. For convenience, these angles have been transformed to angles relative to the disc and named flow angle and yaw angle, the convention adopted for these angles is given in Figure 4Figure 4.4.3.

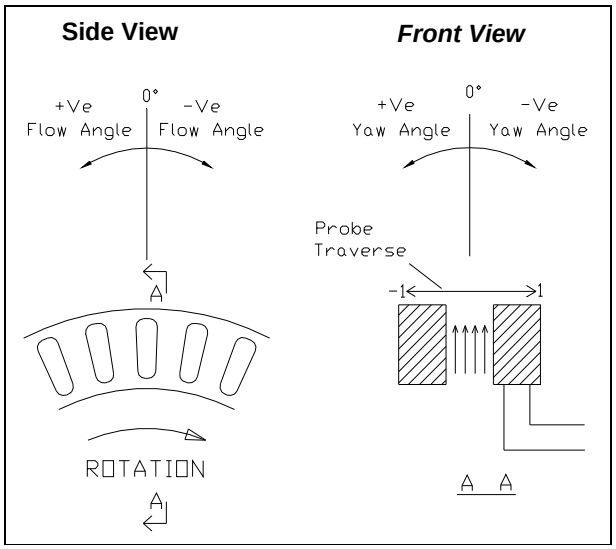

Figure 4 Airflow Angle Convention, for Airflow Through Disc

The flow angles and the yaw angles for all speeds tested are given in Figure 5Figure 4.4.5. It can be seen that the patterns for all speeds are similar.

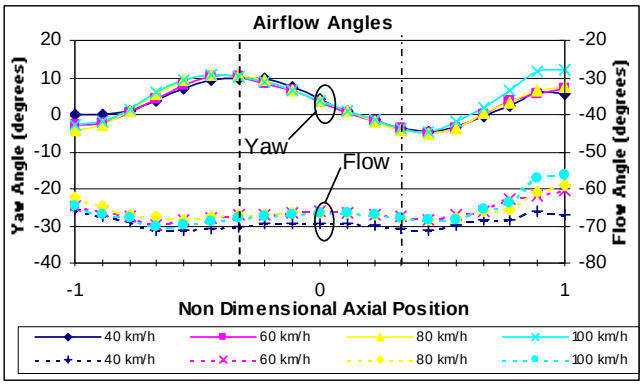

Figure 5 Measured Flow and Yaw Angles for Flow the 303 mm Vented Disc

Real Time Results

In addition to time-averaged measurements, the Cobra probe allows measurement of real time and transient airflows. Figure 6Figure 4.4.6 shows the velocity measurements for one revolution of the disc at an equivalent road speed of 100 km/h, (measured at the centre point of the vent outlet).

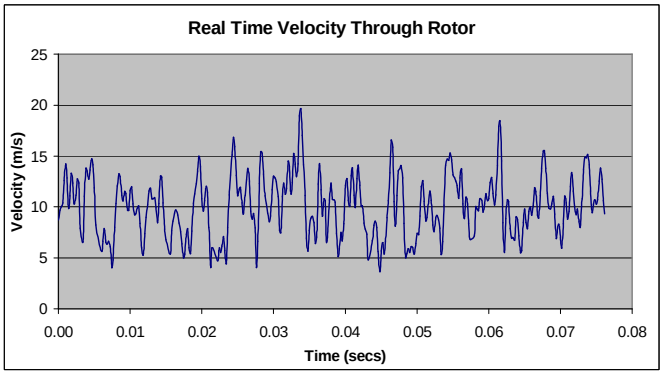

Figure 6 Airflow Velocity for One Revolution of Brake Disc

Spectral analysis was performed on the data using the Cobra probe software, which allows a detailed analysis of the data in the frequency domain. Figure 7Figure 4.4.7 shows the results of the above data (100 km/h equivalent road speed). The frequency is displayed on the x-axis, and the root mean square of the velocity squared is shown on a decibel scale on the y-axis. The software filter cut-off frequency was 1500 Hz, this can be observed in the spectrum as a step change at 1500 Hz. A sharp spike can be observed in the spectrum at about 500 Hz. This is

equivalent to the frequency of the vents in the disc passing the probe head. The disc contains 37 vents and at 100 km/h (816 RPM), the blade passing frequency is:

$$\frac{816}{60} \times 37 = 503.2\ Hz$$

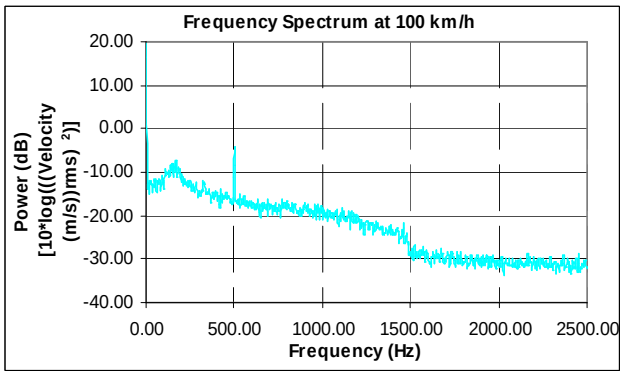

Figure 7 Frequency Spectrum - 100 km/h (816 RPM)

Also observed in the spectrum is a wider spike centred about 180 Hz, which is believed to be vortex shedding. Figure 8Figure 4.4.9 shows the spectra for all speeds measured from 40 to 100 km/h, which are transposed in the y direction for comparison purposes.

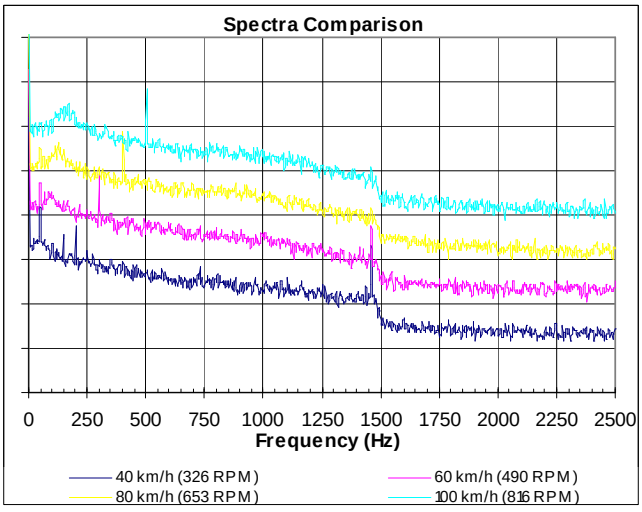

Figure 8 Spectra Plots for Full Range of Speeds.

It can be seen that blade passing and vortex shedding are a function of speed. Vortex shedding frequencies are predicted via Strouhal numbers between 0.2 (circular cylinder) and 0.08 for (rectangle) [8], for Reynolds numbers in the range $40 \leq Re \leq 200000$. Equation 4.4.4 and Equation 4.4.5 were used to determine if the flow through the vanes was with the range for vortex shedding to occur. The results of these equations are outlined in Table 4.4.2. From this table the required conditions for vortex shedding are present.

$$\mathrm{Re} = \frac{V_{vent} L}{\upsilon} \quad \text{- Equation 1}$$

Where

Re = Reynolds Number

V_{vent} = *Air Velocity Through Vent (m/s)*

L = *wetted length of vent (0.044 m)*

υ = *kinematic viscosity (1.4 x 10^{-5} m^2/s)*

$$St = \frac{f_r w}{V} \quad \text{- Equation 2}$$

Where: St = *Strouhal number*

f_r = *frequency of shedding vortices (Hz)*

w = *characteristic width (m)*

V = *velocity (m/s)*

Speed (km/h)	RPM	V_{vent} (m/s)	*Re*	*w* mm	Measured Vortex Shedding Frequency (Hz)	Calculated Strouhal No.
100	816	10.12	24738	6	180	0.11
80	653	8.21	20069	6	125	0.09
60	490	6.30	15400	6	90	0.09
40	326	4.48	10951	6	50	0.08

Table 4 Vortex Shedding Frequencies

CASE 2 – AIRFLOW THROUGH BRAKE DISC IN STILL AIR WITH WHEEL ON

The experimental configuration for case 2 can be seen in Figure 9Figure 4.4.10.

Figure 9 Airflow Measurements with Wheel in Place

The results shown in Figure 10Figure 4.4.11 are the airflow measurements through the disc with wheel in place and no external airflow. The profiles are similar to the free disc case for the inboard portion of the disc, however for the outboard portion of the disc (wheel side) there appears to be significant airflow generated by the wheel. The maximum airflow velocity through the vane section appears similar in magnitude to the free disc case, although the profile is a little flatter.

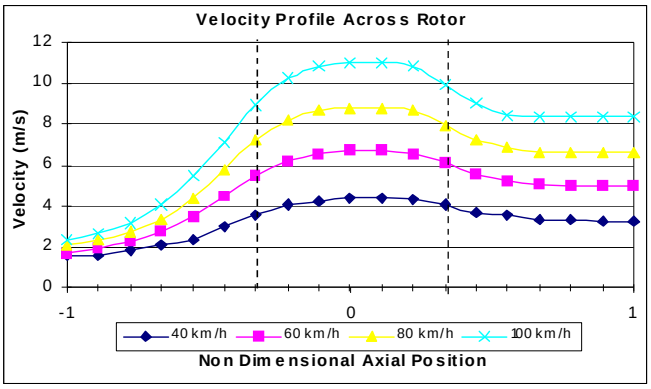

Figure 10 Velocity Profile Across Disc in Still Air (Wheel On)

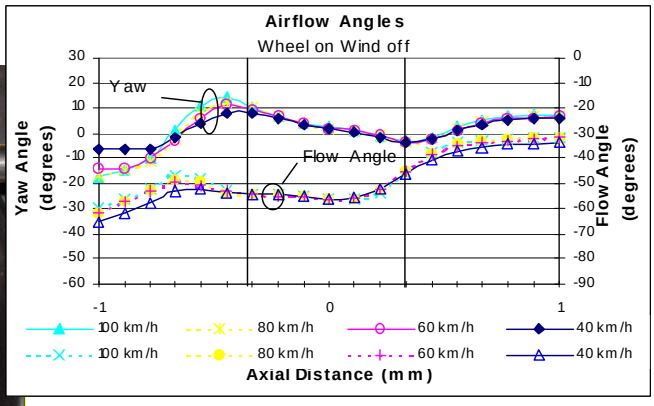

Figure 11 Measured Flow and Yaw Angles in Still Air (Wheel On)

The measured flow and yaw angles for this case are given in Figure 11.

CASE 3 – AIRFLOW THROUGH BRAKE DISC IN MOVING AIR WITH WHEEL ON

Due to the interacting of external flow on the flow through the vents, the airflow around the rotor periphery was no longer axi-symmetric thus the flow was also measured at the front, bottom and back of the rotor. Figure 12 shows the velocity profile across the disc for the wind on and wheel on condition, with the probe in the top position as in the previous set of experiments. The probe angle was kept at -60°. Clearly from this chart the readings were affected by the external flow, and it is unknown if any internal flow was being measured or just the external flow, as no discernible flow jet is observed through the centre portion of the disc. The data rejection rate of the probe for these measurements was also in excess of 30%, indicating that a significant portion of the flow was outside the ± 45° zone of acceptance of the probe head (and extremely turbulent).

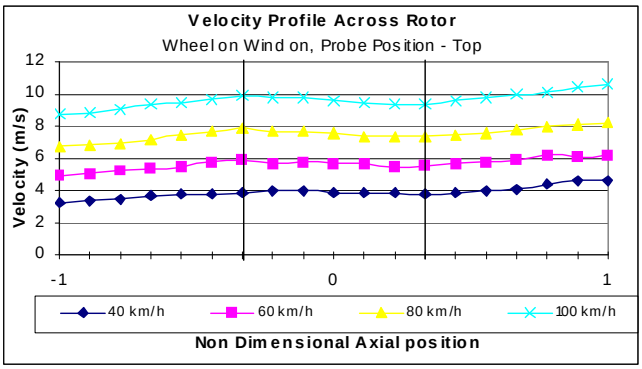

Figure 12 Velocity Profile Across Brake Disc

The results are also given for the measured flow at other points around the disc. Figure 13, Figure 14 and Figure 15 Figure 4.4.15show the velocity profiles for the front, bottom and back of the disc respectively. Apart from the flow measured at the front of the disc, it is not clear whether the air velocity measured is produced mainly by the vent flow or external flow. It is possible that the outlet of the vanes at the front of the disc is within the wake of the wheel and is therefore less affected by the external flow.

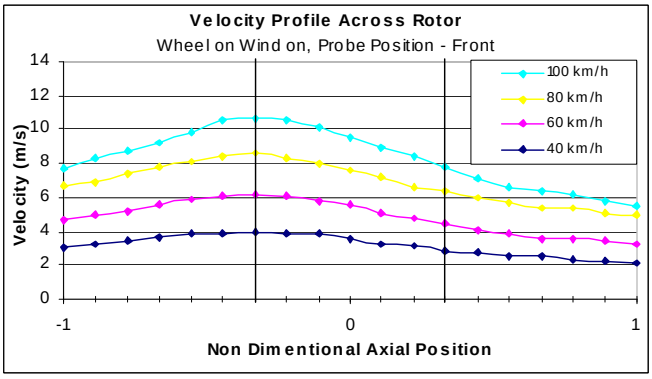

Figure13 Velocity Profile Across Front of Disc

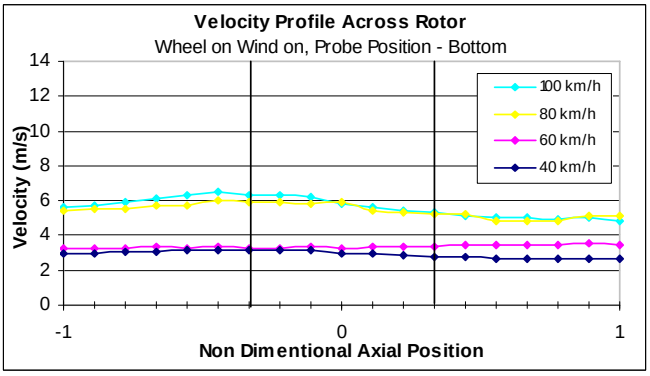

Figure 14 Velocity Profile Across Bottom of Disc

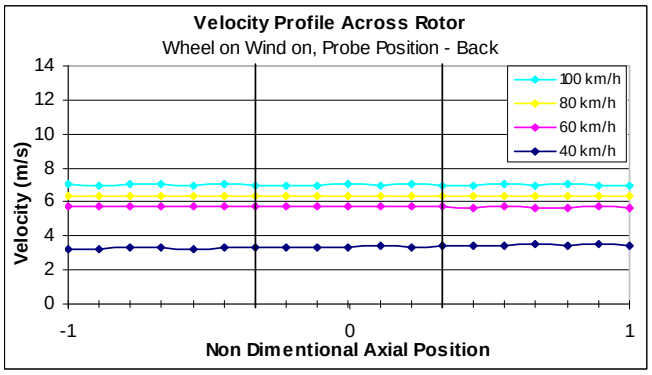

Figure 15 Velocity Profile Across Back of Disc

CASE 4 – AIRFLOW THROUGH BRAKE DISC IN MOVING AIR WITH WHEEL AND QUARTER CAR

As in the previous tests the airflow in this condition was not axi-symmetric. From these results it was difficult to determine if the airflow was being generated though the vanes of the disc in the wind-on condition. As the external airflow was not similar to the normal on-road condition, a further test was performed in a more representative simulation of the real world driving condition. In this test the test wheel was covered with a one-quarter car to represent the front right hand corner of the vehicle, and located close to the side wall of the tunnel, as shown in Figure 16. The blockage area of the ¼ car and associated equipment was approximately 20% (defined as projected frontal area of object divided by cross sectional area of test section). Although many corrections exist for blockage [9], for this work a simple area correction was used and the upstream velocity of the flow was reduced by 20%.

Figure 16 Car Buck Used for Airflow Measurements

Figure 17 shows the velocity measurements for the flow measured at the top of the disc. Although the flow through the vanes appears to be affected by the external flow field, there is still evidence of flow through the vanes, particularly at higher speeds. The flow profiles are similar to the profiles recorded for the wheel on and without external air (Figure 10Figure 4.4.11).

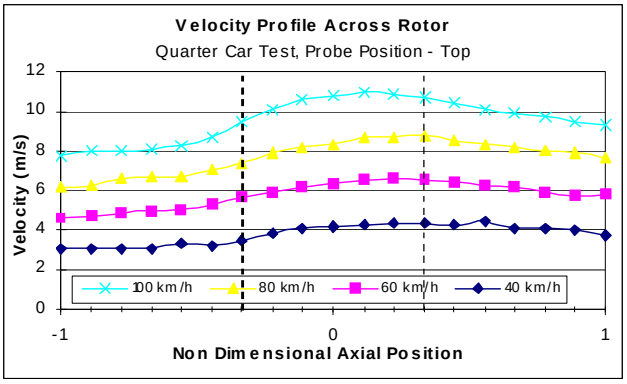

Figure 17 Velocity Profile Across Top of Disc- ¼ Car Tests

The charts shown in Figure 18 are the yaw and flow angles recorded at the top of the disc. The profiles are not significantly different for the case with the wheel on and still air (Figure 11), and are consistent over the range of speeds tested.

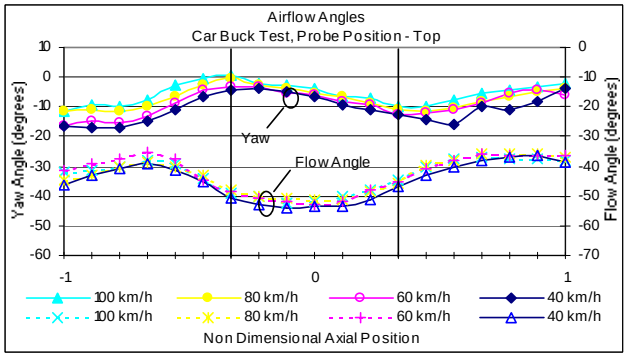

Figure18 Flow and Yaw Angle Plots for - ¼ Car Tests

The velocity plots for the front bottom and back of the disc are given in Figure 19, Figure 20 and Figure 21 respectively. From these plots it appears that no jet of air can be distinguished through the vanes from the front and bottom locations, although some flow is evident through the vanes at the rear.

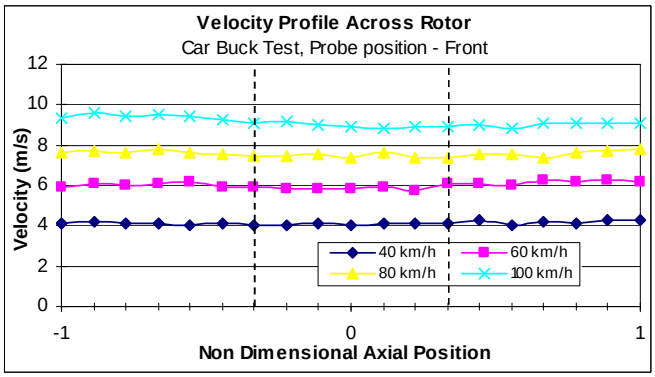

Figure 19 Velocity profile Across Front of Disc - ¼ Car Test

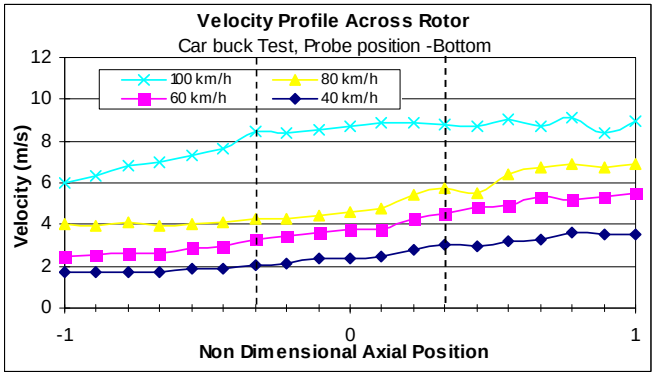

Figure 20 Velocity Profile Across Bottom of Disc - - ¼ Car Tests

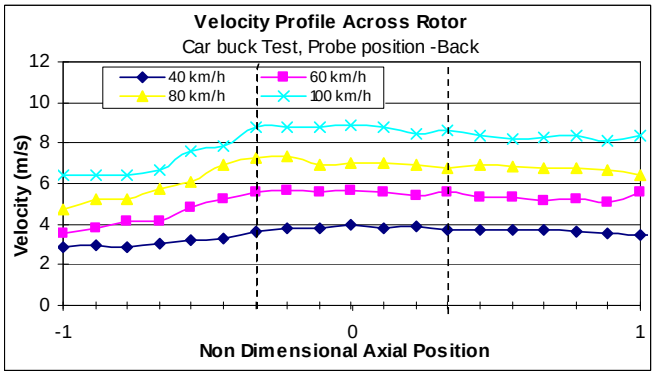

Figure 21 Velocity Profile Across Back of Disc - ¼ Car Tests

From these charts it is evident that some flow occurs through certain segments of the vented disc, in normal driving conditions, even at higher speeds. It is not easy to quantify this flow, as it is difficult to distinguish it from external flow.

DISCUSSION OF RESULTS

Much work has been done to develop vented discs that displace significant airflow for a given rotational speed, however previous research in this area has generally examined the airflow in still air. The results outlined in the still air tests appear to agree with earlier work refereed to in [2, 6, 7] when predicting the expected flow through vented discs. However from the frequency analysis it appears that there is also some other flow disturbance existing through the vanes of the disc, possibly vortex shedding. Kubota *et al.* [10] also found similar disturbances in the flow. It should therefore be possible to further increase the vent flow by reducing these disturbances (i.e. more aerodynamic shaping of the blades) and allow the cooling air to flow through the vents more smoothly.

When the tests simulated the on-road condition it is clear that the disc vent flow is severely influenced by the presence of the wheel vehicle and externally imposed flow (mainly the forward movement of the vehicle). Nothing was found in the public literature that experimentally determined flow through the disc vents in a representative road condition. It was not known how much, or if any, flow occurs through the disc vanes during normal operation, or how this flow was influenced by vehicle velocity. Therefore it may be questionable to attempt to gain more airflow through vented discs if limited airflow exists in its normal operating condition. The presence of the wheel alone around the disc influences this flow significantly as shown in case 2. Figure 22Figure 4.5.2 illustrates how the various interactions effect the flow through the top of the disc at a vehicle speed of 100 km/h. Clearly all these interactions have an effect on the flow, the greatest being the external flow, however the effect of the brake caliper was not examined and should be included in further research.

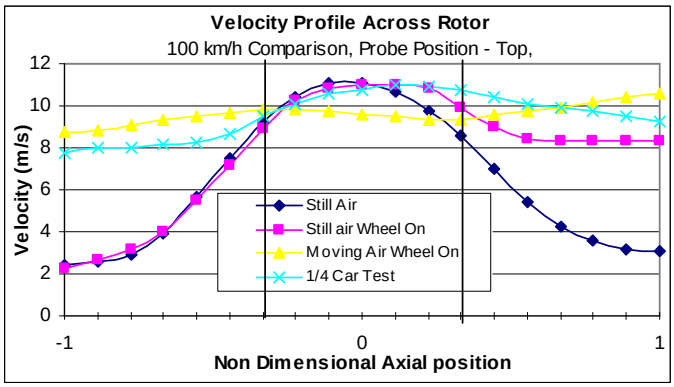

Figure 22 Airflow Through Vented Disc Under Varying Conditions 100 km/h

As observed in Figure 22 the flow jet through the centre of the disc in the ¼ car test (case 4) is similar to the wheel and disc test (case 2). It is interesting to note that the maximum measured vent velocity is similar for cases 1, 2, and 4, at the top of the disc, suggesting that measuring the flow through a disc in still air may indicate the flow in normal operation. However at other positions around the rotor this is not the case. It can therefore be concluded that although the flow through the vents is affected by external airflow, the wheel, and body structure, some airflow still occurs through segments of the disc, even at higher speeds. Therefore a measurable benefit in cooling should be found by using vented brake discs over solid type disc. The results also highlight a contradiction, in the effect of the body shielding created by the vehicle body improves the conditions for the vented disc to operate, (compare case 3 with case 4). This also has the effect of reducing the airflow around the outer surfaces or the disc reducing the overall cooling air interacting with the disc. There may therefore be a greater gain in cooling by increasing the airflow into the region of the brake disc, than what is gained by vented discs, although this will negatively impact on the vehicles aerodynamic drag. Much would appear to depend on the venting of the wheel itself, although additional research is needed to support this.

CONCLUSIONS

Airflow through vented rotors is significantly reduced during on-road driving, compared to when measured in isolation. The main

reason for this is the influence of the flow around the vehicle and its interaction with the wheel and bodywork.

Previously the nature of the flow through vented rotors under normal operating conditions was unknown, nor was the speed dependence understood [3]. However the results outlined in this paper show the non-dimensionalised flow through vented rotors is not particularly affected by vehicle speed.

Air entering the wheel cavity appears to reduce the quantity of air flowing through the vented rotor. Therefore the greatest benefit from vented rotors will be achieved in vehicles where air entering the wheel cavity is limited, such as low drag vehicles.

Increased airflow through vented rotors could be achieved by reducing airflow disturbances (such as vortex shedding) with improved aerodynamic shaping of the internal blades.

Further research should include the measurement of the thermal performance of vented rotors and relate this to the measured vent flow, under representative on-road conditions. This is part of on-going research.

REFERENCES

1. Jerhamre, A. and C. Bergstrom. *Numerical Study of Brake Disc Cooling Accounting for Both Aerodynamic Drag Force and Cooling Efficiency*. (2001-01-0948) in *SAE 2001 World Congress*. 2001. Detroit, Michigan.

2. Hudson, M.D. and R.L. Ruhl. *Ventilated Brake Rotor Air Flow Investigation*. (971033) in *International Congress and Exposition*. 1997. Detroit, Michigan.

3. Limpert, R. *Cooling analysis of Disc Brake Rotors*. (751014) in *Truck Meeting*. 1975. Philadelphia, Pa.

4. Watkins, S., P. Mousley, and J. Hooper. *Measurement of Fluctuating Flows Using Multi-Hole Probes*. in Ninth International Congress on Sound and Vibration, July 2002.

5. Hooper, J.D. and A.R. Musgrove. *Pressure probe Measurements of Reynolds Stresses and Static Pressure Fluctuations in Developed Pipe Flow* in *Twelfth Australasian Fluid Mechanics Conference*. 1995. Sydney, Australia.

6. Sisson, A.E. *Thermal Analysis of Vented Brake Rotors*. (780352) in *Congress and Exposition*. 1978. Detroit, Michigan.

7. Limpert, R. *The Thermal Performance of Automotive Disc Brakes*. (750873) in *Automobile Engineering Meeting*. 1975. Detroit, Michigan.

8. Lawson, T., *Building aerodynamics*. 2001, London: Imperial College Press.

9. Cooper, K.R. *Bluff-Body Aerodynamics as Applied to Vehicles* in *Second International Colloquium on Bluff Body Aerodynamics (BBAA II)*. 1992. Melbourne, Australia.

10. Kubota, M., et al., *Development of a lightweight brake disc rotor: a design approach for achieving an optimum thermal, vibration and weight balance.* JSAE Review, 2000. **21**(3): p. 349-355.

CONTACT

A/Prof. Simon Watkins
Dept of Mechanical & Manufacturing Engineering.
RMIT University
PO Box 71, Bundoora, Vic. 3083
AUSTRALIA
Email: simon.watkins@rmit.edu.au